Rockefeller University
Digital Commons @ RU

Student Theses and Dissertations

2015

Synapse Formation in the Zebrafish Lateral Line

Eliot Dow

Follow this and additional works at: http://digitalcommons.rockefeller.edu/student_theses_and_dissertations

Part of the Life Sciences Commons

Recommended Citation
Dow, Eliot, "Synapse Formation in the Zebrafish Lateral Line" (2015). *Student Theses and Dissertations.* Paper 277.

This Thesis is brought to you for free and open access by Digital Commons @ RU. It has been accepted for inclusion in Student Theses and Dissertations by an authorized administrator of Digital Commons @ RU. For more information, please contact mcsweej@mail.rockefeller.edu.

SYNAPSE FORMATION IN THE ZEBRAFISH LATERAL LINE

A Thesis Presented to the Faculty of

The Rockefeller University

in Partial Fulfillment of the Requirements for

the degree of Doctor of Philosophy

By

Eliot Dow

June 2015

© Copyright by Eliot Dow 2015

SYNAPSE FORMATION IN THE ZEBRAFISH LATERAL LINE

Eliot Dow, Ph.D.

The Rockefeller University 2015

Although much is known about how axons and dendrites are guided to a target tissue, little is understood regarding how pre- and postsynaptic partners are matched for synapse formation. The zebrafish lateral line offers the opportunity for greater insight into this process. Hair cells in the lateral-line neuromast exist as two intermingled subpopulations, anteriorly and posteriorly polarized cells. Afferent neurons form synapses with hair cells of only one subpopulation, and this polarity-specific innervation arises independently of synaptic activity. The research presented in my thesis deepens the understanding of synapse formation in the zebrafish lateral line. First, I examine the neuronal architecture of the neuromast at nanometer-scale resolution by imaging the tissue by serial block-face electron microscopy. The data demonstrate that afferent neurons show a polarity preference at the earliest stages of hair-cell innervation, and additionally that the synaptic arrangement appears to arise from interactions among neurons for access to synaptic ribbons rather than being mediated by an accessory cell. I next describe a novel phenomenon, the extension of transient, dynamic projections from the base of nascent hair cells beginning shortly after mitosis. The projections extend toward nearby mature hair-cell synapses and filopodia arising from afferent terminals extend directly along them toward unoccupied synaptic ribbons. Hair-cell projections lacking stable association of afferent neurons are larger than those that are stably innervated. The appearance of hair-cell projections is contemporaneous with the initiation

of contact between afferent neurons and nascent hair cells, and the disappearance of projections coincides with the appearance of pre- and postsynaptic markers proteins. I propose a model in which hair-cell projections act as cellular scaffolds for the guidance of neurons to available synaptic sites. Finally, I describe a novel method for collecting subpopulations of cells for gene expression analysis, which I employ to compare the transcriptomes of anteriorly and posteriorly polarized hair cells. I identified a number of differentially expressed candidate genes that might mediate polarity-specific afferent innervation. This work expands the repertoire of tools available for investigations of the neuromast and enhances the understanding of synapse formation in the zebrafish lateral line.

ACKNOWLEDGMENTS

I owe immeasurable thanks to my family whose support, encouragement, and love has helped me at every step of the way to completing my Ph.D. Throughout my life, my mother and father, Larry and Sandy Dow, provided me with endless outlets to nurture my curiosity, creativity, and passion for exploring the world around me. Their appreciation for the outdoors brought me in contact with the plants and animals that fostered a love of the natural world in me at a very early age. My sister, Emily Dow, has been a role model to me since we explored the forests of southern Ohio together as children, and her personal and professional accomplishments have served as an inspiration to me ever since. I wish to thank my aunts and uncles for their hugs, compliments, dinners, and unwavering interest in my well-being. My grandmothers, Kathleen Buck and Selma Richwine, were limitless sources of love and encouragement while they were alive, and I think about them often.

There are many friends whose companionship and counsel helped me develop my career goals, adjust to living in new locations, and cope with numerous challenges – Joe, Greg, Jordan, Mike, Tyler, Nick, Greg, Hannah, Vlad, Diego, Prabhjot, Jason, Xiao, Kavi, Dasha, and Josh among others to whom I'm grateful to have known. I also owe thanks to Stephanie Sarbanes for her care and support as I completed my Ph.D. Additionally, I wish to thank my peers and colleagues in the Tri-Institutional community whose insightful conversations and outstanding accomplishments have motivated me immensely during my time as a graduate student.

The Rockefeller University community has been tremendously helpful in aiding me during my time as a graduate student. I have received the assistance of a number of

individuals in Rockefeller's resource centers: Svetlana, Selam, Lily, and Stanka at the Flow Cytometry Resource Center; Alison, Kaye, Pablo, and Tao in the Bio-Imaging Resource Center; and Connie in the Genomics Resource Center. Members of the Hudspeth Lab past and present, including Brian Fabella, Taeryn Kim, Lukasz Kowalik, Sean Low, Suchit Patel, Kim Siletti, Aaron Steiner, Marielle Torres, and Maria Vologodskaia, have contributed to my thesis research in a variety of ways and have taught me a great deal about laboratory techniques. I would like to give a special thanks to Josh Salvi who committed significant time and energy to assisting me with cell collection for the RNA-Seq experiments. Thanks to Beth Dougherty for her administrative support and to Deji Afolalu and Nathan McKenney for overseeing the maintenance, care, and breeding of the zebrafish.

I also wish to thank Ruthie, Elaine, and Renee in the Weill Cornell/Rockefeller/Sloan-Kettering Tri-Institutional MD/PhD Program office as well as the program director Olaf Andersen. Together, their advocacy for the program's students and excellence in administration have contributed to my tenure in the program being enriching and enjoyable. I received assistance from Deyou Zheng and Mingyan Lin at Albert Einstein College of Medicine with analyzing next-generation sequencing data. Additionally, I would like to thank all of the individuals who contributed to the neuromast reconstruction: David Kahler, Sajjad Hossain, Dinara Guliyeva, Daryl Duran, Kattya Gibbs, Nate Aiken, and Anh Ung. I give special thanks to Sajjad Hossain for his additional assistance with the visualization of the reconstructed neuromast and data analysis, as well as Dinara Guliyeva and Kattya Gibbs who contributed their artistic skills to diagrams and figures in this thesis. I also wish to thank Moritz Helmstaedter of the

Max Planck Institute for Brain Research, whom I have had the pleasure of working with in my spare time during graduate school. His investigations with serial block-face electron microscopy served as a scaffold for my own thesis research, and moreover, he has been a role model for taking unorthodox approaches to solving significant scientific challenges.

I am grateful for the keen oversight of my thesis from my faculty advisory committee members, Cori Bargmann, Todd Evans, and Elaine Fuchs. Their years of experience and distinguished careers have not only provided critical insight into my research but also offered lofty career models to which I aspire. I also want to thank Kang Shen for traveling from Stanford University to serve as my external thesis examiner.

Finally, I wish to express my deepest gratitude to my Ph.D. advisor Jim Hudspeth, who is an inexhaustible source of knowledge and guidance. Jim has been supportive of my ideas, encouraging of my independence, tolerant of my shortcomings, and unbounded in his willingness to teach me to become a better scientist and more thoughtful human being. My time spent under Jim's mentorship will continue to have a profound effect on my career and character for many years.

TABLE OF CONTENTS

Acknowledgments……iii

Table of Contents……..……vi

List of Figures……..……vii

List of Abbreviations……ix

Chapter One – Introduction…….……1

Chapter Two – Materials and Methods…….……24

Chapter Three – Nanometer-scale architecture of the neuromast determined by serial blockface electron microscopy……...……...……35

Chapter Four – Cellular projections from sensory hair cells form polarity-specific scaffolds during synaptogenesis…….…….……63

Chapter Five - Hair-cell gene expression reveals candidate genes for polarity-specific synapse formation in the neuromast……...……119

Chapter Six – Conclusions and Future Directions……...…153

Appendix One…….……160

Appendix Two……...…….……164

References……...……194

LIST OF FIGURES

Figure 1-1 Overview of the zebrafish lateral line……..……19

Figure 1-2 In the presence of tetrodotoxin, afferent neurons innervate the same hair-cell polarity at consecutive neuromasts……...……21

Figure 3-1 Preparing the zebrafish PLL neuromast for serial block-face electron microscopy…….……40

Figure 3-2 Serial block-face electron microscopy of the PLL neuromast……42

Figure 3-3 Cellular reconstruction of the serial block-face electron microscopy image data……..…44

Figure 3-4 *In toto* reconstruction of the neuromast and its surrounding cells……..46

Figure 3-5 Exploded-view diagram of the reconstructed neuromast……48

Figure 3-6 *In toto* reconstruction of SBEM image data yielded extensive information about the cells of the neuromast…….53

Figure 3-7 Neurons of all types aggregate beneath hair-cell synapses…….55

Figure 3-8 Anatomy of the PLL afferent dendritic arbor……..……57

Figure 4-1 Dynamic, actin-filled cytoplasmic projections extend from discrete subcellular sites at the base of hair cells following rearrangement……...……67

Figure 4-2 Serial block-face electron microscopy provides a nanoscale resolution view of hair-cell projections and their interaction partners……70

Figure 4-3 Hair-cell projections extend beneath the mature hair cell synapse and make abundant contact with neurons……..……72

Figure 4-4 Hair-cell projections extend toward and are stabilized by PLL afferent neurons at the hair cell synapse…….……76

Figure 4-5 Specimens lacking afferent neurons form erratic hair-cell projections…...…78

Figure 4-6 Specimens lacking afferent neurons form erratic hair-cell projections…...…80

Figure 4-7 Hair-cell projections act as scaffolds for afferents neurons traveling toward the hair cell soma……...…...… 84

Figure 4-8 Hair-cell projections may induce the extension of dynamic offshoots from afferent dendrites……...……86

Figure 4-9 Hair-cell projections preferentially contact a biased subpopulation of neurons that innervate ribbon synapses of the same hair-cell polarity……..……..……90

Figure 4-10 Afferent neurons of both subpopulations are in proximity to hair-cell projections but are displaced from direct contact by polarity-appropriate neurons….....92

Figure 4-11 Polarity-specific differences in hair-cell projections…….....…94

Figure 4-12 Hair-cell projections diminish in size when their bases are stably associated with an afferent nerve fiber……97

Figure 4-13 Hair-cell projections contain presynaptic components……...……101

Figure 4-14 The presynaptic protein Ribeye is present in late differentiating hair cells but not early-differentiating or rearranging hair cells……103

Figure 4-15 The postsynaptic protein MAGUK is present in late differentiating hair cells but not early-differentiating or rearranging hair cells……..……105

Figure 4-16 Polarity-appropriate afferent neurons juxtapose immature synaptic ribbons at the base of hair-cell projections……...……108

Figure 4-17 Hair-cell projections mediate synaptogenesis in nascent hair cells……112

Figure 5-1 Subpopulations of hair cells can be marked and dissociated in Kaede-expressing zebrafish……..…126

Figure 5-2 Photoconverted hair cells can be distinguished and collected using fluorescent-activated cell sorting……..……128

Figure 5-3 Tens-of-thousands of hair cells were collected by fluorescence-activated cell sorting……..……130

Figure 5-4 Hair-cell markers are detected in single-polarity and all-polarity hair-cell samples…….……136

Figure 5-5 Periderm and fin-cell markers are highly expressed in non-hair-cell samples, moderately expressed in single-polarity hair cell samples, and minimally expressed in all-polarity hair-cell samples…….……138

Figure 5-6 PLL neuron, PLL supporting cell, and blood cell markers show variable expression across samples……140

Figure 5-7 *In situ* hybridization confirms hair-cell gene expression in next-generation sequencing data……142

Figure 5-8 Next-generation sequencing samples show reliability in gene expression...144

Figure 5-9 Candidate molecules for polarity-specific synapse targeting and hair-cell polarization……..……148

LIST OF ABBREVIATIONS

ALL	anterior lateral line
cDNA	complementary deoxyribonucleic acid
dpf	days post fertilization
FACS	fluorescence-activated cell sorting
GFP	green fluorescent protein
hpf	hours post fertilization
mCherry	monomeric cherry
OCD	obsessive-compulsive disorder
PBS	phosphate-buffered saline
PBST	phosphate-buffered saline with Tween-20
PLL	posterior lateral line
RNA	ribonucleic acid
SBEM	serial block-face electron microscopy
TTX	tetrodotoxin
Tween-20	polyoxyethylenesorbitan monolaurate

CHAPTER ONE

Introduction

The human brain is an organ of vast capability. It allows us to walk, talk, feel, imagine, and create; every activity that we perform and thought that we possess originates within the brain. But, as vast as the brain is in its function, its structure may be even more astounding. The human brain is composed of nearly 100 billion neurons and at least as many supporting glia; each neuron communicates with hundreds of other neurons through 1,000-10,000 synaptic connections (Azevedo et al., 2009; De Felipe et al., 1999; Herculano-Houzel, 2009). At each synapse, electrical impulses trigger the release of molecular neurotransmitters from the presynaptic membrane, which diffuse across a 20-nanometer synaptic cleft to bind to receptors at the postsynaptic membrane. At the recipient membrane, an electrical signal is produced that may continue transmission of the impulse. Such activity across the synapse is the basis of the input, processing, and output performed by the nervous system. Therefore, proper synaptic connections among neurons are necessary for the brain to meaningfully function.

Development of nervous system connectivity

Axon guidance

Although it is not possible at the present time to compare the full set of synaptic connections within two brains, the faculties of thought, movement, emotion, and perception that nearly every human shares suggests that each individual's nervous system possesses nearly the same connectivity. The faithful arrangement of the brain's 10^{15}

synapses begins in the developing embryo. A first step in nervous-system wiring involves the migration of axons and dendrites from their nascent cell bodies to the location where they will form synapses. Although some neuronal processes extend only a short distance, others extend to targets that are meters away. Navigation over such distances is achieved via a series of targets located at regular intervals. A well-established model for axon guidance involves intermediate target cells, often glial or other non-neuronal cell types, secreting diffusible molecules or bearing molecules on the cell membrane that cause the migrating growth cone to be attracted or repelled. Some of these classical molecular effectors include the semaphorins, netrins, and slits (Brose et al., 1999; Kennedy et al., 1994; Kidd et al., 1999; Kolodkin et al., 1993). The response of the growth cone to these factors is dependent upon the distribution of guidance molecules across the growth cone, the state of its intracellular signaling proteins, and the receptors that it possesses including DCC, Unc5, Robo, Plexin, and Neuropilin (Chan et al., 1996; He and Tessier-Lavigne, 1997; Tessier-Lavigne and Goodman, 1996).

A growth cone's response to chemical-guidance cues can dynamically change, a behavior essential for growth cones to traverse intermediate targets. For example, in the developing spinal cord commissural neurons must cross the midline to reach innervation targets on the contralateral side of the body. Floor-plate cells of the midline secrete Netrin-1, which attracts spinal neuron growth cones by binding to the DCC receptor (Dickson and Gilestro, 2006). However, once the growth cone arrives at the floor plate, intracellular signaling causes the RIG-1 protein to release sequestered ROBO receptors onto the cell membrane. ROBO binds to the molecule SLIT, which is produced by the floor plate cells, and repels the growth cone, thus preventing it from recrossing at the

midline (O'Donnell et al., 2009). The growth cone then uses additional guidance cues to ascend through the contralateral spinal cord toward the brain.

Once a dendrite or axon has been guided to a general region, it forms synapses with particular cellular partners. The assignment of synapses is highly specific: connections are often confined to particular subcellular regions such as the axon hillock, dendritic spine, or axonal arbor of a specific cellular subpopulation. Detailed neuroanatomical studies have found that proximity alone does not determine a neuron's synaptic targets (Batista‐Brito and Fishell, 2009; Briggman et al., 2011; Huang et al., 2007). Therefore, additional mechanisms must exist that specify the formation of synaptic connections.

Activity-dependent synapse formation

One mechanism for the targeting of synapses to particular cellular partners involves the transmission of activity across the synapse. Indeed, anyone who has learned to ride a bike, struggled with verb tenses in a foreign language, or developed perfect pitch can attest that many of the brain's capabilities arise from experience. One of the most thoroughly studied examples of activity-dependent synapse formation is the wiring of the mammalian visual cortex. Pioneering work by Hubel and Wiesel found that sewing shut one eye in a monkey during the first six months of life caused the animal to become permanently blind in that eye even after it was reopened. They found that although retinal ganglion cells depolarized in response to visual stimuli, the axons of the retinal ganglion cells formed normal synapses at the lateral geniculate nucleus, and the second-order neurons successfully carried activity from the lateral geniculate nucleus to the visual

cortex, the neurons of the visual cortex were nonetheless unresponsive. Ultimately they found that the second-order neurons transmitting information from the occluded eye showed significantly diminished innervation of the visual cortex (Hubel and Wiesel, 1977a, b). In sum, although much of visual system formed normally in the absence of visual input, activity was apparently necessary for the elaboration and specificity of cortical wiring.

Similar principles appear to hold in lower vertebrates. In goldfish, retinal ganglion cells extend to the superior colliculus in a pattern that reflects their spatial order across the retina, known as retinotopy. When raised in tetrodotoxin, a compound that inhibits neuronal action potentials, retinal cells retained their retinotopic ordering but their axonal arbors were enlarged and inappropriately overlapped with their neighbors (Schmidt and Edwards, 1983).

However, despite the foregoing, a great deal of nervous-system development occurs independently of input from the environment. In an ingenious demonstration, Roger Sperry removed the eye of a frog and rotated it 180 degrees within the socket. Once the severed retinal ganglion cells reinnervated the optic tectum and lateral geniculate nucleus, the frog was responsive to visual stimuli. However, when a fly was presented above its head, it struck its tongue downward, and conversely, when the fly was placed on the ground it struck its tongue upward. The behavioral results as well as subsequent neuroanatomical examination showed that the retinal ganglion cells had reinnervated their original targets in the brain, resulting in the perception of an inverted external world; the aberrant connectivity did not resolve despite the contradictory synaptic activity provided from the visual input (Sperry, 1945). Altogether, it appears that

although synaptic activity plays an essential role in refining the specificity of nervous system wiring, its role in instructing the initial connectivity of the nervous system is minimal (Katz and Shatz, 1996).

Molecular determinants of synapse formation

Sperry himself suggested that the results of his experiment could be explained by the existence of complementary chemical codes borne on the surfaces of neurons that mediate recognition between synaptic partners (Sperry, 1963). Several decades later, Sperry's hypothesis was validated by the discovery of a molecular mechanism determining the retinotopic wiring of the optic tectum. EphrinA is a membrane-bound molecule that inhibits growth cones bearing its receptor, EphA. Cells of the optic tectum express EphrinA in a gradient that ascends from the anterior to posterior of the structure, whereas retinal ganglion cells express a gradient of EphA that also ascends from anterior to posterior (Egea and Klein, 2007; Frisen et al., 1998). Consequently, migrating retinal ganglion axons residing at the posterior edge of the retina halt their migration at the anterior edge of the optic tectum, whereas low EphA-expressing axons originating from the anterior edge of the retina continue migrating until reaching the posterior edge of the optic tectum. Axons also map retinotopically with respect to the dorsal-ventral axis of the retina wiwth wiring of this dimension at the optic tectum is mediated by an identical scheme that uses counter-gradients of another inhibitory receptor-ligand pair, EphB-EphrinB (Luo and Flanagan, 2007; McLaughlin and O'Leary, 2005).

However, for neurons whose targets are not distributed as a graded field, greater molecular diversity and localization may be necessary to specify proper synaptic wiring.

One intuitive model of molecularly mediated synapse targeting is the binding of complementary adhesion molecules present on the pre- and postsynaptic membranes of partnered neurons. In the developing visual system of the fruit fly, the R7 and R8 photoreceptors form synapses in particular layers of the medulla of the optic lobe (Kunes and Steller, 1993). The leucine-rich-repeat family protein Capricious is expressed in R8 and its associated medullary layer, but not in R7 or the R7 layer of the medulla. In flies with a nullifying frame-shift mutation in *Capricious*, R8 axons stabilize at inappropriate layers of the medulla, whereas when Capricious is inappropriately expressed in R7 photoreceptors, the axons localize ectopically to R8 layers (Shinza-Kameda et al., 2006).

More recently, a different class of adhesion molecules with large extracellular domains containing epidermal-growth-factor repeats, the teneurins, was found to mediate synaptic-partner matching in the developing fruit fly olfactory system. Dendrites from one of 50 classes of projection neurons form synapses with axons from olfactory-receptor neurons at one of 50 discrete olfactory glomeruli (Komiyama and Luo, 2006). Dendrites from the projection-neuron class expressing ten-a colocalized with a class of olfactory receptor neurons expressing teneurin-a; similarly classes of projections neurons and olfactory-receptor neurons that formed synapses both expressed teneurin-m. When the teneurins were expressed in inappropriate cell types or when their expression was eliminated, the neurons formed synapses at inappropriate glomeruli. Interestingly, both teneurin proteins were expressed at moderate levels in glomeruli to which the projections neurons did not target and they were expressed at low levels throughout the glomeruli suggesting that additional factors beyond the teneurins may contribute to synapse partner matching of projection neurons and olfactory receptor neurons (Hong et al., 2012).

Teneurin-a and teneurin-m may also have roles in synapse targeting and organization of the synaptic architecture in the fruit fly neuromuscular junction (Mosca et al., 2012).

Similar mechanisms also appear to operate in the developing vertebrate nervous system. In the chick retina, retinal ganglion cells form synapses with bipolar and amacrine cells across one of at least ten sub-lamina of the inner plexiform layer (Yamagata and Sanes, 1995). Sanes and colleagues identified four homophilic adhesion molecules of the immunoglobulin superfamily, sidekick-1, sidekick-2, dscam, and dscamL, each of which was expressed in the retinal ganglion cells, bipolar cells, and amacrine cells that form synapses in a single retinal sub-lamina. When the molecules were ectopically expressed or expression was eliminated, retinal cells arborized at inappropriate sub-laminae (Yamagata and Sanes, 2008; Yamagata et al., 2002).

An additional mechanism for restricting a neurite's synapses to a particular location is to inhibit its formation of synapses with other nearby cellular targets. One example of this mechanism involves reflex circuits in the mouse. The motor neurons of the triceps muscle receive monosynaptic innervation from proprioceptive afferent neurons, whereas the motor neurons of the cutaneous maximus muscle do not. The proprioceptive neurons express sema3a, a repellant signal, and the motor neurons of the cutaneous maximus, but not of the triceps, express its receptor plexinD1. When the signaling pair is disrupted, the cutaneous maximus motor neurons receive proprioceptive innervation. Additionally, when Sema3e is ectopically expressed, proprioceptive innervation of the triceps muscle is disrupted (Pecho-Vrieseling et al., 2009).

The foregoing models have shown that interaction between molecules residing on pre- and post-synaptic neurons is sufficient to orchestrate partner matching without

assistance from intermediary cells. However, a number of cases have been identified in which non-neuronal cells appear to assist in the matching of synaptic partners. For example, in *Caenorhabditis elegans*, the HSNL neuron forms synapses with the egg-laying vulval muscles with the assistance of so-called guidepost cells. The neuron expresses the immunoglobulin superfamily adhesion molecule SYG-1, and its heterophilic binding partner SYG-2 is expressed by vulval epithelial guidepost cells adjacent to the vulval muscle. Loss of SYG-1 or SYG-2 causes the HSNL synapses to be misplaced onto other cells (Shen and Bargmann, 2003; Shen et al., 2004). Another immunoglobulin superfamily molecule, CHL1, also acts as a synapse-targeting cue via intermediary cells. In this case, expression in glial cells neighboring Purkinje cells are necessary for stellate interneurons to innervate the distal portion of their dendritic arbors. In the absence of CHL1, stellate cell synapses form at inappropriate locations (Ango et al., 2008).

Despite the foregoing examples of synapse targeting, a great deal remains to be learned about how the normal connectivity of the brain arises. First, aside from the work described in the chick retina, few results have been reported in the vertebrate nervous systems. Additionally, although the adhesion of pre- and postsynaptic membranes presents an intuitive model, much remains to be learned about how the physical connection is mediated both on the cellular and molecular levels. Finally, the existing studies can hardly account for the proper wiring of 100,000 neurons of the fruit fly central nervous system let alone the 10^{15} synapses of the human brain.

The zebrafish lateral-line organ

Development of the lateral line

A novel and highly tractable model system for expanding research on nervous system development is the zebrafish posterior lateral line (PLL). Aquatic organisms use the lateral line to sense water currents, a modality that is important for rheotaxis, shoaling, prey detection, and predator avoidance (Montgomery and Macdonald, 1987; Olszewski et al., 2012; Suli et al., 2012). In the embryonic zebrafish, the lateral line is divided into the anterior lateral line (ALL) distributed across the head and the posterior lateral line (PLL) distributed along the tail (Fig. 1-1, A). By five days post fertilization (dpf), the ALL and PLL are each comprised of approximately ten neuromasts, clusters of sensory hair cells surrounded by supporting cells and innervated by afferent and efferent neurons (Fig. 1-1, B) (Metcalfe et al., 1985).

The PLL is derived from a cephalic placode that arises just posterior to the otic placode. Beginning at 22 hours post fertilization (hpf), the placode, or PLL primordium, migrates posteriorly along the midline depositing neuromasts every three to five somites (Metcalfe et al., 1985). The migrating cells reach the posterior end of the tail by 42 hpf (Gompel et al., 2001a). A second primordium migrates from a similar starting position at 48 hpf and deposits an additional set of neuromasts in between the existing neuromasts (Sapede et al., 2002). The PLL continues to expand during the late larval and adult stages with neuromasts budding off into rows of neuromasts known as stitches (Ledent, 2002).

Hair cells: sensory receptors for mechanical stimuli

A hair cell is a sensory cell that detects mechanical stimuli by means of an apical hair bundle. The hair bundle consists of rows of rigid, actin-filled stereocilia of ascending height that culminate in a tall primary cilium, the kinocilium (Fig. 1-1, B) (Hudspeth, 1989). The tips of the stereocilia are connected to neighboring stereocilia by molecular strands of cadherin 23 and protocadherin 15 called as tip links (Kazmierczak et al., 2007). When a force is exerted on the hair bundle, stereocilia bend at their bases, causing the tips to slide along one another and creating tension in the tip links. The tip links are thought to pull on the gating domain of mechanosensitive channels, causing the influx of cations into the hair cell (Hudspeth, 1989; Hudspeth and Jacobs, 1979).

Membrane depolarization, originating from the influx of ions at the hair bundle, propagates through the cell to its base where specialized synapses, known as ribbon synapses, reside (Hudspeth, 1989). The influx of calcium through L-type voltage-gated calcium channels evokes the exocytosis of vesicles, releasing glutamate to the synaptic cleft (Lenzi and Roberts, 1994). Afferent neurons innervating the hair cell transmit this signal to the central nervous system (Fuchs et al., 2003). The ribbon synapse is characterized by rapid, precise synaptic transmission facilitated by the close proximity of voltage-gated calcium channels to glutamatergic vesicles. The ribbon synapse is shared by photoreceptor cells of the retina, a sensory tissue that like the inner ear rapidly transduces environmental stimuli into electrical impulses (Matthews and Fuchs, 2010).

Hair cells appear in a variety of sensory organs. In the cochlea, hair bundles reside in the fluid-filled chamber of the scala media contacting an overlying tectorial membrane. Sound waves in the environment are transmitted from the bones of the middle ear to the

fluid-filled inner ear. The compressive waves in the fluid are then transmitted to the tectorial membrane and subsequently to the hair bundle. Depolarization of the hair cell is transmitted by the eighth cranial nerve to the brain where it is perceived as sound. In the saccule and utricle, hair bundles are attached to an overlying otolithic membrane, a relatively massive object made of matrix proteins and surmounted by crystals of calcium carbonate. Rotation and acceleration of the head shift the otolith, which is in turn transmitted to the hair bundles for the detection of movement and balance. Hair cells in the cupulas of the semicircular canals mediate the detection of rotational motion by hair-bundle deflection through viscous fluid forces (Hudspeth, 1989; Kandel et al., 2012). In the lateral-line organ, hair bundles extend through a gap in the periderm that opens into a gelatinous cylinder called the cupula (Fig. 1-1, B). The cupula projects into the water of the organism's environment, and a deflection of the cupula is transmitted to the hair bundles (Metcalfe et al., 1985).

Hair-cell polarity in the posterior lateral line

The arrangement of the stereocilia and kinocilium of a hair bundle endow it with a vector of maximal mechanosensitivity, sometimes referred to as the cell's polarity. In the PLL a water current traveling in the same direction as the vector of mechanosensitivity causes hair-cell depolarization, whereas a current traveling oppositely to the vector causes a hyperpolarization in the hair cell. A force directed perpendicular to the vector of hair-bundle mechanosensitivity does not incite a response in the hair cell.

In the zebrafish PLL, each neuromast possesses two, roughly equal populations of hair cells with opposite hair-bundle polarity (Flock and Wersall, 1962). Interestingly,

neuromasts deposited by the first primordium contain hair cells that are sensitive along the anterior-posterior axis of the zebrafish, whereas neuromasts deposited by the second primordium contain hair cells sensitive along the dorsal-ventral axis (Gompel et al., 2001a; Sapede et al., 2002). Intrinsic neuromast polarity appears to be endowed by the direction of primordium migration. The first primordium travels from anterior to posterior along the midline, and although the second primordium follows a similar path, the proto-neuromast migrates ventrally prior to maturation (Lopez-Schier et al., 2004).

Hair cells of the PLL regularly turn over and are replaced by supporting cell mitoses. Each mitosis produces a pair of mirror symmetric hair cells arranged such that one posteriorly polarized hair cell lies to the anterior side of the pair, and an anteriorly polarized hair cell lies on the posterior side (Lopez-Schier and Hudspeth, 2006). How the neuromast maintains its intrinsic polarization of the hair cells during development and homeostatic replacement is unclear. However, one clue comes from zebrafish that possess mutations in the canonical planar-cell polarity gene *vangl2*, which have PLL hair cells randomly oriented with respect to the anterior-posterior body axis. Nevertheless, hair bundles retain their normal arrangement of ascending stereocilia and eccentric kinocilia, suggesting that two levels of polarity govern hair-cell orientation: that which orients structures within the cell itself, and that which orients the cell with respect to its environment (Lopez-Schier and Hudspeth, 2006).

Innervation of the lateral-line neuromast

Neuromasts are innervated by afferent and efferent neurons. Efferent neurons arise from the hypothalamus as well as two nuclei in the hindbrain, including the

octavolateral efferent nucleus (Bricaud et al., 2001). Efferent fibers are believed to dampen hair-cell activity by generating inhibitory postsynaptic potentials at the hair-cell synapse (Russell, 1970). PLL afferent neurons reside in the PLL ganglion, which sits just posterior to the inner ear. The earliest afferent neurons co-migrate with the first primordium, innervating the neuromasts as they are deposited (Gilmour et al., 2004). Additional neurogenesis and neuromast innervation occurs at least through 5 dpf (Pujol-Marti et al., 2010).

Afferent neurons form a somatotopic map at their central projections, with the more posteriorly projecting neurons sending their central axons to more dorsomedial portions of the hindbrain. This has been shown both in terms of ALL afferents forming synapses more medially than PLL synapses, as well as more posteriorly projecting neurons within the PLL forming more dorsomedial central synapses than those projecting more anteriorly (Alexandre and Ghysen, 1999). This arrangement appears to be determined prior to contact with a target neuromast, for morphology of the migrating growth cone, neuronal birth order, and somatic position within the PLL ganglion predict a neuron's eventual location of neuromast innervation (Gompel et al., 2001b; Pujol-Marti et al., 2012). One PLL neuron subpopulation has been characterized as arising early, possessing large-diameter dendritic fibers, and having wide receptive fields that often include several of the most posterior neuromasts (Liao and Haehnel, 2012; Pujol-Marti et al., 2012; Sato et al., 2010). Additionally, these neurons, unlike others of the PLL, make direct contact with the Mauthner cell, suggesting that the neurons mediate escape behaviors in the zebrafish (Pujol-Marti et al., 2012). This arrangement is consistent with the neurons having lower input resistance and a lower spontaneous firing rate, suggesting

that the cells are poised to detect fine water currents that could signify the presence of a predator (Liao and Haehnel, 2012). Interestingly, this subpopulation expresses high levels of neuroD, and overexpression of that transcription factor is sufficient to induce the phenotype in PLL afferent neurons (Sato and Takeda, 2013).

The PLL afferent neurons have other diverse and stereotyped patterns of innervation. Afferent neurons may innervate more than one consecutive neuromast, with documented receptive fields sometimes stretching across five of the sensory units (Faucherre et al., 2009; Nagiel et al., 2008). Within neuromasts, afferent neurons arborize extensively and dilate beneath hair cells. It was confirmed by electron microscopy that afferent neurons and hair cells form true ribbon synapses, at the sites of dilatation (Nagiel et al., 2008). Beginning by 2.5 dpf, afferent neurons were found to form synapses with hair cells of a single polarity. This was true even when afferents innervated more than one neuromast (Faucherre et al., 2009; Nagiel et al., 2008). The majority of neurons innervated less than half of the hair cells in a neuromast. The innervation specificity suggested by the structure of the dendritic arbor was confirmed with electrophysiology of afferent neurons, which appear to fire with stimulation in only one direction (Liao, 2010; Obholzer et al., 2008). Finally, after the ablation of all of the hair cells in the neuromast the afferent neuron reforms selective innervation with the same hair-cell polarity as before ablation, suggesting that the afferent neuron's polarity specificity is intrinsic to the cell (Faucherre et al., 2010; Nagiel et al., 2008).

Mechanisms of polarity-specific innervation of hair cells

How might afferent neurons innervate hair cells of a single polarity? In the neuromuscular junction, presynaptic cells can change identity based upon the postsynaptic target, inspiring the hypothesis that a particular hair-cell polarity could be endowed by its innervating afferent neuron (Fox and Umemori, 2006; Salmons and Sreter, 1976). However, in *neurogenin1* mutant zebrafish, which lack PLL neurons, hair cells retain normal polarization ratios and behaviors (Nagiel et al., 2008). Another hypothesis suggested that since hair cells share a vector of mechanosensitivity and would depolarize simultaneously in response to a water current, neurons might detect coincident firing. This is reflective of the activity-dependent synaptic specification mechanism at work elsewhere in the nervous system. However, zebrafish with inactivating mutations in tmie or pcdh15a, the genes encoding two proteins essential for hair bundle function, retained polarity-specific afferent synapses. The additional possibility that each hair-cell subpopulation possesses a unique, intrinsic pattern of spontaneous depolarization was ruled out by observing wild-type synapse specificity in zebrafish with disruptions of the genes for the L-type voltage-gated calcium channel, *cav1.3a*, or the glutamate transporter, *vglut3*, which eliminated neurotransmitter release at the synapse (Nagiel et al., 2009).

However, other research groups reached an opposite conclusion regarding the role of hair-cell activity in polarity-specific afferent synapse formation suggesting that *tmie* mutants, in fact, made more frequent synapse-targeting errors (Faucherre et al., 2010). Since the determination of what constitutes a synapse is based on the relative size of a

portion of the dendritic arbor as well as its proximity to a hair cell, it is possible that different investigators make different judgments regarding some marginal synapses.

Therefore, I conducted an experiment in which *Tg(ET4)* zebrafish with fluorescently labeled hair cells and single afferent neurons labeled with an injected *HuC:mCherry* plasmid were immersed in a 2 mM bath of tetrodotoxin (TTX) beginning at 28 hpf. In TTX, an inhibitor of voltage-gated sodium channels, fish are totally immobilized and their PLL ganglia show the complete cessation of activity (Fig. 1-2 A-B). This system allowed me to determine whether afferent neurons select the same hair-cell polarity between consecutive neuromasts in the absence of action potentials transmitted across the nerve fiber. Indeed, TTX fish showed no significant difference from fish raised in the absence of TTX in the proportion of afferents that innervated a majority of hair cells of the same polarity across two consecutive neuromasts (Fig. 1-2 D-H).

Altogether, the evidence weighs in favor of neither evoked nor spontaneous hair-cell activity playing an essential role in polarity-specific afferent innervation. An alternative to activity-dependent mechanisms is that each polarity of hair cell possesses unique molecular features that mediate the formation of polarity-specific synapses. The present work seeks to better understand the process of polarity-specific afferent innervation of hair cells and to identify the proteins that mediate synapse targeting.

Zebrafish: an ideal model organism for the study of vertebrate synapse targeting

The zebrafish neuromast represents an excellent model system for understanding the mechanisms involved in synapse targeting. New hair cells regularly arise in the

neuromast and are innervated by afferent and efferent nerves. Moreover, each pair of new hair cells represents a binary choice of innervation for afferent neurons. Zebrafish are optically transparent and the neuromast lies below less than 5 μm of periderm, allowing it to be imaged at high resolution without sectioning or staining. In the embryonic stage, zebrafish survive mounting in agarose for days, making long-term, high-resolution *in vivo* imaging possible. Zebrafish produce ample clutches of embryos that can be used for investigations of the PLL as soon as 2 dpf. Finally, zebrafish are highly amenable to genetic investigations. Genes can be targeting for knockdown using morpholinos that render particular RNAs untranslatable (Nasevicius and Ekker, 2000). Moreover, a rigorous method of stably targeting a gene for mutation is available in the form of the CRISPR-Cas system, which has been successfully adapted for the zebrafish (Hwang et al., 2013).

Figure 1-1

Overview of the zebrafish lateral line

A. The posterior lateral-line organ of the embryonic zebrafish is comprised of a series of neuromasts positioned at regular intervals down the length of the tail. Neuromasts are innervated by 20-40 afferent neurons that arise in the PLL ganglion. Their central projections extend to the hindbrain. Single afferent neurons may innervate 1-5 consecutive neuromasts. B. The neuromast contains sensory hair cells surrounded by supporting cells and mantle cells. At their apex, a hair cell contain the hair bundle, a mechanosensory structure comprised of stereocilia and a kinocilium. In zebrafish, the hair bundles lie in a gelatinous cupula that is extends from the periderm cells into the water surrounding the organism. At the base of hair cells, ribbon synapses transmit electrical activity evoked at the hair bundle to afferent nerves. Efferent nerve endings modulate hair-cell activity.

A

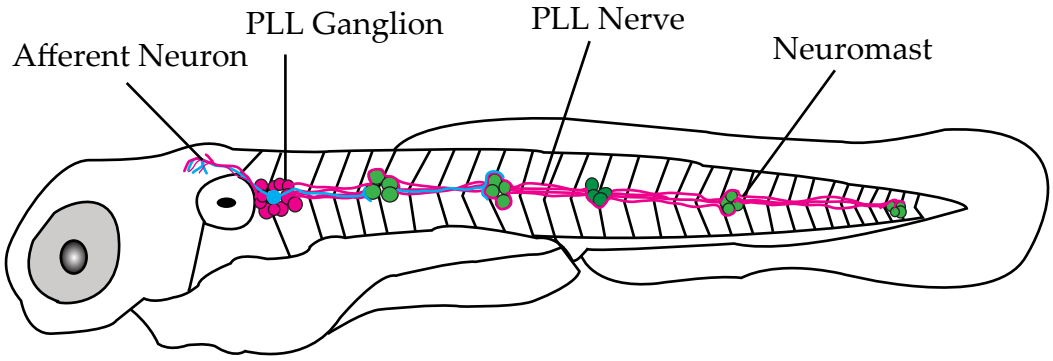
Afferent Neuron
PLL Ganglion
PLL Nerve
Neuromast

B

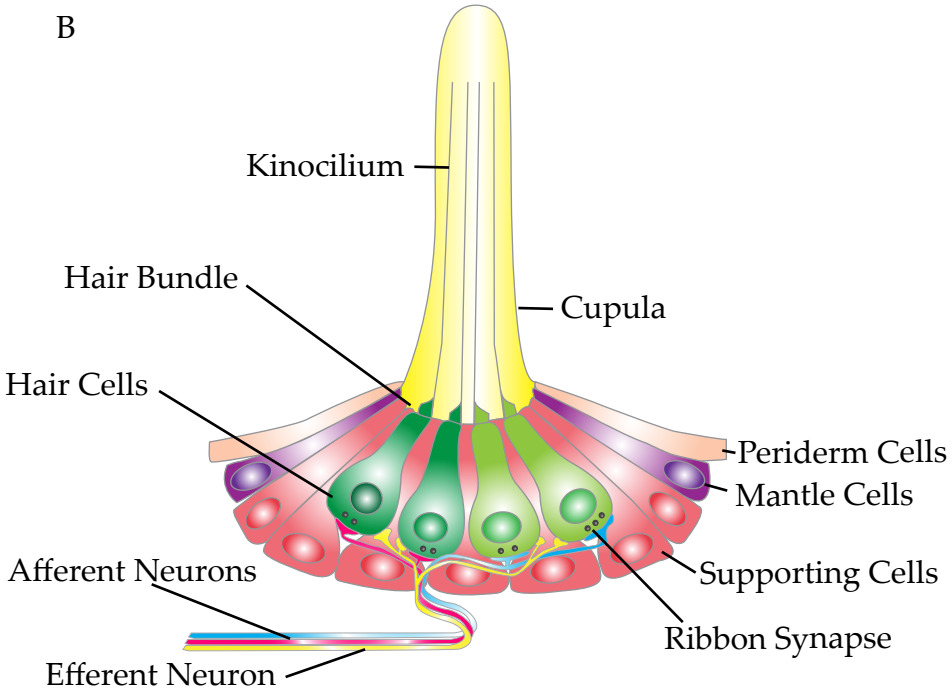
Kinocilium
Hair Bundle
Cupula
Hair Cells
Periderm Cells
Mantle Cells
Afferent Neurons
Supporting Cells
Ribbon Synapse
Efferent Neuron

Figure 1-2

In the presence of tetrodotoxin, afferent neurons innervate the same hair-cell polarity at consecutive neuromasts

A. At 28 hpf, zebrafish embryos have spontaneous movement and readily respond to touch. B. In a bath of E3 medium containing 2 mM tetrodotoxin, spontaneous movement and movement in response to tapping or prodding are eliminated within minutes. C. Near-field voltage-clamp electrophysiology at the posterior lateral-line ganglion detects action potentials. However, after the addition of 2 mM tetrodotoxin (red asterisks), action potentials are eliminated. D-G. Neuromasts showing GFP-expressing hair cells and a single afferent nerve fiber expressing an injected *HuC:mCherry* plasmid. Shown in two examples, the afferent fibers innervate hair cells of the same polarity across consecutive neuromasts. D and E are consecutive neuromasts in fish 1; F and G are consecutive neuromasts in fish 2. White asterisks mark posteriorly polarized hair cells. Anterior is left, dorsal is up. H. Zebrafish raised in E3 medium with tetrodotoxin and in normal E3 medium show no difference in the propensity of afferent neurons to innervate hair cells of the same polarity across consecutive neuromasts (E3 = 13/14 samples, E3+TTX = 11/12 samples).

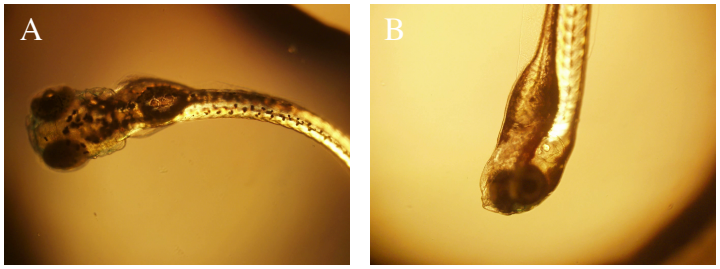
A
B

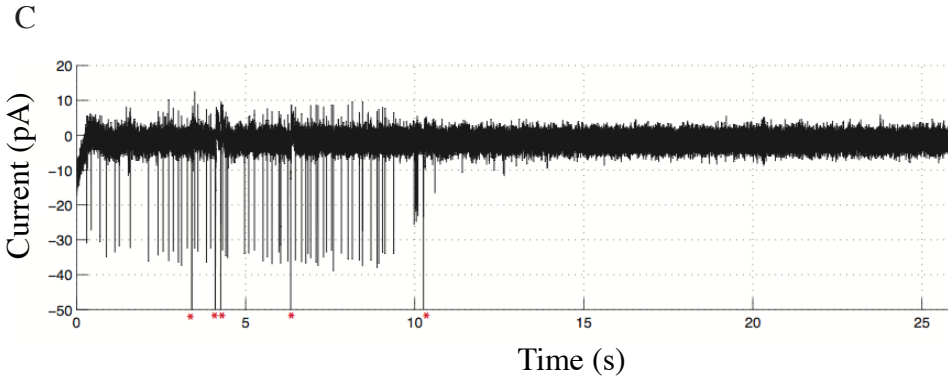
C
Current (pA)
Time (s)
20
10
0
−10
−20
−30
−40
−50
0
5
10
15
20
25

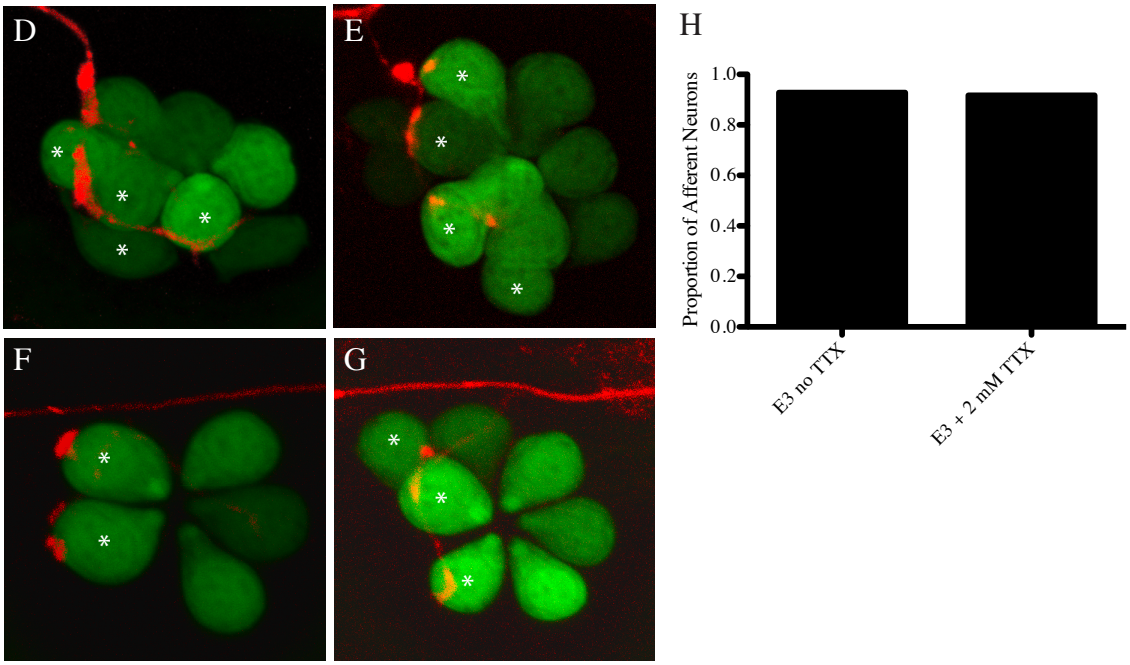
D
E
F
G
H
Proportion of Afferent Neurons
1.0
0.8
0.6
0.4
0.2
0.0
E3 no TTX
E3 + 2 mM TTX

Synapse formation and dysfunction in human disease

A rigorous understanding of synapse formation in a vertebrate system, including the zebrafish lateral line, has the potential to shed light on how the process occurs in the human brain. How normal connectivity develops or fails to develop in the human brain is of great importance to the understanding of psychiatric illness. Several psychiatric and neurological diseases, most notably autism, obsessive-compulsive disorder (OCD), and schizophrenia are believed to arise from a dysfunction in synapse formation or development (Guilmatre et al., 2014; Penzes et al., 2013). Two neuroligin genes, *nlgn3* and *nlgn4*, have been identified as monogenetic causes of autism in humans (Jamain et al., 2003; Laumonnier et al., 2004; Lawson-Yuen et al., 2008; Yan et al., 2005). The neuroligins are expressed on the postsynaptic membrane where their intracellular domain binds to the synaptic scaffold protein PSD95 while their extracellular domain adheres to presynaptic neurexins. The neurexin-neuroligin complex binds the synapse together and mediates cell-cell signaling necessary for the progression of synaptogenesis (Sudhof, 2008; Varoqueaux et al., 2006). The neurexin genes have also been associated with autism as well as schizophrenia (Reichelt et al., 2012).

Shank genes, which encode for multi-domain proteins that scaffold essential synaptic molecules, have also been implicated in autism (Durand et al., 2007; Gauthier et al., 2009; Leblond et al., 2012). Loss-of-function deletions in *shank3*, in particular, is the cause of the autism spectrum disorder Phelan-McDermid Syndrome (Wilson et al., 2003). The shank family of genes appears to be a particularly interesting point of intersection for a number of neuropsychiatric diseases. In mice, duplication in *Shank3* causes symptoms of mania and seizures, and humans with a similar *Shank3* deletion had hyperkinetic

disorders (Han et al., 2013). Mice mutant for *Sapap3*, whose protein directly interacts with Shank3 at the postsynaptic density display OCD-like symptoms (Welch et al., 2007). In fact, the obsessive thoughts and compulsive behaviors that characterize OCD may share a pathophysiological basis with the restricted, repetitive interests that are diagnostic for autism spectrum disorders (Jacob et al., 2009).

In addition to the ways in which a thorough understanding of synapse formation in the neuromast may generalize to the vertebrate central nervous system, it is important to consider that the research may directly apply to the one of the most prevalent nervous system dysfunctions, hearing loss. Hair cells of the cochlea are lost throughout life by a variety of insults including viral infections, side effects of prescription drugs, and loud noise. In the mammalian inner ear, cochlear hair cells are no longer produced after the early postnatal period. At present, nearly 20% of teenagers and 50% of older adults have clinical hearing loss (Cruickshanks et al., 1998; Shargorodsky et al., 2010). Recent research has encouraged the idea that therapeutic interventions may allow hair cells in the human cochlea to be replaced including by the reactivation of latent progenitor cells, guiding the differentiation of induced pluripotent stem cells, or directing the transdifferentiation of supporting cells (Gubbels et al., 2008; Mizutari et al., 2013; Oshima et al., 2010; Sinkkonen et al., 2011). However, for replacement hair cells to convey the sensation of sound, they must be innervated by neurons of the vestibulocochlear nerve. Knowledge of hair-cell synapse formation in the PLL may bear directly on reinnervation of hair cells in the human cochlea.

CHAPTER TWO
Materials and Methods

Animal Care and Breeding

Experiments were conducted in accordance with Rockefeller University's Institutional Animal Care and Use Committee. Zebrafish were kept under standard conditions (Westerfield, 2000). Embryos were maintained at 28.0° C and kept in E3 medium (5 mM NaCl, 0.17 mM KCl, 0.33 mM $CaCl_2$, and 0.33 mM $MgSO_4$) with 1 μg/ml methylene blue. All experiments used larvae at 2-4 dpf. The transgenic zebrafish lines included *Tg(Brn3c:GFP)*, *Tg(myo6b:mCherry), Tg(pvalb3:Ribeye-mCherry), Tg(HGn39D)*, *Tg(Et4),* and *Tg*(*myo6b:actin-GFP*) (Faucherre et al., 2009; Kindt et al., 2012; West and McDermott, 2011). The *Tg(hspGFF4A;UAS:nfsb-mCherry*) transgenic line was obtained from an enhancer-trap screen conducted by K. Kawakami (Kawakami et al., 2010). The *Tg(s1097t;s1999t)* transgenic line was created by the lab of H. Baier and received through the Zebrafish International Resource Consortium (Scott et al., 2007).

Tetrodotoxin Experiments

Zebrafish embryos were injected at the one-cell stage with 100 nl of *HuC:mCherry* plasmid. Fish were dechorionated at 28 hpf and placed into bath of E3 medium with 2 mM of dissolved tetrodotoxin citrate (Tocris Biosciences) or into a control bath of only E3 medium. Zebrafish in TTX showed complete cessation of movement in response to tapping or pinching with forceps within one minute. At 3 dpf,

fish were screened for single PLL afferents expressing the injected plasmid and contacting two or more consecutive neuromasts. Zebrafish raised with or without TTX did not show differences in the number of hair cells per neuromast or the total number of somites; however, TTX-treated fish had slightly fewer PLL afferent neurons than controls. Samples were mounted in 1% low melting-point agarose on a 35-mm glass-bottomed dish and imaged on an Olympus IX81 confocal microscope with Fluoview FV1000 laser-scanning system.

Electrophysiology experiments were conducted in collaboration with Suchit Patel. Zebrafish of the *Tg(HGn39D)* line were anesthetized with tricaine solution and immobilized on coverslips. Loose-seal voltage-clamp recording in the PLL was performed in solution containing 112 mM Na^+, 2 mM K^+, 1.5 mM Ca^{2+}, 119 mM Cl^-, 3 mM D-glucose, 2 mM creatine, 1 mM pyruvate, 600 μM 3-aminobenzoic acid ethyl ester methanesulfonate, and 5 mM HEPES at pH 7.3. The sample was visualized through a 40x objective with differential-interference-contrast optics. After the electrode was stably positioned with near-gigaohm seal and action potentials were observed, concentrated TTX solution was added to the bath solution for a final concentration of 2 mM.

Tissue preparation for electron microscopy

Following confocal pre-imaging of the 4 dpf *Tg*(*myo6b:actin-GFP*) zebrafish, the sample was removed from 1% low melting-point agarose and transferred to a 600 μM solution of 3-aminobenzoic acid ethyl ester methanesulfonate for anesthetization. Anesthetized fish were then immersed at 4° C in 200 mM glutaraldehyde, 400 mM formaldehyde, 75 mM sodium cacodylate, 10 mM sucrose, and 1 mM $CaCl_2$ for fixation

for 3 hours. Samples were dissected at the tail 200 μm posterior to the target neuromast before being returned to the fixation solution overnight. Samples were washed in 75 mM sodium cacodylate, 10 mM sucrose, and 1 mM $CaCl_2$ before osmication at 4° C for 1.5 h in 80 mM OsO_4, 75 mM sodium cacodylate, 10 mM sucrose, 35 mM K^+ ferrocyanide·3 H_2O, and 1 mM $CaCl_2$. Samples were washed in distilled water and then treated at 60° C for 30 min with 100 mM thiocarbohydrazide. Samples were once again washed in distilled water, and then treated at room temperature for 1 h with 80 mM OsO_4. After samples were washed in distilled water, they were treated at 4° C for 16 h in 25 mM uranyl acetate. Washes in distilled water were followed by treatment at 60° C for 30 min in 20 mM lead (II) nitrate ($Pb(NO_3)_2$ dissolved in 30 mM L-aspartic acid solution adjusted to pH 3.5 with 25 mM KOH. After washing, samples were dehydrated in a graded series of ethanol concentrations leading to immersion in 100% ethanol at room temperature twice for 45 min. Then, samples were transferred to propylene oxide twice for 45 min.

Samples were placed in a 50% propylene oxide/50% plastic mixture (EMbed-812 resin, dodecenyl succinic anhydride, nadic methyl anhydride, and 2,4,6-tri(dimethylaminomethyl)phenol) for 24 h. Then samples were transferred to a 100% plastic mixture and mixed with slow rotation for 24 h before being placed in a 2 mm deep layer of plastic and cured in a vacuum oven at 60° C for 48 h. Plastic-embedded samples were trimmed by hand and glued onto stubs for thick sectioning. One-micron semi-thin sections were trimmed from the block face before halting approximately 5 μm posterior to the target neuromast.

Serial block-face electron microscopy imaging

Block faces were trimmed to approximately 200 μm x 200 μm. Samples were sent to Renovo Neural, Inc. for imaging on a Zeiss Sigma VP scanning electron microscope with a Gatan 3View high-precision ultramicrotome. The ultramicrotome cut the block face at 50 nm increments. Samples were imaged in high-vacuum mode with lateral resolution of 5 nm x 5 nm per pixel. Overnight imaging resulting in approximately 1000 consecutive images of the tissue sample, which were aligned using the SIFT algorithm (FIJI).

SBEM data annotation and rendering

One data set that includes one nearly complete neuromast was chosen for *in toto* reconstruction of the cell membranes. Data-annotation technicians were contacted through Craigslist. All prospective technicians passed a work sample test before being hired. Each cell in the neuromast was given a unique identification number and annotators were provided with a set of starting coordinates in the cell from which to begin annotating. Cells were reconstructed by outlining the cell membrane across serial EM sections using the free software Reconstruct on the user's home computer (Fiala, 2004). Challenging areas for annotation were flagged and evaluated by the author resulting in no areas of significant ambiguity. Cell contours were compiled into a master file that was checked twice independently for accuracy. Surfaces of the cells were rendered from contours in Reconstruct, and then, additional rendering and post-production was performed in MeshLab and Blender. Volume and distance measurements

were performed in Reconstruct. Surface area contact measurements were performed in FIJI. The contact areas of projections in SBEM data were calculated by multiplying the contact lengths by the sectioning interval.

Live Imaging

Larvae of 2-4 dpf were anesthetized in 600 μM 3-aminobenzoic acid ethyl ester methanesulfonate in E3 medium and mounted in 35-mm glass-bottomed dish in 1% low-melting-point agarose. Laser-scanning confocal imaging was performed with an inverted Zeiss Axio Observer Z1 with LSM 780 system equipped with a 60X oil immersion objective. Neuromasts were imaged as Z-stacks acquired at 0.7 μm intervals under 488 nm and 561 nm laser excitation. Images were deconvoluted using AutoQuant X3 software (Media Cybernetics) and processed into maximum-intensity Z-projections or movies and analyzed with FIJI. Hair-cell projections were segmented and measured in deconvoluted image stacks imported into Imaris (Bitplane). Projections were formally measured beginning at the dilatation of the soma that departed from the normal curvature of the cell membrane. A technician with no knowledge of the sample identities or hypotheses performed the segmentation. All image data are oriented with anterior to the left and dorsal up unless otherwise noted.

Spinning-disk confocal imaging was performed on an inverted Zeiss Axiovert 200 with Perkin-Elmer disk-spinning unit and 63X PlanApochromat objective. Neuromasts were imaged as Z-stacks acquired at 0.7 μm intervals under 491 nm and 561 nm laser excitation. Images were processed and analyzed using FIJI.

Image analysis

Contact between afferent terminals and nascent hair cells was judged by their colocalization in image stacks acquired by spinning-disc confocal microscopy. Ribeye and MAGUK puncta were segmented manually and their areas measured in FIJI. A projection was considered stable if between successive time points it did not retract more than 50% of its length or shift in azimuthal position by more than 30˚ as viewed along the apicobasal axis. A projection was considered for analysis only if it was clearly distinguishable from neighboring GFP-positive hair cells. As a result, approximately one-third of the projections analyzed by confocal microscopy extended toward the center of a neuromast whereas two-thirds extended toward the periphery. The epoch of projection was considered complete when the hair cell no longer extended projections exceeding 1 mm in length. Stable innervation was determined based on whether the same fiber remained associated with the hair cell base for more than one hour, a definition of nerve stability used elsewhere (Faucherre and Lopez-Schier, 2014). Hair-cell projections were segmented and measured in deconvolved image stacks imported into Imaris (Bitplane). Each projection was measured beginning at the dilatation of the soma that departed from the smooth contour of the cell membrane. A technician with no knowledge of the sample's identity performed the segmentation.

Injections and labeling

Plasmid DNA was injected on a Drummond Nanoject II Auto-Nanoliter Injector. Through a fine glass needle, 4.6 nl of DNA in distilled water was injected at a concentration of 5-10 ng/µl. The SILL1 plasmid DNA, expressed in PLL afferent

neurons, was provided by the Lopez-Schier lab (Pujol-Marti et al., 2012). The *UAS:gap43-citrine* plasmid was provided by the Raper lab (Dell et al., 2013). Embryos were screened 24-48 h after injection on a Zeiss Axioplan 2 wide-field fluorescence microscope.

Antibody labeling

For antibody labeling, 3.5 dpf *Tg*(*myo6b:actin-GFP*) larvae were fixed in 4% PFA overnight at 4° C then washed with 0.1% Tween-20 phosphate buffered solution (PBST). Larvae were blocked in 2 mg/mL bovine serum albumin in PBST for 1 hour at room temperature before the addition of the primary antibody overnight at 4° C. After wash, an AlexaFluor 568 anti-mouse secondary antibody was applied for 4 h at room temperature. Pan-MAGUK antibody (NeuroMab) was used at 1:500, mouse anti-acetylated tubulin (Sigma-Aldrich) at 1:500, and AlexaFluor 568-conjugated anti-mouse secondary antibody (Life Technologies) was applied at 1:500. Imaging was performed on the Olympus IX81 confocal microscope with Fluoview FV1000 laser-scanning system. Images were processed and analyzed with FIJI. For MAGUK-stained and Ribeye-mCherry zebrafish, hair cell pairs were categorized as rearranging, early maturity, late maturity, or fully mature based upon morphological characteristics: rearranging hair-cell soma are tightly adherent to one another, lacked discernible kinocilia, lack hair-cell projections, and are dimly fluorescent in the *Tg(myo6b:actin-GFP)* transgenic line; early maturity cells possess hair-cell projections, may appear to have elongated somata when viewed along the apicobasal axis, and have hair bundles with central kinocilia; late-differentiating hair cells have small or absent projections and have polarized kinocilia but

a smaller hair bundle than mature hair cells; and mature hair cells have strongly polarized kinocilia, large hair bundles, rotund somata, and convex bases (Kindt et al., 2012).

In situ hybridization

Linearized DNA was used to create DIG-labeled RNA with a standard kit (Roche) with Promega RNA Polymerase. At 3.5 dpf, embryos were fixed at 4° C in 4% phosphate-buffered paraformaldehyde solution. After washing with PBS, fixed embryos were immersed in a graded series of methanol concentrations up to 100% before the tissue was rehydrated in a decreasing series of methanol concentrations ending in 100% PBS with 0.1% Tween-20. Embryos were treated at 37° C with proteinase K, then refixed in 4% phosphate-buffered paraformaldehyde and washed. Anti-sense probes or sense-control probes were diluted 1:50 in hybridization buffer consisting of 50% formamide, 5X SSC, 500 μg/mL tRNA, 50 μg/mL heparin, 0.1% Tween-20, and 9.2 mM citrate and applied to samples at 65° C overnight. Samples were rinsed and blocked with 5% sheep serum before being incubated with α-DIG-AP Fab fragments at room temperature overnight. Finally, samples were washed and incubated with indoxyl-nitroblue tetrazolium (BCIP-NBT) to create a color reaction at the site of DIG-labeling. Reactions were monitored on a Zeiss Axioplan 2 wide-field fluorescence microscope and quenched with PBS rinse and application of 5 mM EDTA. Samples were mounted on a coverslip and imaged on an Olympus IX81 confocal microscope with Fluoview FV1000 laser-scanning system.

PLL ganglion ablation

Zebrafish of the *Tg(hspGFF4A;UAS:nfsb-mCherry;myo6b:actin-GFP)* line at 2 dpf were anesthetized in 600 μM 3-aminobenzoic acid ethyl ester methanesulfonate in E3 medium and mounted in 35-mm glass-bottomed dish in 1% low-melting-point agarose. Fluorescence-positive PLL ganglia were identified on a Nikon Eclipse Ti inverted widefield fluorescence microscope with Micropoint laser ablation system (Andor). Five high-powered shots from a coumarin 440 dye laser obliterated the PLL ganglion and nearby tissue. The absence of mCherry-fluorescent neurons was confirmed immediately after laser firing as well as during follow-up imaging 24 hours later. Efferent neurons, which pass through the PLL ganglion region, were also assumed to be ablated by the severe tissue damage, a finding that was affirmed in *Tg(HuC:GFP)* zebrafish.

Kaede photoconversion

At 4 dpf, *Tg(s1097t;s1999t)* zebrafish were anesthetized in 600 μM 3-aminobenzoic acid ethyl ester methanesulfonate in E3 medium and mounted in 35-mm glass-bottomed dish in 1% low-melting-point agarose. Specimens were viewed on an inverted Olympus IX81 confocal microscope with Fluoview FV1000 laser-scanning system or an inverted Zeiss Axio Observer Z1 with LSM 780 system and scanned for neuromasts with hair cells in a two-column arrangement. Hair-cell apices were observed to determine the position of the kinocilia when possible. Hair cells were exposed to a 405 nm laser for 10-20 seconds with imaging restricted to approximately one-third of the cell interior. This caused significant photoconversion and minimal photo-bleaching in the target cell as well as minimal photoconversion in neighboring cells. Hair cells of a single

polarity were photoconverted in each accepted neuromast. Ultraviolet light-exposed zebrafish were removed from agarose for further processing.

Cell dissociation and Fluorescence-activated Cell Sorting

Photoconverted zebrafish were anesthetized in 600 μM 3-aminobenzoic acid ethyl ester methanesulfonate in frog saline (110 mM NaCl, 2 mM KCl, 1 mM $CaCl_2$, 5 mM HEPES, 10 mM glucose). Fine forceps were used to remove the periderm and place it into frog saline on ice. Periderm tissue was immersed in 400 μl Accumax (Millipore) and 400 μl 0.25% trypsin/0.913 mM EDTA solution (Gibco) at 28.5° C for 7 minutes. 30% FBS was added to halt the dissociation and samples were triturated with 25-gauge needle. Samples were filtered through an 8-micron pore mesh. Samples were spun down at 400 x g for 5 minutes. The supernatant was removed, and the cell pellet was resuspended in fresh frog saline. Samples in the *Tg(myo6b:mCherry;Brn3c:GFP)* experiments were treated identically except they were not exposed to the photoconversion steps.

Cells were sorted by the FACSAriaII (BD Biosciences) using an 85-μm nozzle. Events identified as belonging to the kaede-red population based upon a high red-fluorescence signal and low green-fluorescence signal were isolated directly into the RNeasy Micro Kit cell lysis buffer (Qiagen) containing 130 mM β-mercaptoethanol. Collected cells were stored at −80 °C until RNA extraction. For *Tg(myo6b:mCherry; Brn3c:GFP)* experiments, events with a high red-fluorescence and green-fluorescence signal were captured. Additionally, events from three other portions of the scatter plot were collected: high green fluorescence/low red fluorescence, low green fluorescence/high red fluorescence, and low green fluorescence/low red fluorescence.

Processing RNA and next-generation sequencing

Total RNA was isolated from collected cells with the RNeasy Micro Kit (Qiagen). Recovered samples were concentrated to 5 µl of RNase-free water with an unheated vacuum concentrator (Thermo). The samples showed two distinct peaks and RNA integrity scores above 8.0 when measured on the 2100 Bioanalyzer (Agilent). An estimated one nanogram of total RNA was converted to cDNA and amplified using the Ovation V2 kit (NuGen). One microgram of amplified cDNA was acoustically sheared and then prepared for sequencing using the TruSeq RNA Sample Prep Kit (Illumina). Single-polarity samples underwent 100-basepair, paired-end sequencing in individual lanes of the HiSeq 2000 (Illumina) yielding approximately 150 million reads per lane. Samples in the *Tg(myo6b:mCherry;Brn3c:GFP)* experiments were multiplexed three to a lane yielding approximately 60 million reads per sample. Reads were aligned to the zebrafish genome zv9 using TopHat software and assembled with Cufflinks software (Trapnell et al., 2012). The fold change in gene expression between pairs of anteriorly and posteriorly polarized samples was calculated for each gene and a p-value assigned for the distance from zero.

CHAPTER THREE

Nanometer-scale architecture of the neuromast determined by serial blockface electron microscopy

Previous work at the light-microscopic level has characterized the neuromast as being comprised of five cell types: afferent neurons, efferent neurons, supporting cells, mantle cells, and hair cells (Ghysen and Dambly-Chaudiere, 2007). The hair cells may be further subdivided as anteriorly polarized or posteriorly polarized, and the afferent neurons may be subdivided as innervating anteriorly polarized or posteriorly polarized hair cells. Supporting cells regularly give rise to new hair cells, each of which become stably innervated within hours of cell division. How does the ensemble of neuromast cells ensure that afferent synaptogenesis occurs at the correct subcellular location of the appropriately polarized hair cell? This chapter seeks to establish a framework for addressing this question. It introduces a technique whose application is novel to the study of the neuromast, serial block-face electron microscopy (SBEM) and *in toto* reconstruction of the cellular membranes, to achieve a nanometer-scale description of the neuronal architecture of the neuromast.

RESULTS

The neuromast is highly amenable to serial block-face electron microscopy and *in toto* reconstruction of cellular membranes.

Serial block-face electron microscopy is a recently developed technique that allows its user to acquire with high fidelity thin consecutive electron micrographs across a volume of tissue (Denk and Horstmann, 2004). A serial block-face electron microscope consists of a scanning electron microscope along with a specialized microtome. The flat

surface of a prepared specimen is imaged by a scanning beam of electrons before the sample is advanced a short distance above the blade of a diamond knife and this superficial layer is scraped away by the knife. By repeating this automated process hundreds or thousands of times, a volume of tissue can be imaged at electron-microscopic resolution (4-5 nm/pixel) at intervals as small as 20 nanometers (Helmstaedter et al., 2013). The high resolution of SBEM allows many of the smallest cellular structures, including thin axons and dendrites, to be fully appreciated in three-dimensions. The technique has been adopted for studying the dense connectivity of neuropil in the brain, but has not previously been applied to the zebrafish neuromast. In order to study the intricate architecture of lateral-line afferent neurons and hair cells, I performed SBEM imaging on the neuromast.

To reduce imaging time and sample charging, a key challenge in SBEM is to track a region of interest throughout the sample's pretreatment, fixation, staining, embedding, and cutting so that one can home-in on the desired location during imaging (Fig. 3-1, A). In this respect, I found that the myotomes visible in the larval zebrafish act as fiducials for tracking a desired PLL neuromast. In a line of transgenic zebrafish expressing GFP fused to monomeric actin under the control of the early hair-cell gene promotor myo6b, *Tg(myo6b:actin-GFP),* I performed preimaging on a target neuromast. Neuromasts lie directly over the intersection of consecutive myotomes whose features are visible under white light, so I counted the total number of myotomes anterior to the neuromast (Fig. 3-1, B). I also noted the location of melanophores and other biological landmarks such as the anal fin or gut. After fixing the fish, I viewed the zebrafish under a

dissection microscope and, using the myotomes and other landmarks, made a single axial cut two myotomes posterior to the neuromast. (Fig. 3-1, C)

The dissected tissue was prepared using a new protocol adapted from traditional SBEM staining protocols including treatments with osmium tetroxide, thiocarbohydrazide, lead aspartate, and uranyl acetate. Following embedding of the sample in resin, I cut away one-micrometer sections of the sample block by hand using a microtome. Using images of the sample prior to staining, I could determine the distance from the end of the sample to the target neuromast (Fig. 3-1, C). Additionally, the myotomes, which overlap and taper to a point from posterior to anterior, acted as an excellent guide to identifying the distance from the block surface to the neuromast of interest (Fig. 3-1, B and D). Melanophores visible under white light both before and after sample fixation acted as a second set of landmarks for homing-in on the neuromast (Fig. 3-1, B-D). These cues allowed me to cut down the block until its face was less than 5 μm posterior to the target neuromast (Fig. 3-1, A). The trimmed neuromast fit easily within a single viewport during SBEM imaging, and samples were imaged in a single overnight run with lateral resolution of 5 nanometers per pixel and 50-nanometer intervals. All cell types were distinguishable at high resolution, including anteriorly and posteriorly polarized hair cells, supporting cells, mantle cells, periderm, and neurons. Subcellular structures and organelles were also visible including ribbon synapses, synaptic vesicles, kinocilia, and stereocilia (Fig. 3-2).

I wished to reconstruct *in toto* the cell membranes of all of the cells in and around the neuromast. A major issue surrounding the use of SBEM is how to segment structures of interest in the enormous amounts of image data generated by the technique. Computer

algorithms for segmentation are poor at recognizing biological structures in electron-microscopic data with high accuracy (Helmstaedter, 2013; Helmstaedter and Mitra, 2012). Fully manual reconstruction of a neuromast takes one thousand hours exceeding a reasonable amount of time that a researcher may devote. But good results have been obtained by distributing the segmentation of SBEM data to large numbers of minimally trained workers, an approach also known as "crowdsourcing" (Helmstaedter et al., 2011).

I found that individuals without any scientific training could accurately identify the boundaries of a cell in the neuromast across a series of SBEM images when the outline of the cell was provided in the first image (Fig. 3-3, B-C). Consequently, twelve individuals were employed to perform annotation of the neuromast data using free software and their home computers. Annotators and editors flagged any areas of uncertainty and the coordinates were sent to the author for evaluation (Fig. 3-3, A). Accuracy of the annotation was confirmed through a hierarchical strategy in which one experienced annotator inspected and edited traces submitted by the other annotators, followed by a second experienced annotator evaluating the plausibility of the three-dimensional objects. The work culminated in a high-resolution reconstruction of the membranes of all cells of the neuromast and those surrounding it (Fig. 3-4 and 3-5).

Figure 3-1

Preparing the zebrafish PLL neuromast for serial block-face electron microscopy

A. Flow diagram for the preparation of a zebrafish for SBEM (for details see Materials and Methods). B. High-resolution confocal pre-imaging was performed on a target neuromast (arrowhead) followed by the overview images depicted in B. The desired final block-face position is indicated by the white line. The ratio of myotome boundaries can be correlated to structures viewed in (D). Melanophores (asterisk) provide additional landmarks. C. Formaldehyde- and gluteraldehyde-fixed embryo with a single axial cut two myotomes posterior to the target neuromast (arrowhead). The dotted line represents a measurement of the distance from the end of the tissue sample to the region of interest, which will be sectioned away by hand prior to SBEM imaging (approximately 78 μm + 74 μm across two myotomes). This pre-imaging can also be used to calculate the distance of the neuromast below the midline (approximately 8 μm). D. One-micrometer thick sections from the specimen block face can be monitored for proximity to the target neuromast using the ratio of myotome widths. The arrowhead marks a neuromast.

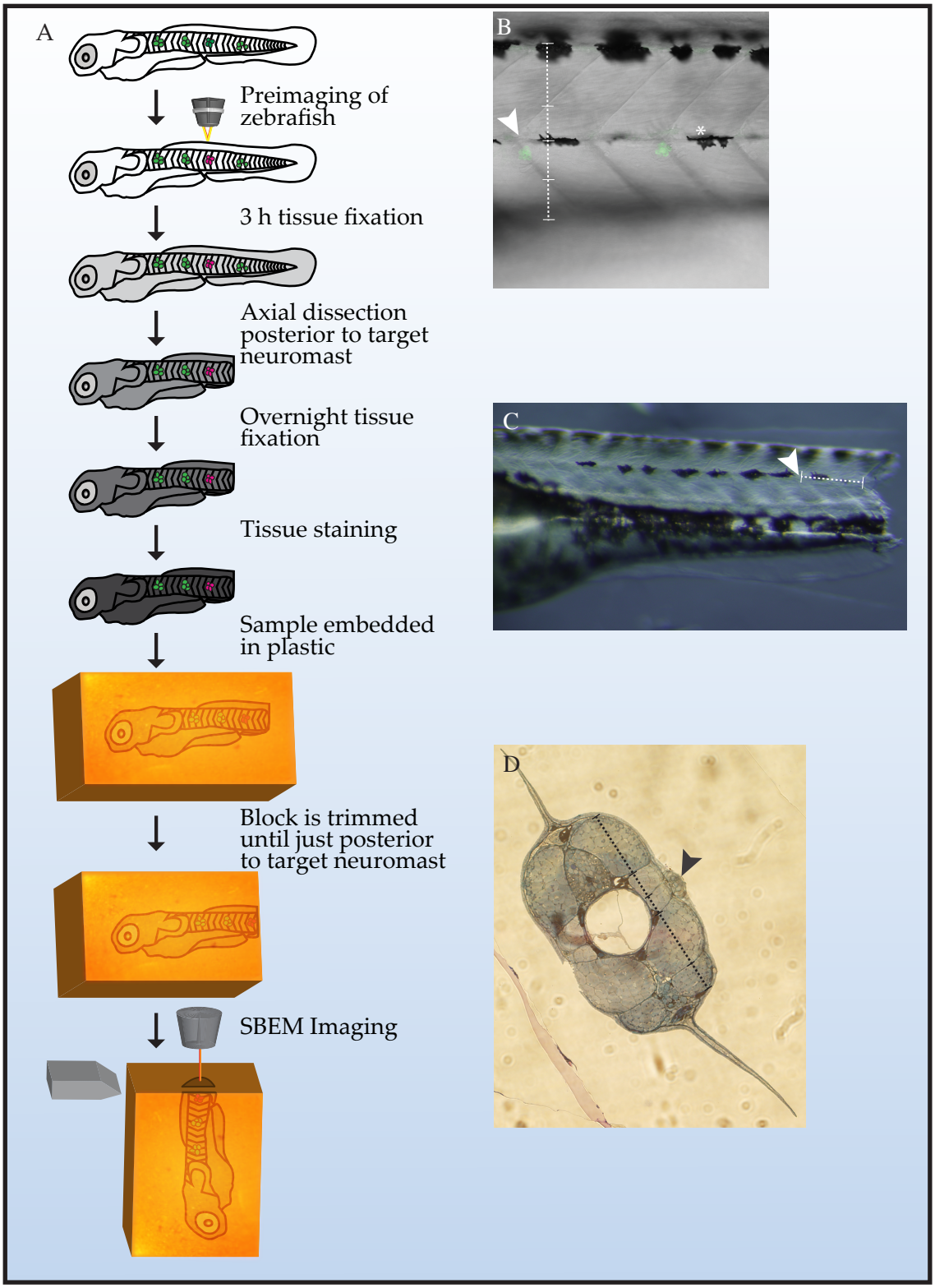
A
Preimaging of zebrafish
3 h tissue fixation
Axial dissection posterior to target neuromast
Overnight tissue fixation
Tissue staining
Sample embedded in plastic
Block is trimmed until just posterior to target neuromast
SBEM Imaging
B
C
D

Figure 3-2

Serial block-face electron microscopy image of the PLL neuromast

An electron micrograph depicting a cross section of a PLL neuromast. More than 700 consecutive images span the neuromast without loss of a single section. All cell types of the neuromast and surrounding tissue can be identified as well as a variety of organelles and subcellular ultrastructure.

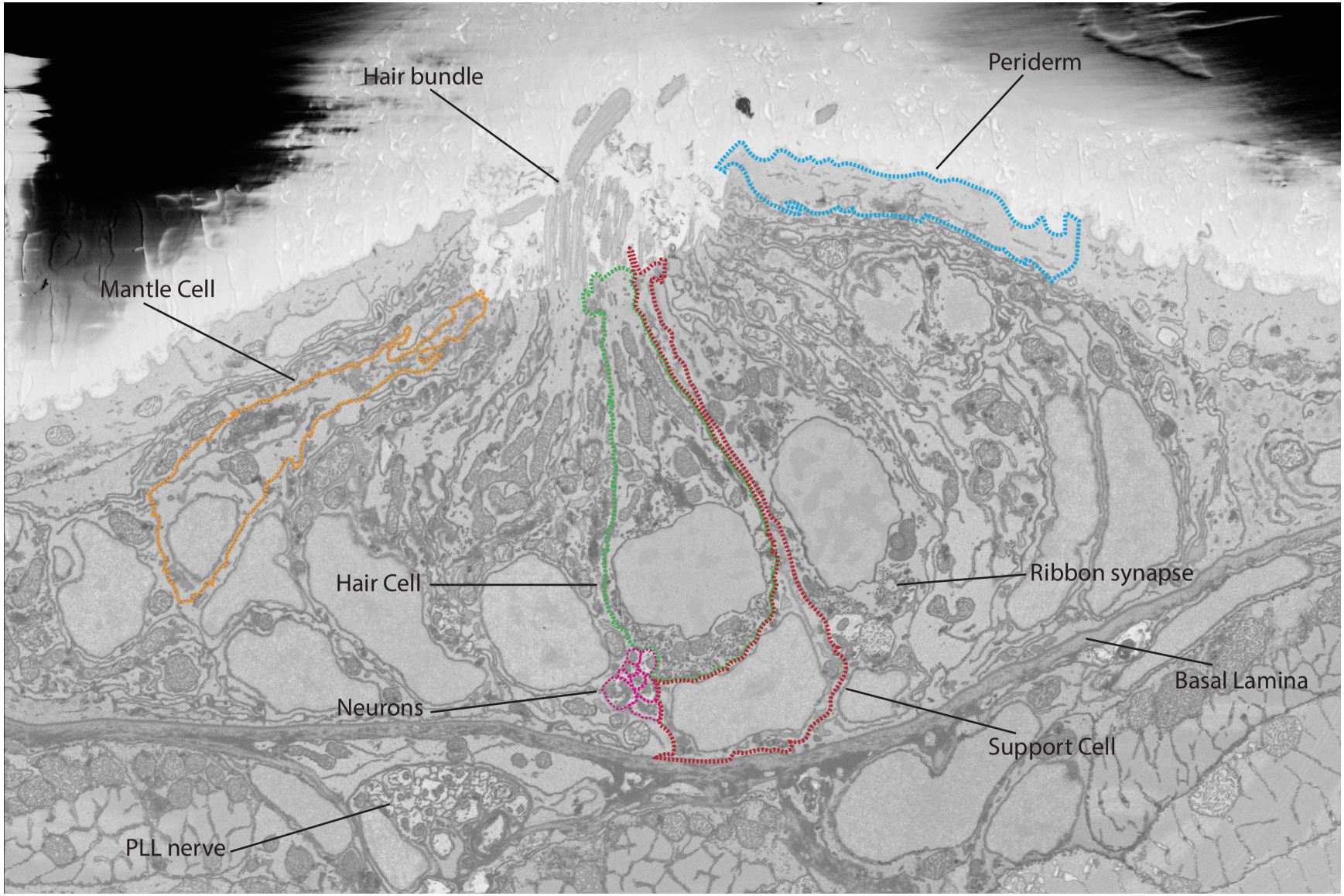
Hair bundle
Periderm
Mantle Cell
Hair Cell
Ribbon synapse
Basal Lamina
Neurons
Support Cell
PLL nerve

Figure 3-3

Cellular reconstruction of the serial block-face electron microscopy image data

A. Flow diagram for the process of "crowdsourced" data reconstruction. Each cell in the data set was identified and given an ID as well as a set of starting coordinates. Data sets were downloaded by hired data analysts or provided via USB drives. Analysts received cell assignments by email and performed complete contouring of the cell starting at its given coordinates. Contours were returned via email. A master file of contours was checked and edited twice. All questionable areas were flagged by analysts and resolved by an expert. B-D. Cell contours from work tests performed by untrained individual prior to hiring. The contours match an expert's work except for one error in (C) (arrowhead).

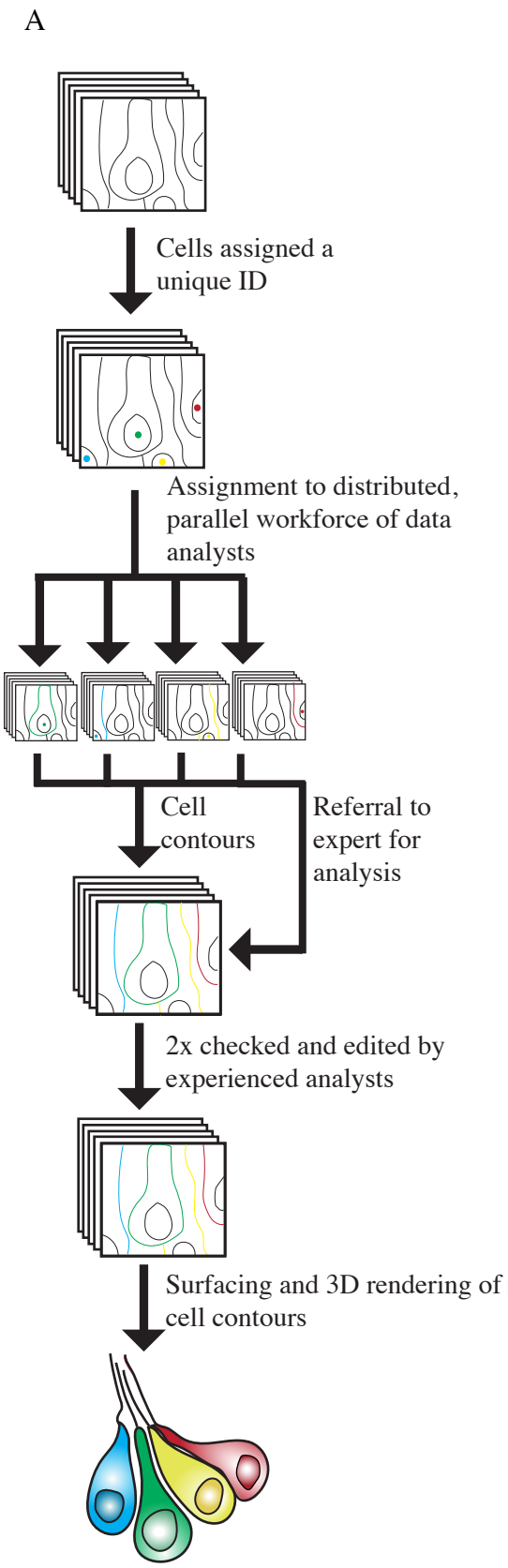
A
Cells assigned a unique ID
Assignment to distributed, parallel workforce of data analysts
Cell contours
Referral to expert for analysis
2x checked and edited by experienced analysts
Surfacing and 3D rendering of cell contours

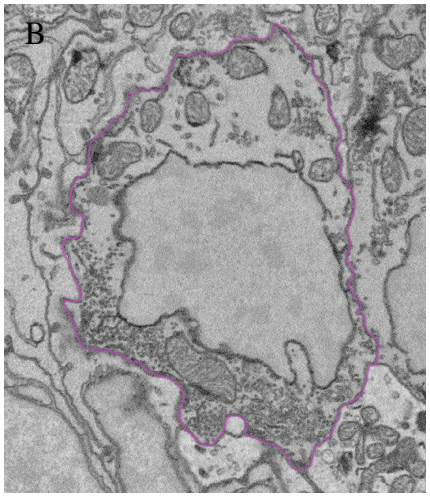
B

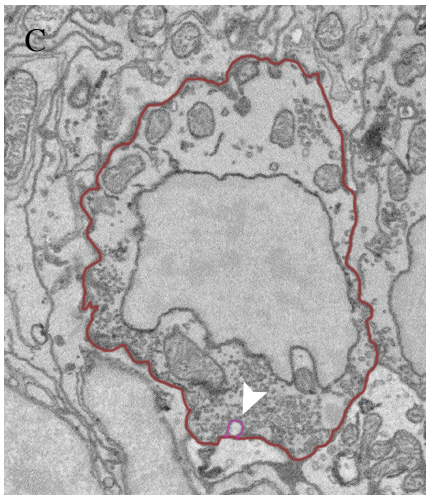
C

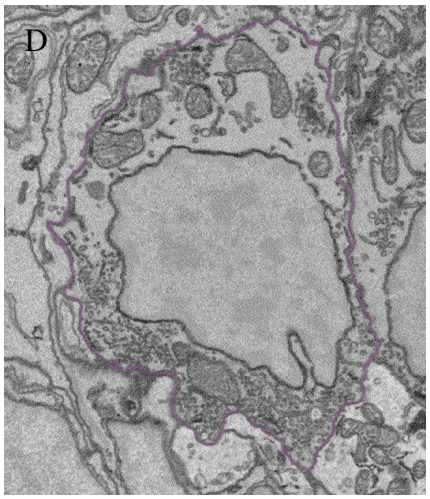
D

Figure 3-4

In toto reconstruction of the neuromast and its surrounding cells

Nearly 1000 hours of manual annotation resulted in a complete reconstruction of the neuromast and its surrounding cells.

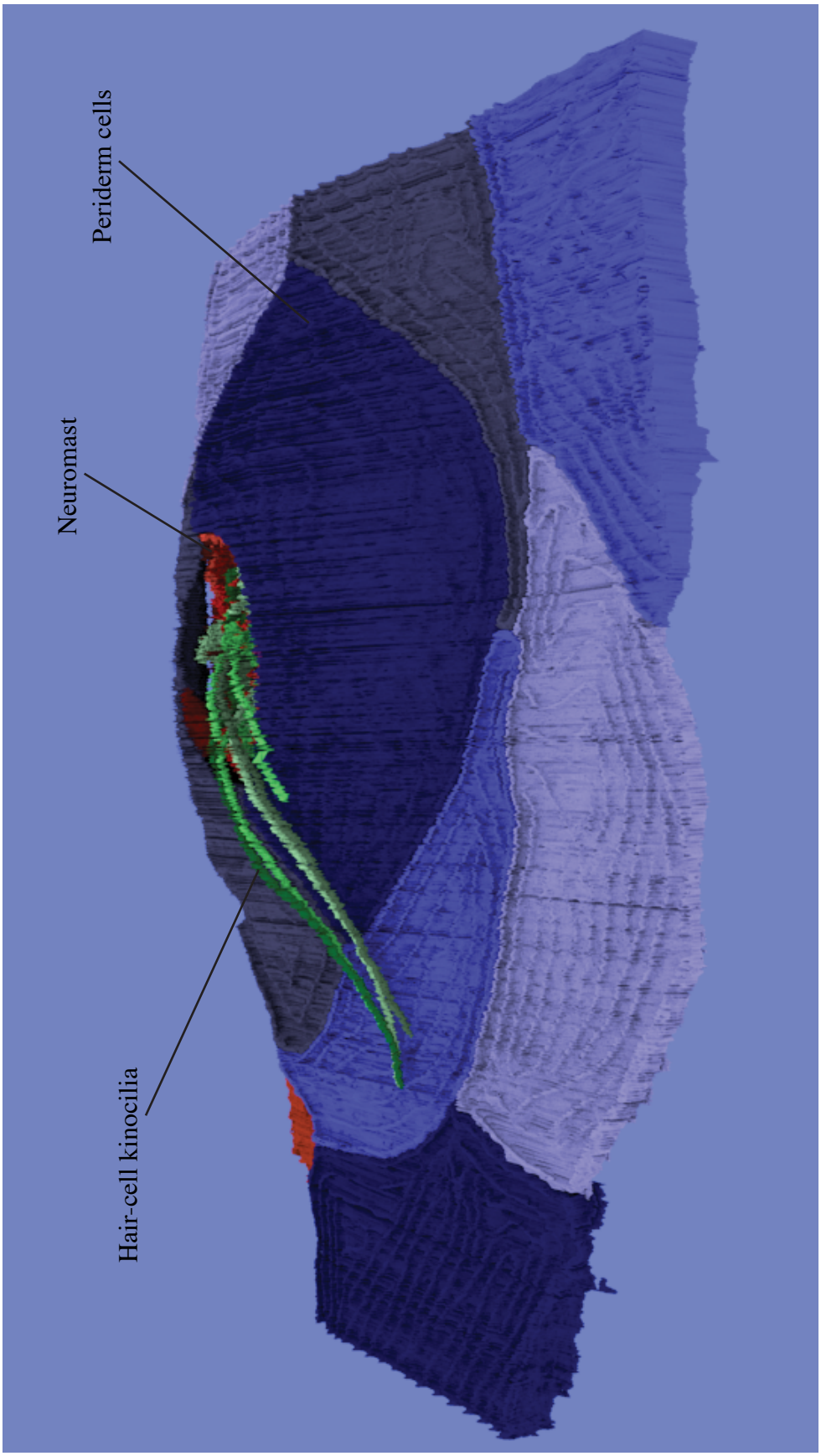
Periderm cells
Neuromast
Hair-cell kinocilia

Figure 3-5

Exploded diagram of the reconstructed neuromast

The reconstruction comprised 81 cells: 10 hair cells, 48 mantle and supporting cells, 9 periderm cells that overlaid the neuromast, 9 neurons, and 5 cells of an unknown type that abutted the neuromast.

Periderm Cells
Supporting Cells
Hair Cells
Afferent and Efferent Neurons

Reconstruction of the neuromast reveals the nanoscale architecture of the ribbon synapse.

The reconstruction yielded an extensive description of the cellular architecture of the lateral-line neuromast. Altogether, the reconstruction comprised 81 cells: ten hair cells, 48 mantle and supporting cells, nine periderm cells that overlaid the neuromast, nine neurons, and five cells of an unknown type that abutted the neuromast. Intracellular structures were also revealed including mitochondria, nuclear membranes, Golgi apparatus, endoplasmic reticula, synaptic vesicles, and ribbon synapses.

Hair-cell stereocilia were fully visualized in the SBEM imaging as were kinocilia down to the level of the axoneme microtubules. Hair-cell synaptic ribbons, uniformly semi-dense circles surrounded by a ring of synaptic vesicles, were also readily appreciable in the SBEM data. Of the 10 hair cells, one pair was deemed immature and will be described more fully in the next chapter, and another pair was judged to be partially mature, since they were similar to the remaining six mature hair cells but had markedly shorter kinocilia, fewer synaptic ribbons with smaller diameters, and fewer stereocilia (Fig. 3-6).

Although neuronal somata were not present in the sample, I could confirm the individual identities of the cells because each PLL neuron innervating the hair cells is represented by a single branch extending from the PLL nerve to the neuromast. Of the nine neurons extending branches into the neuromast, six were determined to belong to afferent neurons because they juxtaposed hair-cell ribbon synapses, and two additional branches likely belonged afferents since they were in the vicinity of the ribbon synapse although they did not directly juxtapose them. Afferent terminals associated with high specificity to synaptic ribbons of one polarity type: out of 53 ribbons, only one was

juxtaposed to an inappropriate afferent terminal (Fig. 3-6). One cell was determined likely to be an efferent neuron, because it associated extensively with all of the hair cells but none of the synaptic ribbons (Fig. 3-6). Putative synaptic vesicles were observed within the portions of the efferent terminal next to the hair cells.

Afferent terminals innervated 31 out of 32 ribbons in the mature hair cells, eight out of nine ribbons in the partially mature pair of hair cells, and six out of 12 ribbons in the immature pair of hair cells. Interestingly, although there were terminals belonging to eight afferent neurons, only four terminals abutted 96% of the synaptic ribbons (Fig. 3-6). In several cases, a ribbon synapse resided within a narrow extension of the cell membrane that was bordered on both sides by different afferent terminals suggesting that a ribbon synapse may possess more than one active zone (Fig. 3-7, C). Altogether, the specificity of afferent innervation appears to begin in immature hair cells and is maintained in mature hair cells. Finally, the proportion of synaptic ribbons that are innervated increases throughout hair-cell maturation.

The afferent terminal arbors consisted of several stereotyped structures. First, each neuron entered the neuromast as a single branch from the PLL nerve by passing through a perforation in the basal lamina (Fig. 3-8, D). Upon entry into the neuromast, each afferent terminal branched and extended arched branches beneath the mature hair cells (Fig. 3-8, A-B). Portions of afferent terminals lying beneath ribbon synapses of the appropriate polarity tended to expand in surface area and volume (Fig. 3-8, A-B) (Nagiel et al., 2008). Afferent terminals of each functional polarity nonetheless resided beneath each hair cell often having direct contact with the hair-cell base (Fig. 3-7, A-C). Typically, aggregations of afferent terminals surrounding hair-cell synapses included

only nerve fibers without any association with supporting cells or other cell types (Fig. 3-7, B-C). Aggregations of afferent terminals of both functional polarities also contacted the immature hair cells. Polarity-specific synapse formation, therefore, may be mediated by competition among terminals for access to synaptic ribbons.

Expansions of an afferent terminal at the hair-cell synapse were joined as an arbor by long, tubular tracts (Fig. 3-8, A-B). All portions of a neuronal terminal had a high degree of fasciculation with other terminals and were nearly always in contact with at least one other neuronal process. Additionally, a large number of filamentous filopodia with blind ends grew predominantly from the expanded portions of the afferent terminal and occasionally from the tubular portion (Fig. 3-8, A-C). They varied in length and orientation, but were uniformly unbranched, thin, and directed away from their sites of origin. In a few instances in which a filopodia was juxtaposed to a synaptic ribbon, the portion next to the ribbon slightly enlarged as it were transforming into a postsynaptic structure. These morphological features suggested that these postsynaptic filopodia are instrumental in selecting presynaptic targets and forming synapses. Postsynaptic filopodia have been characterized in the hippocampus, pyramidal neurons of the cortex, *Drosophila* neuromuscular junction, and other areas of the developing nervous system (Marrs et al., 2001; Trachtenberg et al., 2002). Current models suggest that postsynaptic filopodia search for presynaptic targets of innervation, form stable contact with them, and differentiate into postsynaptic structures (Hu and Hsueh, 2014; Kohsaka and Nose, 2009).

Figure 3-6

In toto reconstruction of SBEM image data yielded extensive information about the cells of the neuromast

Cellular membranes, synaptic ribbons, stereocilia, and kinocilia were contoured. Reconstructions of the contours produced volume measurements. Hair-cell polarity was judged by hair-bundle orientation. Innervation partners were judged by the neuron juxtaposed to the synaptic ribbon; if more than one fiber abutted the synaptic ribbon, the closer one was considered its innervation partner.

	Differentiation Status	Polarity	Cell Volume (µm3)	Number of Ribbons	Number of Innervated Ribbons	Innervating Neurons	Average Ribbon Size (µm3)	Size of Kinocilium (µm3)	Number of Stereocilia
HC-A	Immature	A	26.281	7	5	B	0.012	0.024	22
HC-B	Immature	P	32.073	5	1	D	0.006	0.029	15
HC-C	Mature	A	34.954	4	4	B, C	0.072	0.405	37
HC-D	Mature	A	41.308	4	4	C, B	0.093	0.466	41
HC-E	Mature	P	41.285	7	7	D, E, I	0.081	0.526	31
HC-F	Early Mature	A	35.578	4	4	B, G, D	0.038	0.193	33
HC-G	Mature	A	40.002	7	7	C, B	0.097	0.475	40
HC-H	Mature	P	48.448	6	5	D	0.115	0.573	34
HC-I	Early Mature	P	38.530	5	4	D, E	0.043	0.259	29
HC-J	Mature	P	43.125	4	4	D, E	0.090	0.584	30

	Neuron Type	Innervated Hair-cell polarity	Cell Volume (µm3)	Innervated in Mature Anteriorly Polarized HCs	Innervated in Mature Posteriorly Polarized HCs	Innervated in Immature Anteriorly Polarized HCs	Innervated in Immature Posteriorly Polarized HCs	Contact with HC-A projections (µm2)	Contact with HC-B projections (µm2)
NeuronA	Efferent	both	8.972	0	0	0	0	7.97	9.31
NeuronB	Afferent	A	12.148	6	0	5	0	24.29	3.30
NeuronC	Afferent	A	9.375	11	0	0	0	19.01	1.65
NeuronD	Afferent	P	12.432	1	16	0	1	3.19	18.35
NeuronE	Afferent	P	4.883	0	3	0	0	1.56	6.77
NeuronF	Afferent	-	1.758	0	0	0	0	0	0
NeuronG	Afferent	A	0.546	1	0	0	0	0	0
NeuronH	Afferent	-	0.494	0	0	0	0	0	0
NeuronI	Afferent	P	1.604	0	1	0	0	0	0

Figure 3-7

Neurons of all types aggregate beneath hair-cell synapses

A. An apicobasal view of the nine reconstructed neurons of the neuromast as well as 41 synaptic ribbons (immature ribbons not included). Neurons of both polarities are present beneath hair cells of each polarity. B-C. Two anteriorly polarized hair cells possess presynaptic ribbons (arrowheads) surrounded by synaptic vesicles. They are juxtaposed by polarity-appropriate afferent neurons (AP) and some ribbons even encounter more than more polarity-appropriate afferent neuron (C, black arrowhead). Polarity-inappropriate (PP) afferent fibers are contiguous with polarity-appropriate neurons but are displaced from direct contact with the synaptic ribbon by them. The efferent neuron (E) makes contact with the base of the hair cell but not at the ribbon synapse. Scale bars are 200 nm.

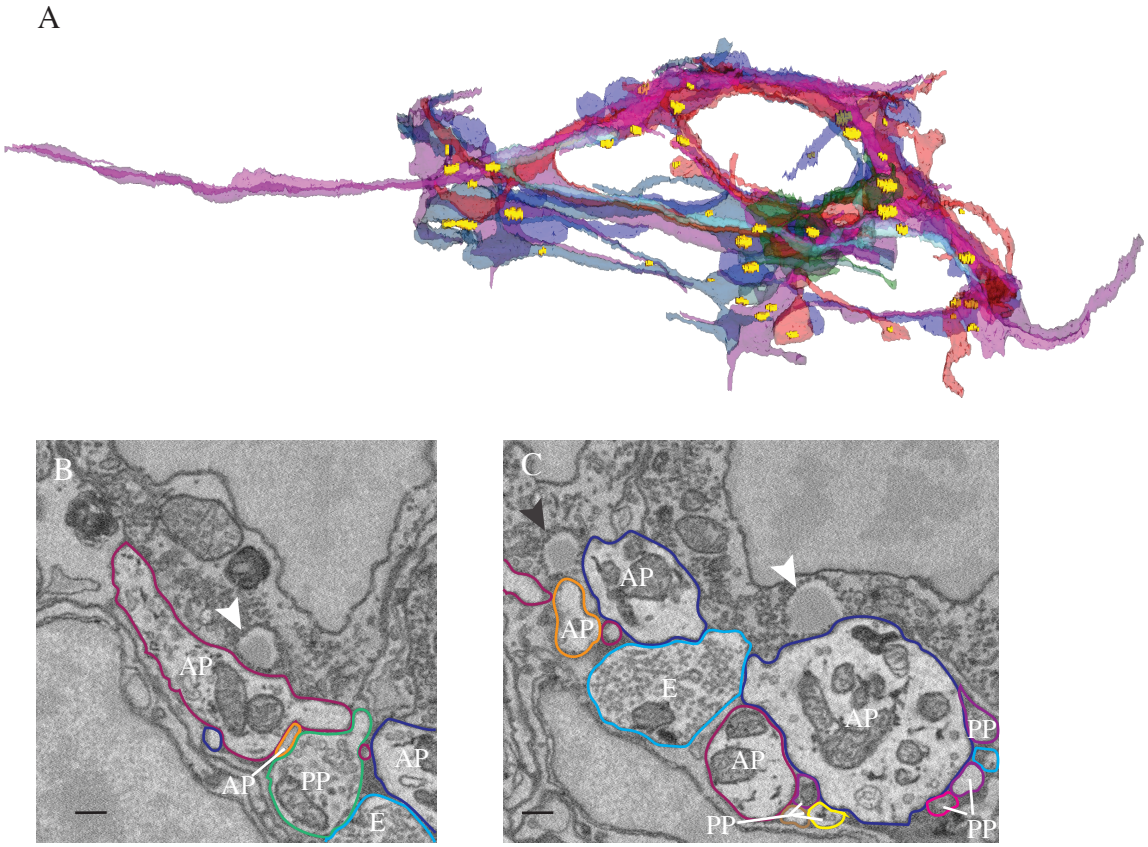
A
B
AP
AP
PP
AP
E
C
AP
AP
E
AP
AP
PP
PP
PP

Figure 3-8

Anatomy of the PLL afferent dendritic arbor

A-B. Examples of two reconstructed dendritic arbors along with synaptic ribbons from all hair cells of the polarity that the neurons innervate. Thick tubular portions of the dendritic arbor connect together expanded portions that lie beneath the hair-cell synapses (arrowheads). Thin, unbranched filopodia arise predominantly from the expanded portions of the dendritic arbor. C. A closer view of an expanded portion of the dendritic arbor as well as filopodial offshoots (arrowhead). D. Each neuron has one fiber in the PLL nerve (arrowhead) and extends a single innervating branch into the neuromast.

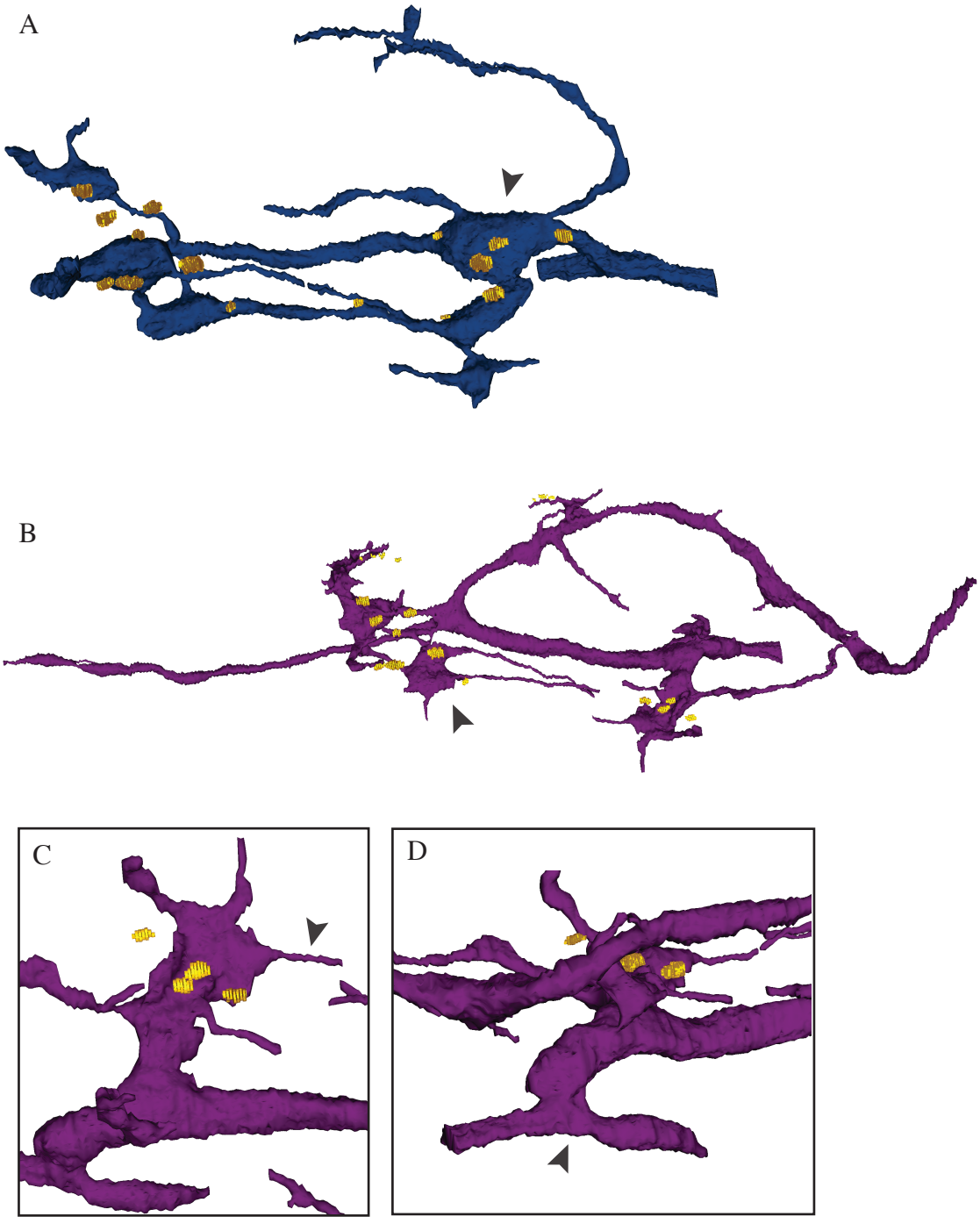
A
B
C
D

DISCUSSION

Serial blockface electron microscopy reveals tissue structure at high resolution.

Serial block-face electron microscopy offers a number of advantages for the fields of cellular and developmental biology. First, the technique holds at least a ten-fold increase in resolution over state-of-the-art light microscopy. This allows one to appreciate fine features of cells including small dendrites, cellular processes, and intracellular organelles. Moreover, one can appreciate these features in every cell in the sample rather than just a subset of cells as in a standard transgenically labeled preparation. Importantly, the resolution also allows an investigator to confirm direct membrane contact between cells. Finally, upon reconstruction of SBEM image data, the investigator possesses a remarkably clear and navigable three-dimensional representation of the tissue environment that can be rapidly measured and analyzed.

The zebrafish neuromast is highly amenable to investigation by SBEM for several reasons. First, the neuromast can be imaged at high resolution by light microscopy prior to SBEM adding valuable information about the cellular identity or state of differentiation. I have successfully obtained SBEM data from samples that were imaged by time-lapse confocal microscopy continuously for up to 34 hours prior to tissue fixation.

Secondly, the neuromast can readily be tracked across experimental steps using visible landmarks in the zebrafish. In addition to melanophores and gross biological structures, the myotomes provide a highly reliable system for homing-in upon the

neuromast of interest. Consequently one can investigate a particular neuromast by light microscopy and recover the same neuromast in SBEM image data with high efficiency.

Third, the roughly 40-micrometer diameter of the semi-spherical neuromast allows it to be imaged with SBEM during a single overnight run of the microscope, significantly less time than the weeks or months of continuous imaging that many investigators are faced with in studying other areas of the nervous system. Consequently, the 1000 man-hours required for *in toto* reconstruction is considerably smaller than the 25,000 man-hours needed for partial dense reconstruction of a subsection of the murine retina (Helmstaedter et al., 2013).

Finally, the neuromast appears to be a self-contained organ that performs its functions through the interactions of the cells within its 50-micrometer confines. These functions include the detection and transmission of mechanical stimuli, regeneration of sensory receptors, planar cell polarization of cells, and innervation of sensory receptors. The only neuromast cells not entirely contained within the neuromast are the neurons, which can nevertheless be individually identified, classified as afferent or efferent, and considered as independent processing units. Therefore, there are no cells of unknown origin or incomplete structure to limit interpretation of the neuromast architecture.

SBEM does have several downsides at the present. Access to the hardware required for data acquisition is limited to a few major research institutions. However, the microscopes are becoming more prevalent including within the walls of The Rockefeller University. An additional obstacle to widespread use is the time involved in data annotation. Manual annotation through crowdsourcing has shown promise for making a legitimate contribution to scientific research. Internet connectivity, online tools, and a

broad public interest in contributing to science make a large, distributed workforce possible for any standard biomedical laboratory. Additionally, computer algorithms for automated segmentation of electron microscopy data are steadily improving. In fact, some research groups have found success with a symbiotic combination of manual and automated annotation in which portions of SBEM data that cannot be reliably segmented by computer algorithms are flagged for evaluation by crowdsourced labor; the human-annotated data in turn improves the accuracy of the algorithms. Computer algorithms for the automated segmentation of neuromast cells and classification of subcellular structures integrated with a work flow for focused annotation by humans will allow examination of the neuromast architecture by SBEM to be a regular tool for the investigator.

The nanoscale neuronal architecture of the neuromast

The neuronal architecture of the neuromast revealed by SBEM indicates that hair-cell innervation is both extensive and accurate: 94% of ribbons were innervated in fully mature hair cells and 100% of the ribbons were innervated by their polarity-appropriate afferent terminal. In the pair of immature cells, although only 50% of ribbon synapses were innervatd, 100% of the synaptic contacts were polarity-specific. Out of the nine ribbons in a partially mature pair of hair cells, one was uninnervated and a second was innervated by a polarity-inappropriate afferent terminal. These results indicates that innervation of hair cells begins early in hair-cell differentiation and is polarity specific even during this stage. Additionally, the existence of a large number of uninnervated synaptic ribbons in immature hair cells suggests that the location of synaptic ribbons are established independently of afferent terminals.

It was interesting to observe that although the neuromast contained eight presumed afferent terminals, only four of them were innervated by more than one of the 53 ribbon synapses in the sample. The four neurons included two that were innervated by posteriorly polarized hair cells and two neurons that were innervated by anteriorly polarized hair cells. It has previously been estimated that each neuromast is predominantly innervated by two to four afferent neurons (Liao, 2010; Nagiel et al., 2008). The redundancy may allow each neuron to receive a strong signal in response to mechanosensory stimuli while also ensuring that sensory information from the neuromast is still relayed to the brain if one of the neurons dies.

The remaining four afferent neurons had comparatively small dendritic arbors with little volume, branching, or contact with hair cells. This is consistent with observations I have made using sparse labeling of afferent neurons, in which afferent terminals tend to form extensive dendritic arbors with one or two consecutive neuromasts along with extending sparse innervation into neighboring neuromasts. A mechanism that disallows these low-resource afferent arbors to be juxtaposed to ribbons would concentrate the sensory signal into a few robust neurons. Additionally, an afferent neuron acting as the dominant terminal in just one or two neuromasts would increase a neuron's spatial resolution.

Finally, it appears that juxtaposition with synaptic ribbons by the neuromast's most robust, polarity-appropriate afferent neurons is mediated by the neurons themselves. Aggregations of afferent neurons occupied circumscribed portions of roughly half to one-third of the hair-cell base. Afferent terminals of both functional polarities were represented in these aggregations and even made contact with the hair-cell base, but were

juxtaposed to ribbons of the inappropriate polarity only once out of 53 synapses. This indicates both that polarity-inappropriate terminals are able to innervate either polarity of hair cell but that a robust mechanism prevents this from happening very often. Supporting cells bordered the aggregations of afferent terminals and were sometimes interleaved with the nerve fibers, but often only terminals were displacing other terminals without any other intervening cell type. This observation suggests that a competitive process occurs among PLL afferent terminals for access to the hair-cell synaptic ribbon.

CHAPTER FOUR

Cellular projections from sensory hair cells form polarity-specific scaffolds during synaptogenesis

The somata of hair cells are generally regarded as stable, quiescent structures. However, the following chapter suggests that during synaptogenesis hair cells are not simply passive recipients in the process of innervation. Using fluorescence confocal microscopy and serial block-face electron microscopy, I identified dynamic cytoplasmic projections that emerge from immature hair cells soon after mitosis to act as scaffolds for the remodeling of the axon terminal arbor. Nerve fibers fasciculate with the projections in a subpopulation-biased manner and migrate toward the projection base where presynaptic components reside. Stable association of nerve fibers with the proximal projection is associated with a decrease in projection size. I propose a model in which hair-cell projections act as scaffolds that guide specific subpopulations of afferent neurons to unoccupied sites for synaptogenesis. This represents a novel cellular mechanism for synapse targeting and synapse specification.

RESULTS

Dynamic cytoplasmic projections extend from the base of a hair cell following rearrangement.

Mature hair cells of the zebrafish posterior lateral-line organ appear round and quiescent. However, in transgenic zebrafish expressing GFP fused to monomeric actin under the control of the early hair-cell gene promoter myosin 6b, *Tg(myo6b:actin-GFP),* I identified hair cells possessing long, cytoplasmic projections from their bases (Fig. 4-1, A-C). Projections often had an arched shape and were diverse in morphology, appearing raggedly branched, filamentous, or as stumpy elongations of the soma.

Time-lapse laser-scanning fluorescence confocal microscopy of cells revealed that projections arose 41 ± 25 minutes after rearrangement, a behavior that pairs of sibling hair cells undergo during the two to three hours following mitosis (Fig. 4-1, D). The projections behaved in various ways, sometimes extending, retracting, or changing shape over the course of minutes, while at other times they remained stable in their position for more than two hours (Fig. 4-1, D-G). The projections extended up to 15 μm and were between 0.1-0.5 μm wide at their site of origin at the soma. Some projections grew at up to 2 μm per minute. Projections originated from one to three relatively consistent sites on the hair cell soma that tended to include the anterobasal and posterobasal edge of the cell and occasionally the medial edge. Projections typically oriented toward nearby mature hair cells or the cell's immature sibling (Fig. 4-1, E-G). Hair cells occasionally shifted their somatic position by a few micrometers, but hair-cell projections did not consistently precede the movement nor did most projecting hair cells migrate. Projections were abundantly labeled by the actin-GFP fusion and additionally showed labeling of the

microtubule-associated protein Map1b indicating the presence of both cytoskeletal components (Fig. 4-1, H-K). Projections persisted for 11.5 ± 2.5 hours before new hair cells became rotund and quiescent like their mature counterparts.

Figure 4-1

Dynamic, actin-filled cytoplasmic projections extend from discrete subcellular sites at the base of hair cells following rearrangement

A-C. Three examples of hair-cell projections (arrowheads) extending from the base of actin-GFP-expressing PLL hair-cells. D-G. Time-lapse confocal microscopy showed that hair-cell projections are absent in rearranging hair cells (D) but appear less than one hour after rearrangement (E) and persist for approximately 12 hours (F-G). Time is listed as minutes from the end of hair-cell rearrangement. H-K. Immunofluorescence staining for β-tubulin. A pair of early differentiating hair cells as indicated by their immature hair bundles (H) shows no staining in hair-cell projections (arrowheads) across three z-positions in an image stack (I-K). All scale bars are 5 μm. Zebrafish are 2.5-3.5 dpf. D-G are maximum projections through the Z-axis.

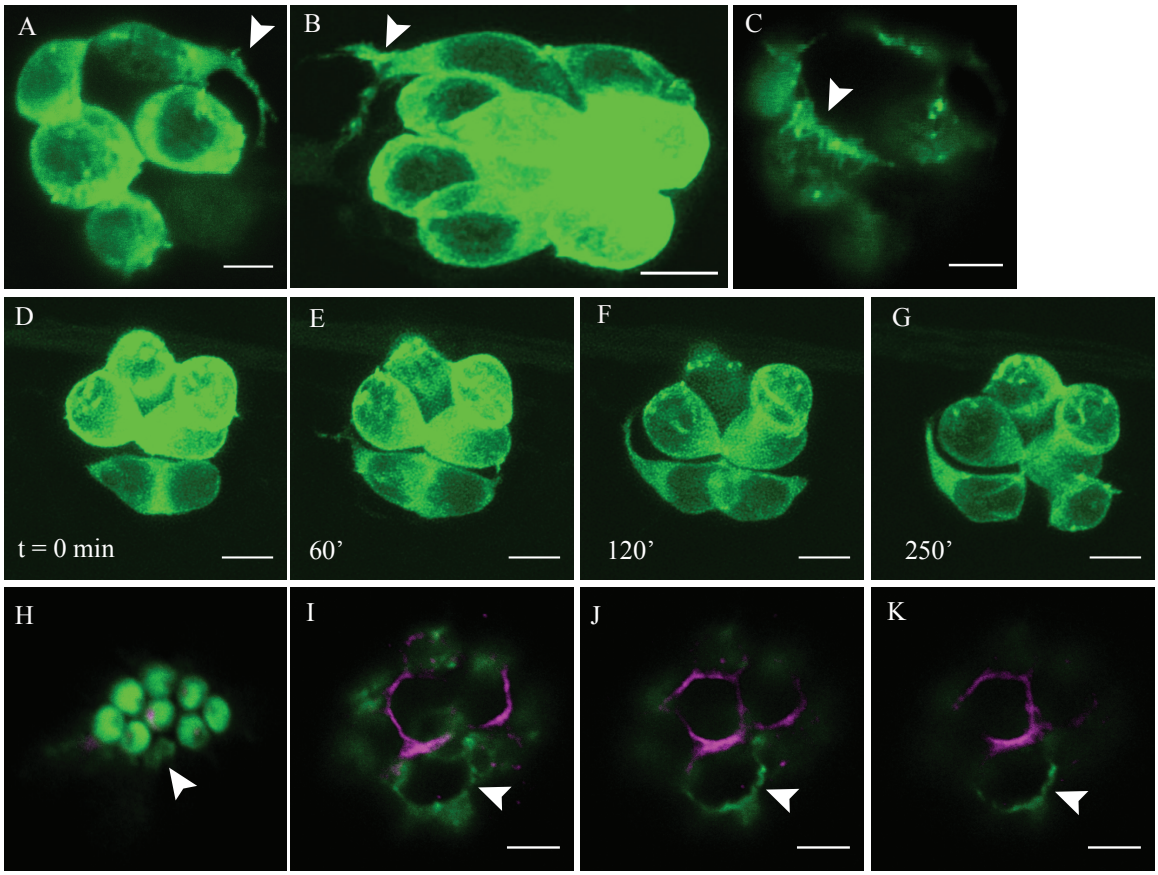
A
B
C
D
t = 0 min
E
60’
F
120’
G
250’
H
I
J
K

Serial block-face electron microscopy provides a nanometer-resolution view of hair-cell projections and their interaction partners.

Given the long, thin structure of hair-cell projections, I sought to obtain a complete view of their morphology as well as to precisely identify the cellular partners with which they interact. To do so, I examined the *in toto* reconstruction of the neuromast from serial block-face electron microscopy. The reconstruction provided a detailed view of two immature hair cells shortly after hair-cell rearrangement (Fig. 4-2, A-B and C-D). Projections arose from two basolateral sites on each immature hair cell and extended below the bases of the mature hair cells and above the supporting-cell nuclei. The projections had diverse morphology including branches, thin filamentous offshoots, flattened portions, and somatic elongations. Similar basal projections were not seen in any of the mature hair cells (Fig. 4-2, A-E).

All four hair-cell projections made abundant cell-cell contacts with PLL afferent terminals and to a lesser extent with efferent terminals (Fig. 4-3, A). Interestingly, all four hair-cell projections extended toward and intermingled with nearby aggregations of neuronal terminals directly underlying the mature hair-cell ribbon synapses (Fig. 4-3, B-C). Hair-cell projections made direct cell-cell contact with supporting cells, and the projections' stereotypical arched morphology arose from their maneuvering around neighboring supporting cells. But, supporting cells did not appear to have any other specialized morphology related to the projections that would suggest a more important role in their structure or genesis. Additionally, despite orienting toward nearby hair cells, projections made minimal direct contact with other hair cells (Fig. 4-3 A).

Figure 4-2

Serial block-face electron microscopy provides a detailed view of hair-cell projections and their interaction partners

A-C. Serial block-face electron-microscopy imaging of hair-cell projections (outlined in blue and green). Scale bar is 200 nm. B-D. Lateral view of 3D reconstruction of two immature hair cells from serial block-face electron microscopy data. Each cell contains an immature hair bundles are at the top and two hair-cell projections extending from their bases. E. A basal view of three-dimensional reconstructions of the six full maturity, two late maturity, and two early maturity hair cells in the neuromast from serial block-face electron microscopy data.

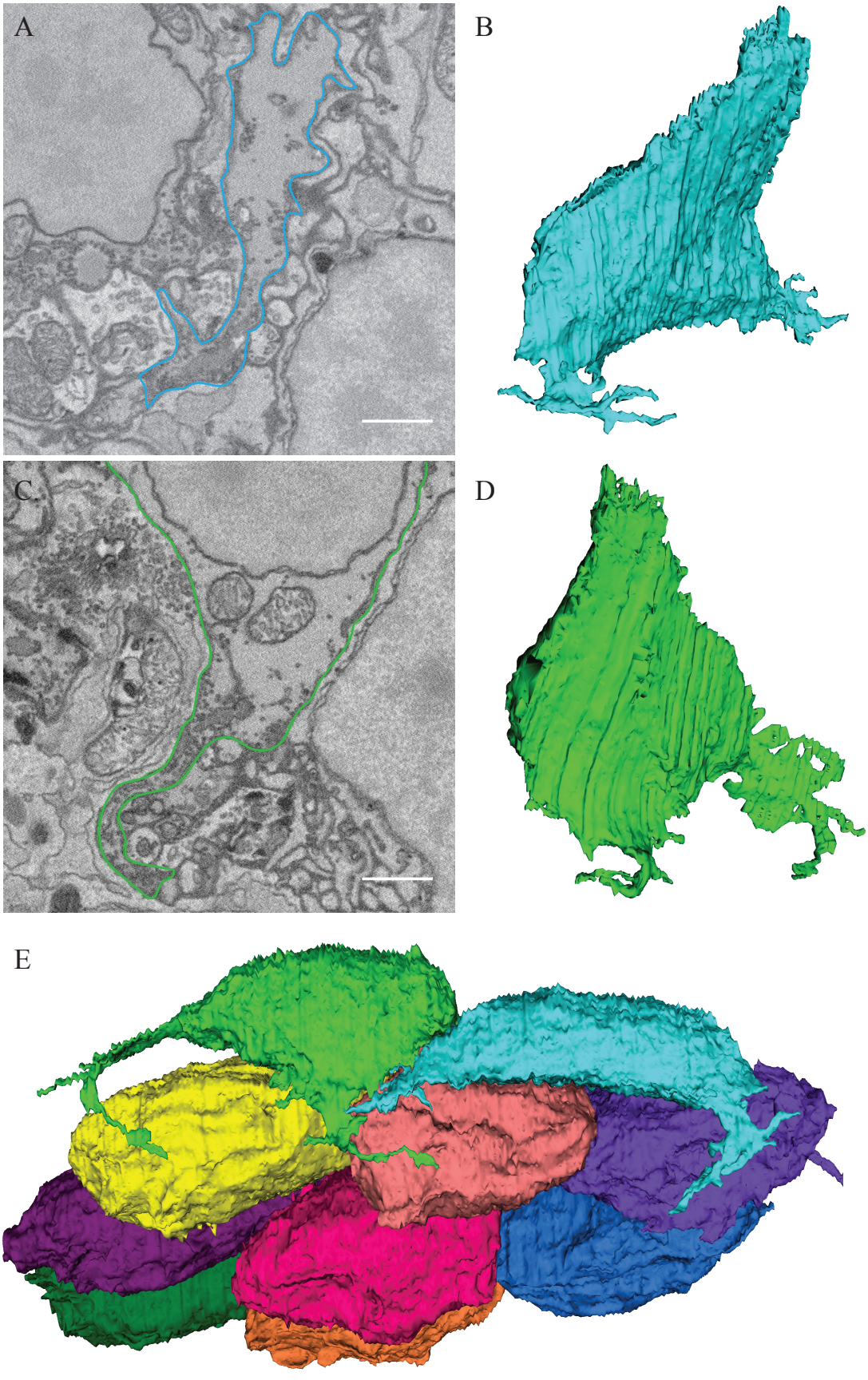
A
B
C
D
E

Figure 4-3

Hair-cell projections extend beneath mature hair-cell synapses and make abundant contact with neurons

A. After analysis by serial block-face electron microscopy, direct contact between hair-cell projections and cell membranes was measured for afferent neurons, efferent neuron, mature hair cells, and sibling immature hair cells. B-C. Apical-to-basal views of immature hair cells show their projections (blue at left; green at right) insinuating into aggregations of afferent neurons (variously colored and partially translucent). Aggregations of neurons occurred beneath mature hair-cell synapses, indicated by the yellow cylindrical puncta representing mature synaptic ribbons.

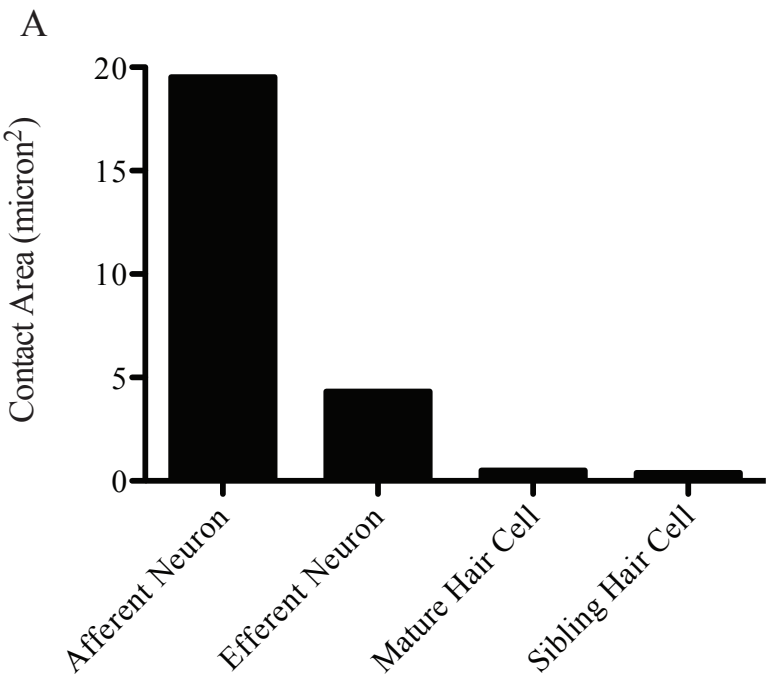
A
20
15
10
5
0
Contact Area (micron^2)
Afferent Neuron
Efferent Neuron
Mature Hair Cell
Sibling Hair Cell
Cell Type in Contact with Projection

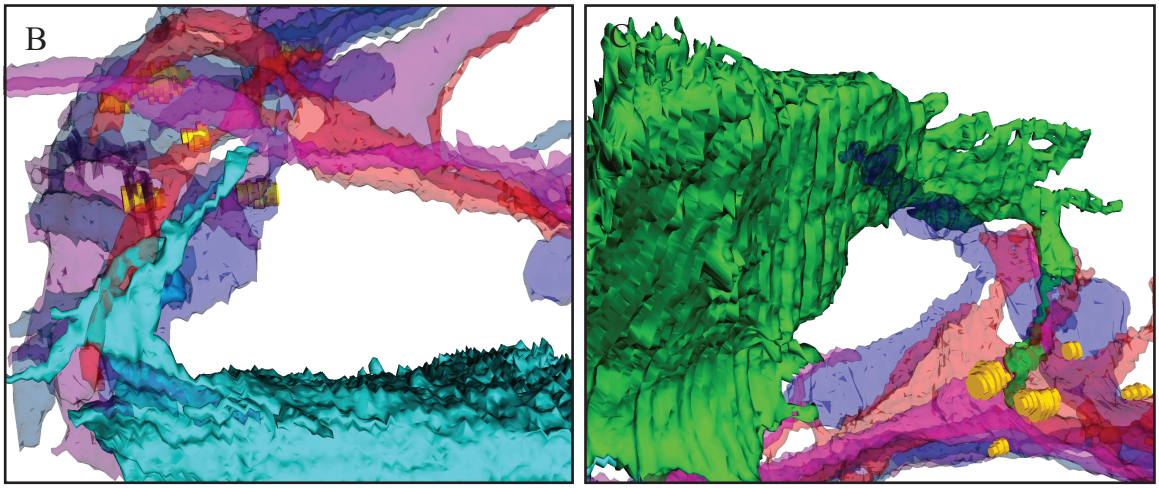
B

Hair-cell projections extend toward and are stabilized by PLL afferent neurons at the hair-cell synapse.

Given the significant contact between hair-cell projections and lateral-line afferent terminal, I focused on the relationship between the two. In order to study the interaction of projections and afferent terminals across time, I used the zebrafish line *Tg(myo6b:actin-GFP;hspGFF4A;UAS:nfsb-mCherry)* in which the fluorescently labeled hair cells are accompanied by mCherry-expressing PLL afferent terminals. Time-lapse confocal microscopy showed that the frequency of contact between projections and afferent neurons was nearly absent during rearrangement before sharply increasing upon appearance of the projections and increasing over time. In agreement with the SBEM reconstruction data, hair-cell projections closely associated with the afferent terminals residing beneath mature hair cells synapses, and in 95% ± 9% of the confocal microscopy time points, the distal portion of the hair-cell projection co-localized with afferent terminals (Fig. 4-4, A-D). Although projections appeared to orient toward large aggregations of afferent neurons, much of the contact along the length of the projection occurred with thin filopodia arising from the afferent terminal arbors. Hair-cell projections originated predominantly from the lateral edge away from the sibling hair cell (Fig. 4-4, E). I never observed any projections extending any from the center of the neuromast.

To better understand the role of afferent neurons in the genesis or stability of hair-cell projections, I performed laser ablation of the posterior lateral-line ganglion, which contains the soma of all afferent neurons innervating PLL neuromasts. Ganglia were ablated at 28 hpf, and within 30 minutes the lateral-line nerve had undergone complete degeneration. Time-lapse confocal imaging of the samples commenced 24 hours after

ablation. In neuromasts lacking PLL afferent neurons, hair-cell projections formed shortly after rearrangement, confirming that afferent terminals are not necessary for the formation of projections (Fig. 4-5, A-D). However, the projections tended to arise from a wider range of locations on the hair cell compared to specimens with intact afferent neurons (Fig. 4-5, E). Additionally these projections often appeared to be thicker, more sheet-like, and more meandering as if lacking orientation to a target (Fig. 4-5, A-D).

I assessed the stability of projections by determining whether between two consecutive time intervals a projection changed position by at least 45 degrees, decreased its length or volume by half, or grossly changed in morphology. Wild-type projections demonstrated stability for significantly longer time intervals than projections from specimens lacking the lateral-line afferents, which moved rapidly and erratically throughout the neuromast (Fig. 4-6, A). In zebrafish possessing lateral-line neurons, I observed several instances in which the distal tip of a hair-cell projection extended along a stable portion of the dendritic arbor, supporting the notion that the afferent dendrite acts as an anchor for projection adhesion (Fig. 4-6, B-C). Altogether, these results suggest that although the lateral-line afferents do not give rise to hair-cell projections, they do contribute to their stability.

Figure 4-4

Hair-cell projections extend toward and are stabilized by PLL afferent neurons at the hair-cell synapse.

A-D. Time-lapse confocal microscopy showing a hair-cell projection (arrowheads) extending to a neighboring aggregation of afferent neurons and interacting with postsynaptic filopodia (magenta). Zebrafish is 3 dpf. Time is given as minutes from the end of rearrangement. A-D are maximum projections through the Z-axis. Scale bars are 5 μm. E. A plot shows the point of origin on the soma from which hair-cell projections extend for all wild-type samples across all time points. Measurements are relative to a ventrally arising, posteriorly polarized hair cell (180 = away from sibling hair cell, 0 = toward sibling hair, 90 = toward the center of the neuromast, 270 = away from the neuromast).

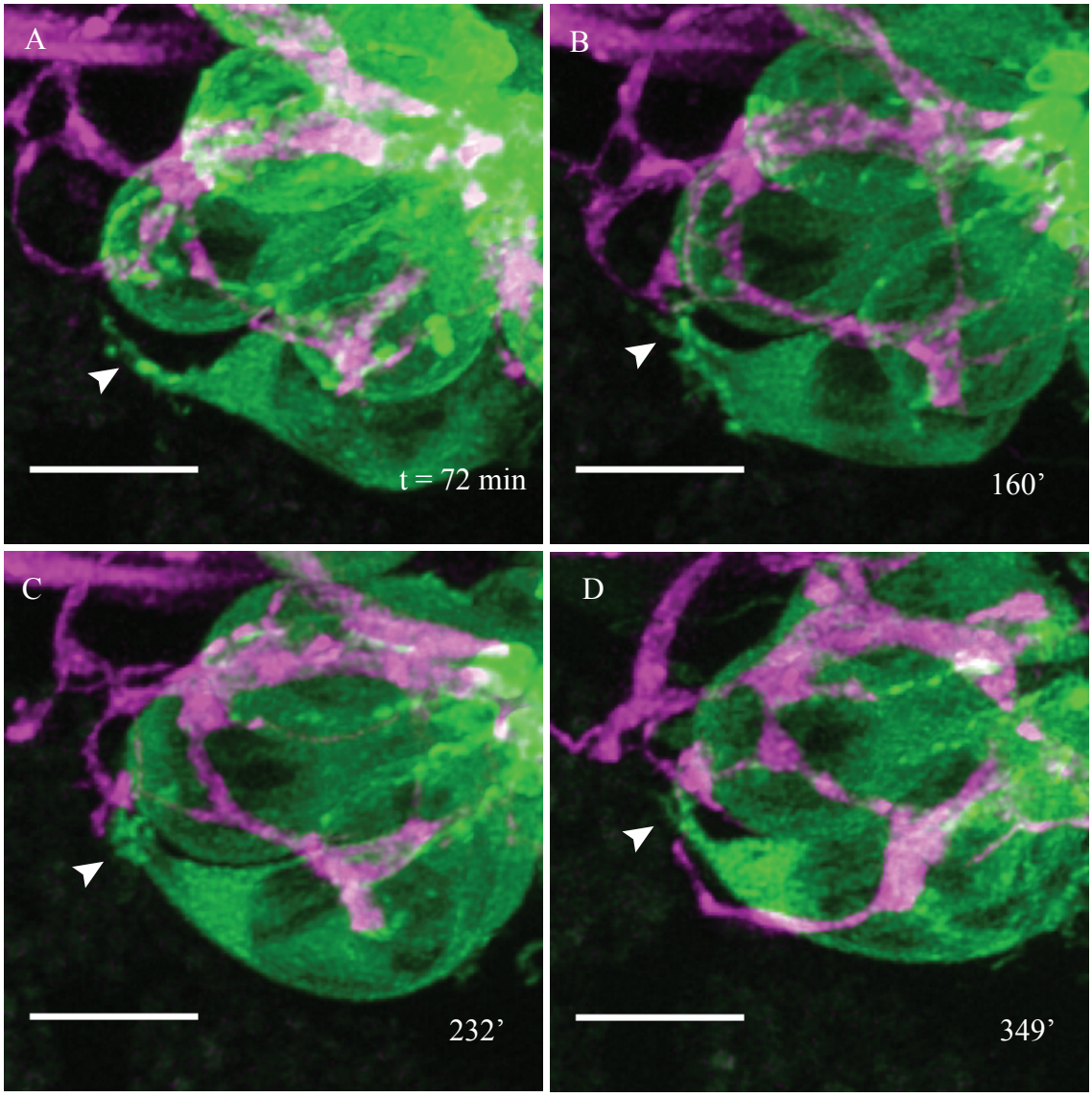
A
t = 72 min
B
160’
C
232’
D
349’

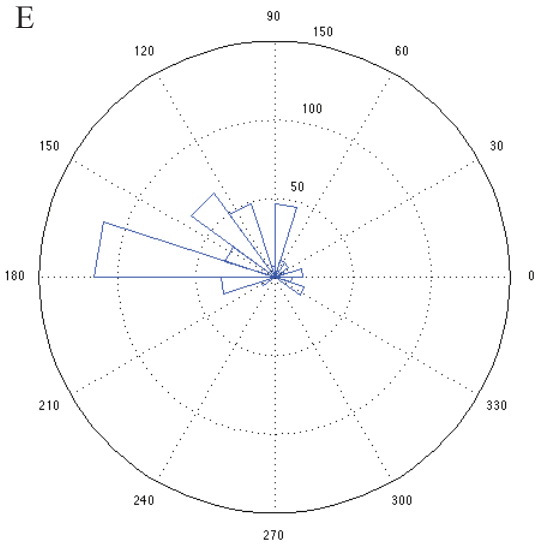
E
90
150
60
120
100
150
30
50
180
0
210
330
240
300
270

Figure 4-5

Specimens lacking afferent neurons form erratic hair-cell projections

A-D. Two immature hair cells in *Tg(myo6b:actin-GFP;hspGFF4a;UAS:nfsb-mCherry)* whose PLL ganglion was ablated at least 24 hours prior to imaging. Both cells show diffuse, erratic projections (arrowheads) that arose less than an hour after hair-cell rearrangement. Images are maximum projections through the Z-axis. Scale bars are 5 μm. Time is given as minutes from the end of hair-cell rearrangement. E. A plot shows the point of origin on the soma from which hair-cell projections extend for all PLL ganglion ablation samples across all time points. Measurements are relative to a ventrally arising, posteriorly polarized hair cell (180 = away from sibling hair cell, 0 = toward sibling hair, 90 = toward the center of the neuromast, 270 = away from the neuromast).

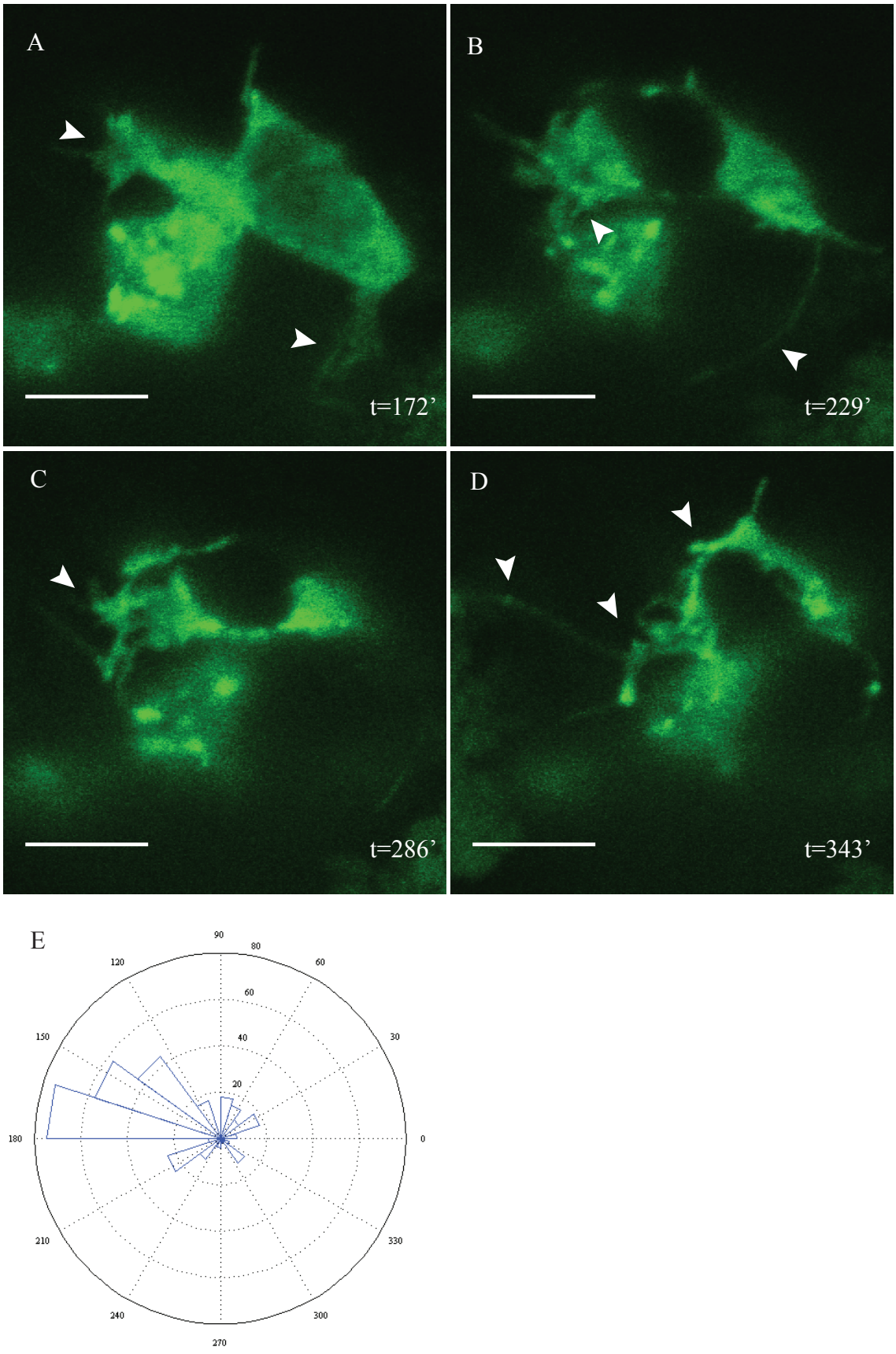
A
t=172’
B
t=229’
C
t=286’
D
t=343’
E
90
80
60
120
60
30
150
40
20
180
0
210
330
240
300
270

Figure 4-6

Specimens lacking afferent neurons form erratic hair-cell projections

A. Hair-cell projections in specimens lacking PLL afferent neurons showed decreased stability, frequently collapsing, extending, and changing orientation. (two-tailed t-test $p<0.009$). B-C. Arrowheads indicate two examples of hair-cell projections in direct contact with and extending along stable portions of the dendritic arbor. In B, the hair-cell projection is green and an afferent nerve is red; in C, the hair-cell projection is blue and the afferent nerve is purple; and in both frames, the ribbon synapses are yellow punctate cylinders.

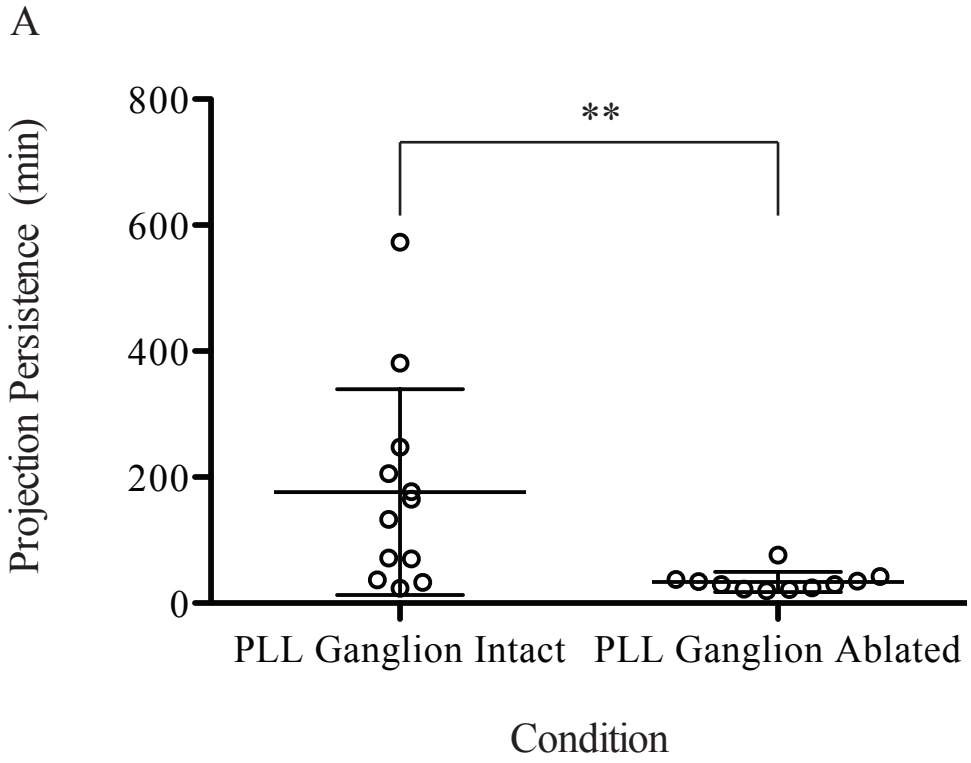
A
800
600
400
200
0
**
Projection Persistence (min)
PLL Ganglion Intact
PLL Ganglion Ablated
Condition

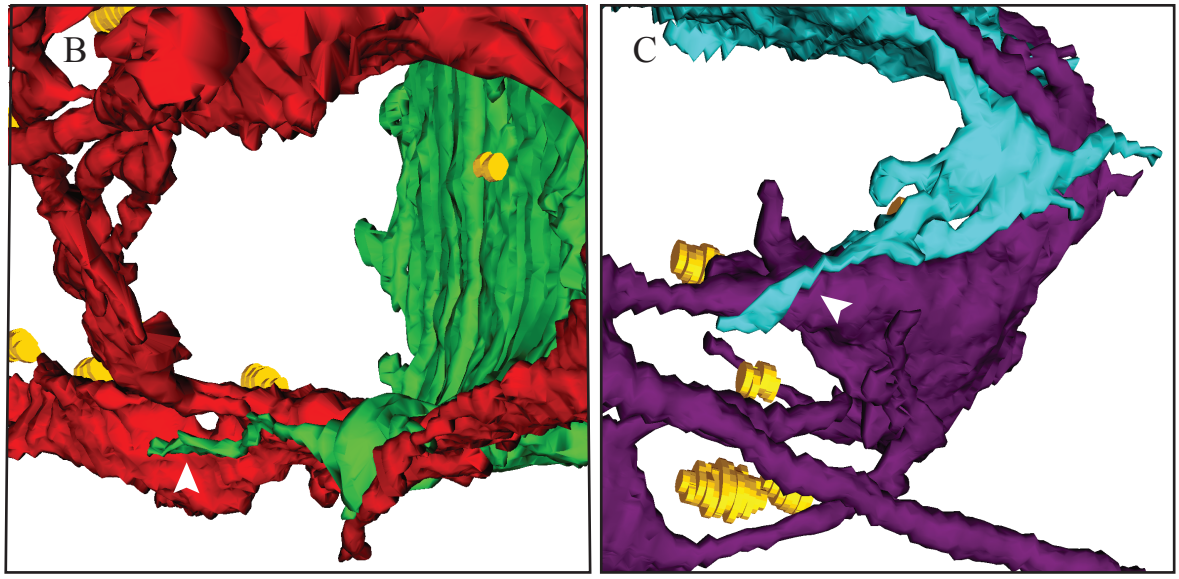
B
C

Hair-cell projections act as scaffolds for afferent neurons traveling toward the hair cell soma.

Immature hair cells finish rearrangement with no stable innervation, but by 14 hr after mitosis afferent neurons are stably associated with the hair-cell base (Fig. 4-7, A-B). I observed in the time-lapse confocal microscopy data that 94% of afferent fibers that reach the immature hair cell do so by traveling across a site of a hair-cell projection. Likewise, in the SBEM reconstruction data, all of the afferent neurons contact the hair-cell soma by traversing one of the four hair-cell projections (Fig. 4-7, C).

In the time-lapse confocal-microscopy data, I frequently observed dynamic filopodia arising from afferent terminals and extending the length of a hair-cell projection toward its soma before rapidly retracting (Fig. 4-7, D-F). The SBEM data showed similar examples in which thin afferent filopodia arising from stable portions of the neuronal arbor traversed the hair-cell projection (Fig. 4-8, A-B). Each projection was in contact with multiple neuronal terminals, and the terminals were often in direct longitudinal contact with one another. These observations suggest that the hair-cell projection may act as a cytoplasmic scaffold for afferent terminals to accelerate their search for and extension toward the immature hair cell.

It is possible that hair-cell projections serve as a target and means of guidance for filopodia that arise from neuronal terminals independent of hair-cell projections. Alternatively, hair-cell projections could, in fact, induce the formation of afferent filopodia. The former possibility is supported by the observation that postsynaptic filopodia exist throughout the neuromast, not only at the locations near hair-cell projections. However, I also observed several examples in which a hair-cell projection contacted a portion of the afferent terminal arbor that lacked filopodia only for a

filopodium to appear immediately afterward (Fig. 4-8, C-H). Similarly, in the SBEM reconstruction, I observed an budding afferent terminal filopodium at the location where a hair-cell projection had contacted the terminal arbor (Fig. 4-8, I).

Figure 4-7

Hair-cell projections act as scaffolds for afferents neurons traveling toward the hair-cell soma

A-B. Two examples of pairs of rearranging hair cells that lack contact with afferent neurons. C. A reconstructed immature hair cell in light blue viewed from apex to base. Five variously colored neurons extend across the projections at either end of the hair cell. D-F. A postsynaptic filopodia crosses and then extends along a hair-cell projection. Hair cells in green, afferent neurons in magenta. Time is given as minutes from the end of hair-cell rearrangement. All scale bars are 5 μm.

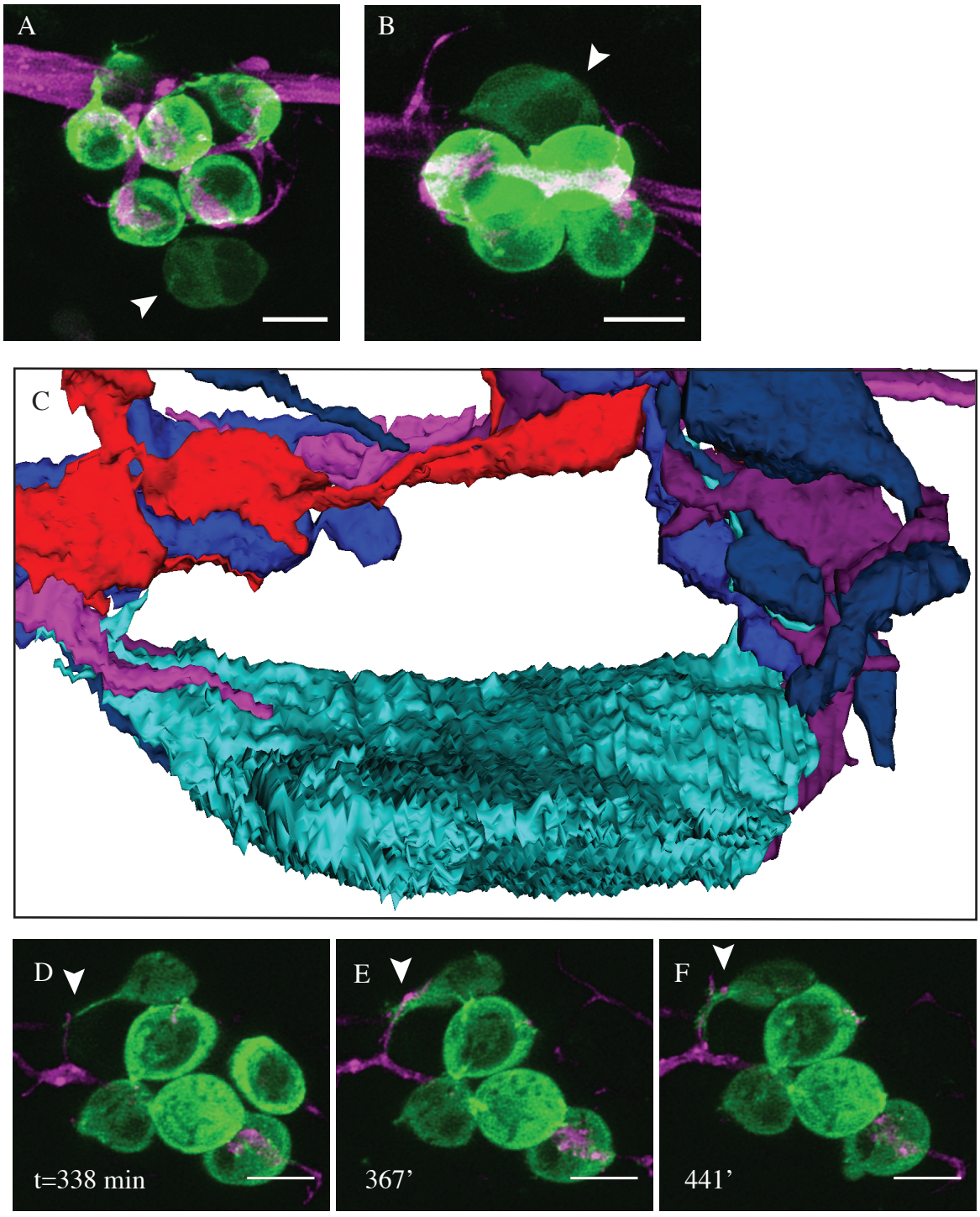
A
B
C
D
t=338 min
E
367’
F
441’

Figure 4-8

Hair-cell projections may induce the extension of dynamic offshoots from afferent terminals

A-B. Afferent neurons make direct contact with and fasciculate along hair-cell projections (arrowheads). C-H. A hair-cell projection contacts a portion of the axonal terminal arbor lacking any postsynaptic filopodia (C-D); and thereafter a filopodium forms (E-F) that extends along the projection (G-H). Hair cells in green, afferent neurons in magenta. Time is given as minutes from the end of hair-cell rearrangement. Scale bars are 5 μm. I. A hair-cell projection (green) contacts a stretch of afferent neuron (purple) containing no postsynaptic filopodia except a nascent one at the point of contact (arrowhead).

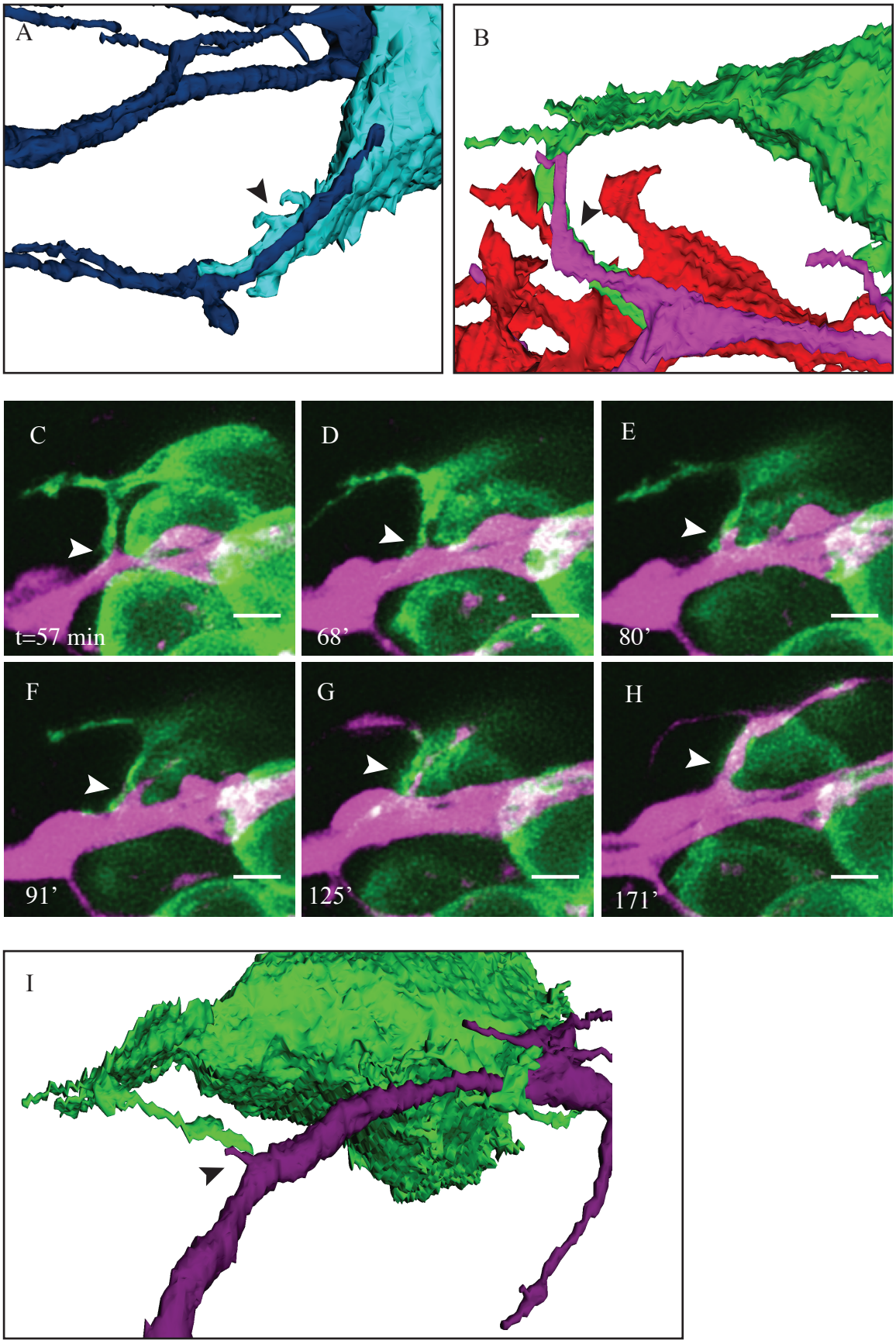
A
B
C
t=57 min
D
68’
E
80’
F
91’
G
125’
H
171’
I

Hair-cell projections preferentially contact afferent neurons of the same functional polarity.

Afferent terminals of the posterior lateral line are biased to innervate a single polarity of hair cell (Faucherre et al., 2009; Nagiel et al., 2008). I identified two neurons in the SBEM data that together juxtaposed synaptic ribbons of all of the anteriorly polarized hair cells, and two other neurons that together juxtaposed synaptic ribbons of all of the posteriorly polarized hair cells. Interestingly, hair-cell projections from the immature posteriorly polarized hair cell made direct contact preferentially with the two afferent terminal arbors innervating ribbon synapses of the mature posteriorly polarized hair cells (Fig. 4-9, A-B). Similarly, projections from the immature anteriorly polarized cell made preferential contact with the two afferent terminal arbors innervating ribbon synapses of the mature anteriorly polarized hair cells (Fig. 4-9, C-D). This bias did not appear to be due to access to the projection, since terminals of both subpopulations were within the vicinity of the projection (Fig. 4-10, A). In fact, terminals of the opposing subpopulation extended in parallel with the projection and its polarity-appropriate afferent fibers and made occasional direct contact with it. But neurons of the polarity-appropriate afferent subpopulation were larger and appeared to displace the polarity-inappropriate terminals from direct contact with the projection (Fig. 4-10, B). Further confirming this, two projections, one from an anteriorly polarized cell and one from a posteriorly polarized cell, extended into the same aggregation of neuronal terminals but nevertheless showed a significant bias toward contact with their polarity-appropriate afferent terminals. Hair-cell projections also showed specialized morphology such as cupping around the polarity-appropriate terminals that they did not display for the opposing afferent subpopulation.

Hair-cell projections tended to extend preferentially to the area beneath hair cells of their same polarity (Fig. 4-11, A). The behavior was not simply due to proximity because hair-cell synapses of either polarity were often equally close to the nascent hair cell. Moreover, I noticed examples in which projections avoided neighboring hair cells of the opposite polarity in favor of more distant hair cells of the same polarity. The observation could be accounted for by projections having greater adhesion or attraction to polarity-appropriate terminals, which tend to be in greater abundance beneath hair cells of the same functional polarity.

Another interesting difference between hair-cell polarities was the observation that in the time-lapse confocal data projections from posteriorly polarized hair cells were, on average, more than twice as large as those from anteriorly polarized hair cells (Fig. 4-11, B). Likewise, the average volume of the posteriorly polarized hair-cell projections in the SBEM data was larger than that of the two anteriorly polarized projections. This difference may arise due to differences in the polarity-appropriate afferent subpopulations for each hair-cell polarity. Specimens lacking lateral line afferent neurons showed a similar, albeit not statistically significant, trend toward larger posteriorly polarized projections, suggesting that the size difference may be intrinsic to the hair-cell subpopulations.

Figure 4-9

Hair-cell projections preferentially contact a biased subpopulation of neurons that innervate ribbon synapses of the same hair-cell polarity

A-B. Contact area between each of the two anteriorly polarized hair-cell projections and each neuron or hair cell. C-D. Contact area between each of the two posteriorly polarized hair-cell projections and each neuron or hair cell. Afferents A1 and A2 innervate only ribbon synapses in mature anteriorly polarized cells. Afferents P1 and P2 innervate ribbon synapses in posteriorly polarized cells.

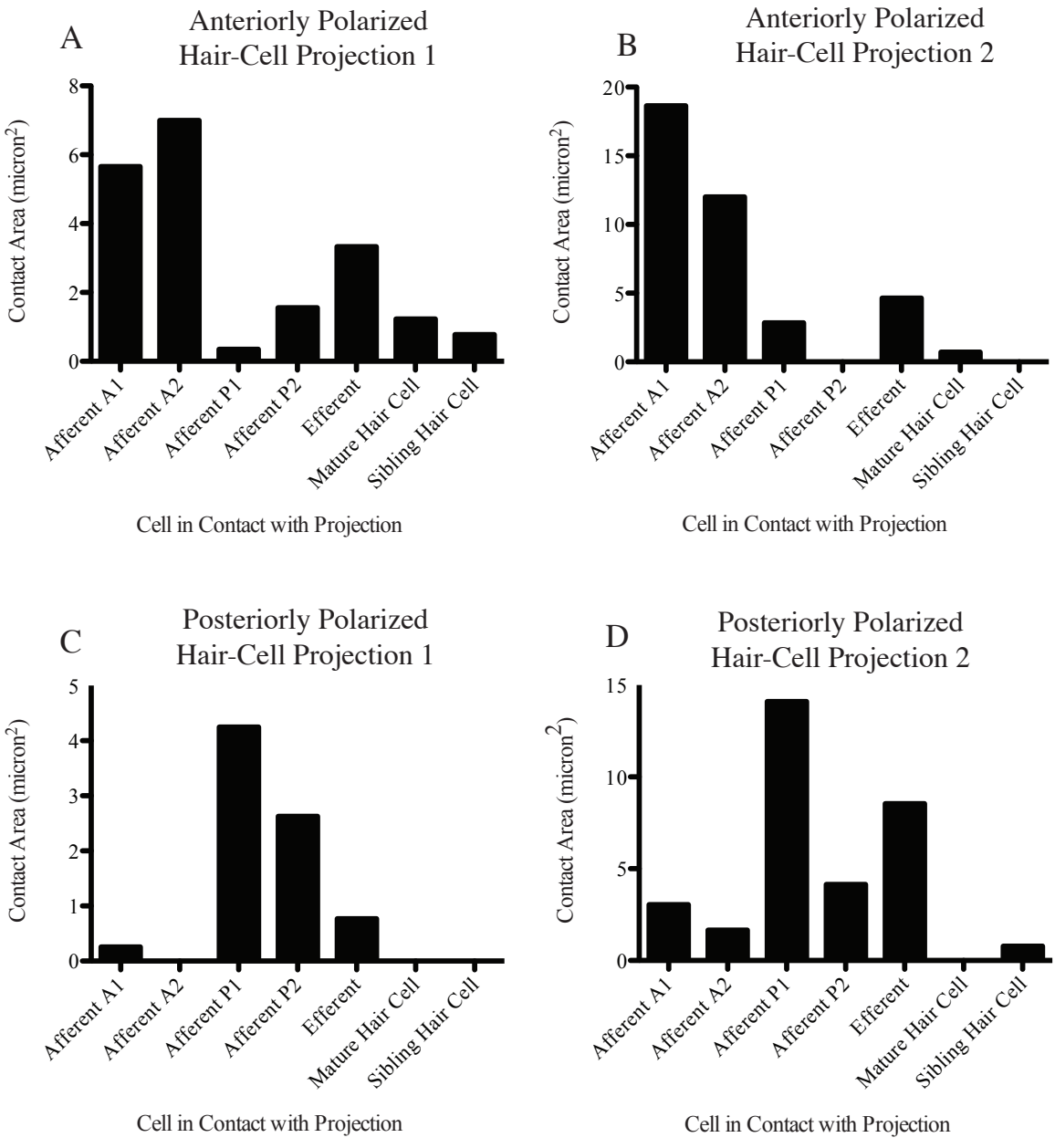
A
Anteriorly Polarized
Hair-Cell Projection 1
Contact Area (micron2)
0
2
4
6
8
Afferent A1
Afferent A2
Afferent P1
Afferent P2
Efferent
Mature Hair Cell
Sibling Hair Cell
Cell in Contact with Projection
B
Anteriorly Polarized
Hair-Cell Projection 2
Contact Area (micron2)
0
5
10
15
20
Afferent A1
Afferent A2
Afferent P1
Afferent P2
Efferent
Mature Hair Cell
Sibling Hair Cell
Cell in Contact with Projection
C
Posteriorly Polarized
Hair-Cell Projection 1
Contact Area (micron2)
0
1
2
3
4
5
Afferent A1
Afferent A2
Afferent P1
Afferent P2
Efferent
Mature Hair Cell
Sibling Hair Cell
Cell in Contact with Projection
D
Posteriorly Polarized
Hair-Cell Projection 2
Contact Area (micron2)
0
5
10
15
Afferent A1
Afferent A2
Afferent P1
Afferent P2
Efferent
Mature Hair Cell
Sibling Hair Cell
Cell in Contact with Projection

Figure 4-10

Afferent neurons of both subpopulations are in proximity to hair-cell projections but are often displaced from direct contact by polarity-appropriate neurons

A. The projection from an immature anteriorly polarized hair cell (light blue) is associating with afferents that innervate mature anteriorly polarized hair cells (dark blue and maroon), mature posteriorly polarized hair cells (red and pink), and an efferent neuron (blue). B. The projections from anteriorly (AP) and posteriorly polarized (PP) hair-cells insinuate among nerve fibers of both subpopulations (A1 and A2 innervate mature anteriorly polarized hair cells; P1 and P2 innervate mature posteriorly polarized hair cells; E is an efferent nerve) but nevertheless make direct contact predominantly with afferent neurons of the polarity-appropriate subpopulation.

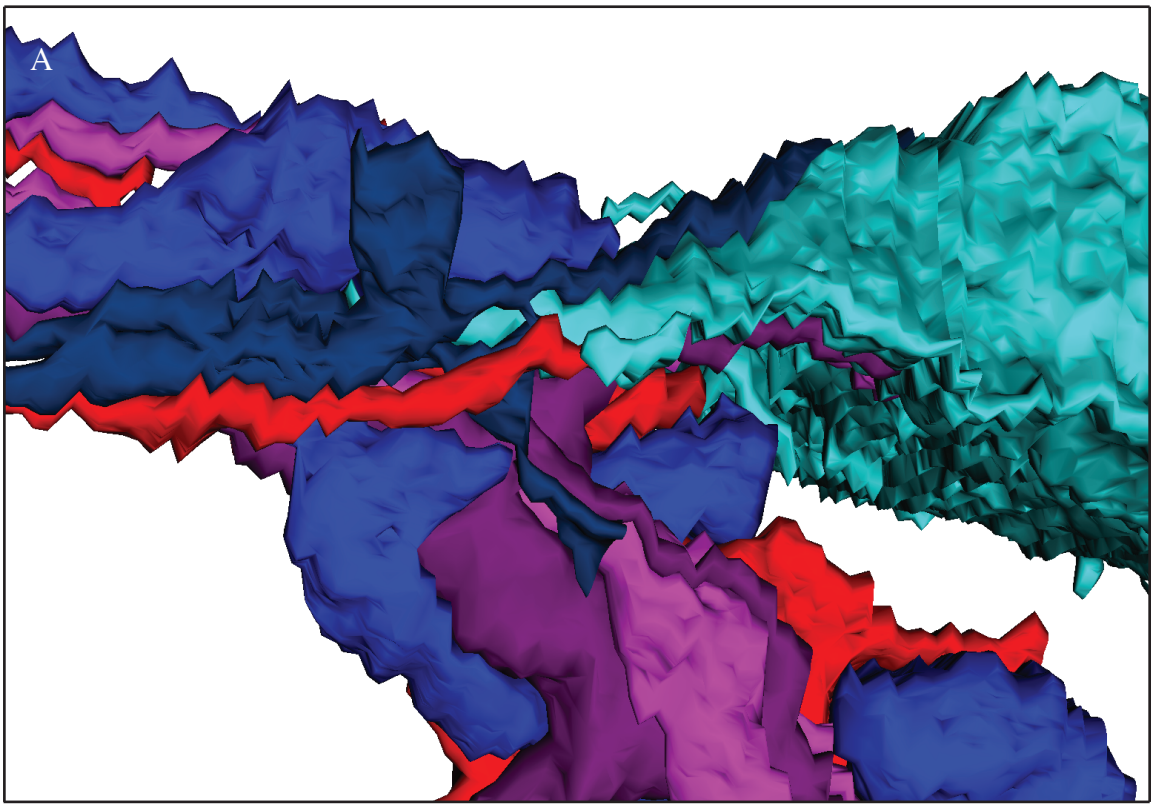
A

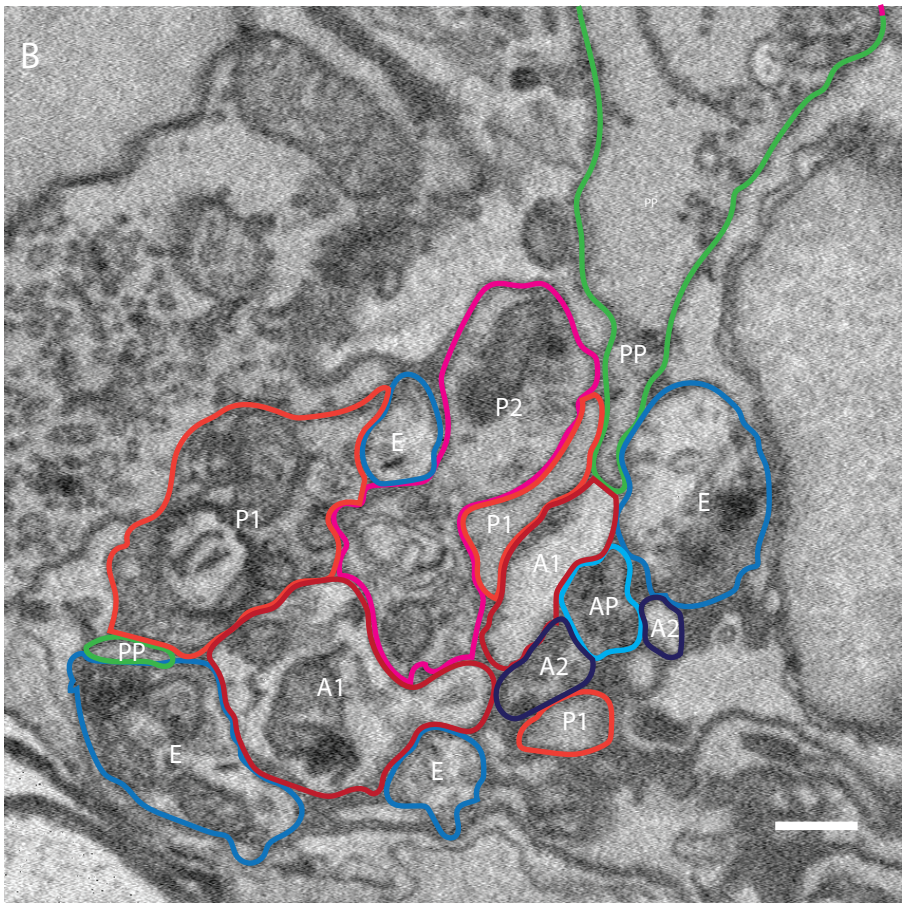
B
PP
P2
E
P1
P1
A1
AP
A2
PP
A2
A1
P1
E
E
E

Figure 4-11

Polarity-specific differences in hair-cell projections

A. Time-lapse confocal microscopy indicated the proportion of time projections spent with their tips colocalized at mature anteriorly polarized hair cells, mature posteriorly polarized hair cells, sibling hair cells, or non-hair-cell targets (most likely supporting cells, which were not fluorescently labeled in the preparation). Afferent neurons were not included in the analysis. Neuromasts were imaged every 20 minutes for six to eight hours. Zebrafish were 2-4 dpf. Anteriorly polarized hair-cell projections targeting A>P, $p<0.0002$. Posteriorly polarized hair-cell projections targeting P>A, $p<0.0001$). B. Hair-cell projection volume was quantified in the same time-lapse confocal microscopy data as well as in time-lapse microscopy data from PLL ganglion-ablated specimens. Projections were divided by hair-cell polarity and whether or not the specimen contained afferent neurons. Posteriorly polarized hair-cell projections are on average larger than anteriorly polarized hair-cell projections ($p<0.04$).

A

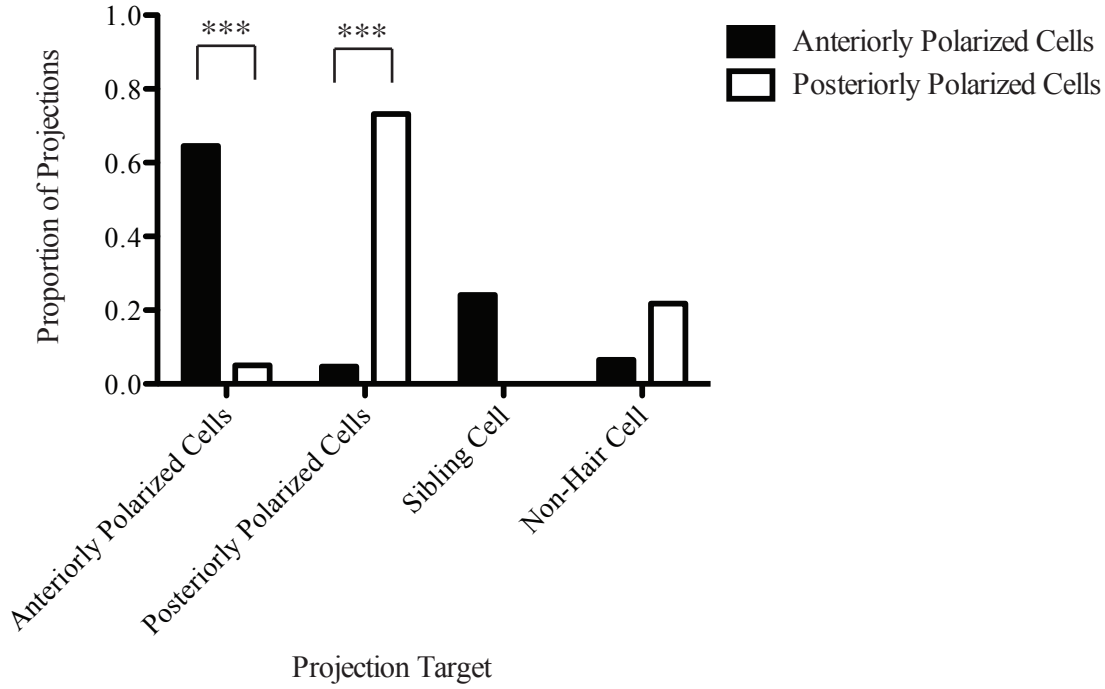
1.0
0.8
0.6
0.4
0.2
0.0
Proportion of Projections
***
***
Anteriorly Polarized Cells
Posteriorly Polarized Cells
Anteriorly Polarized Cells
Posteriorly Polarized Cells
Sibling Cell
Non-Hair Cell
Projection Target

B

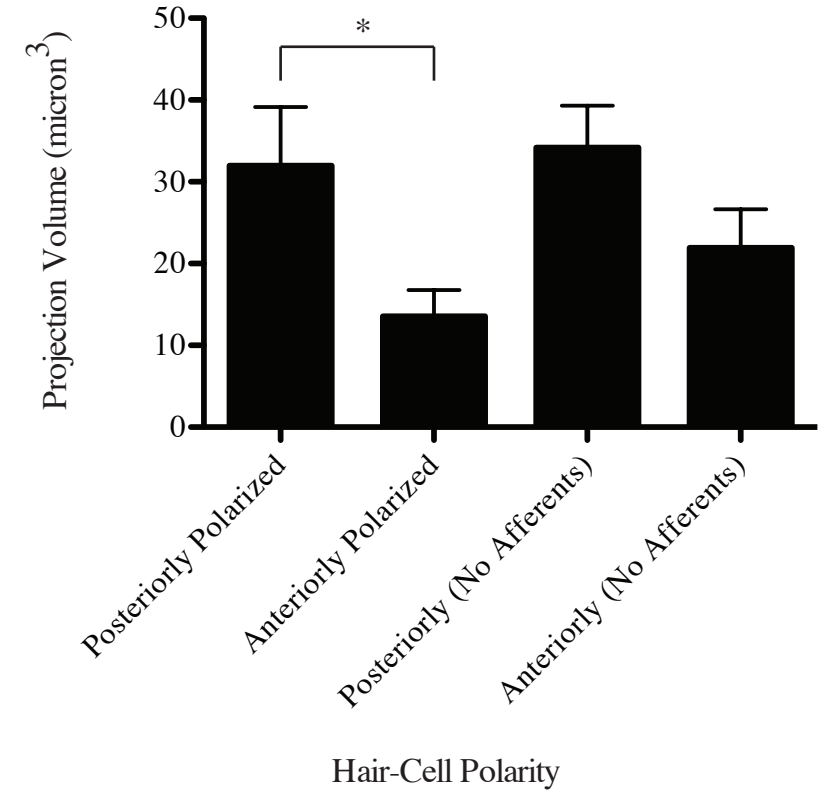
50
40
30
20
10
0
Projection Volume (micron3)
*
Posteriorly Polarized
Anteriorly Polarized
Posteriorly (No Afferents)
Anteriorly (No Afferents)
Hair-Cell Polarity

The stable association of an afferent terminal with the hair-cell base causes projections to diminish.

Early in the period of hair-cell projection, the afferent filopodia tended to transiently contact the projection often retracting in less than 30 minutes; later in hair-cell differentiation larger afferent terminals migrated toward the soma. Afferent terminals eventually stabilized at the base of the hair cell. I observed that a projection tended to be smaller when an afferent neuron was stably associated near its base, whereas the largest projections almost invariably lacked stable afferent innervation (Fig. 4-12, A-F, J).

Furthermore, projections in specimens whose posterior lateral-line ganglion was ablated by a focused laser beam, thus eliminating hair-cell innervation, tended to be larger than projections in specimens possessing lateral-line neurons (Fig. 4-12, J). In fact, nascent hair cells in specimens lacking afferent terminals sometimes became extremely elongated with much of the cell's cytoplasm allotted to the projection (Fig. 4-12, G-I). Finally, neuromasts in *Tg(myo6b:actin-GFP;hspGFF4a;UAS:nfsb-mCherry)* zebrafish with intact PLL ganglia as well as zebrafish whose PLL ganglia had been ablated by a focused laser beam were recorded with spinning-disc time-lapse confocal microscopy for 24 hours. Hair cells extended projections for a greater duration in specimens lacking PLL ganglia compared to those with intact lateral-line afferent neurons (Fig. 4-12, K).

Figure 4-12

Hair-cell projections diminish in size when their bases are stably associated with an afferent nerve fiber

A-F. Time-lapse confocal microscopy reveals the diminution of a hair-cell projection (arrowhead) as an afferent nerve (magenta) becomes stably associated with the soma. A second hair-cell projection in the image series (E, asterisk) is not stably innervated at the base and remains large. G-H. Time-lapse confocal microscopy of a specimen lacking PLL afferent neurons. J. Projection volume was plotted for every frame of time-lapse confocal imaging data. Projections were significantly larger in the absence of stable afferent association with the projection base ($p<0.0007$). K. Spinning-disc time-lapse confocal microscopy was conducted for 24 hours in zebrafish with PLL ganglia ablated or zebrafish with intact ganglia. The duration of projections was longer in those lacking PLL ganglia ($p<0.008$). Zebrafish in all experiments were 2-4 dpf. Time is given as minutes from the end of hair-cell rearrangement. Scale bars are 5 μm.

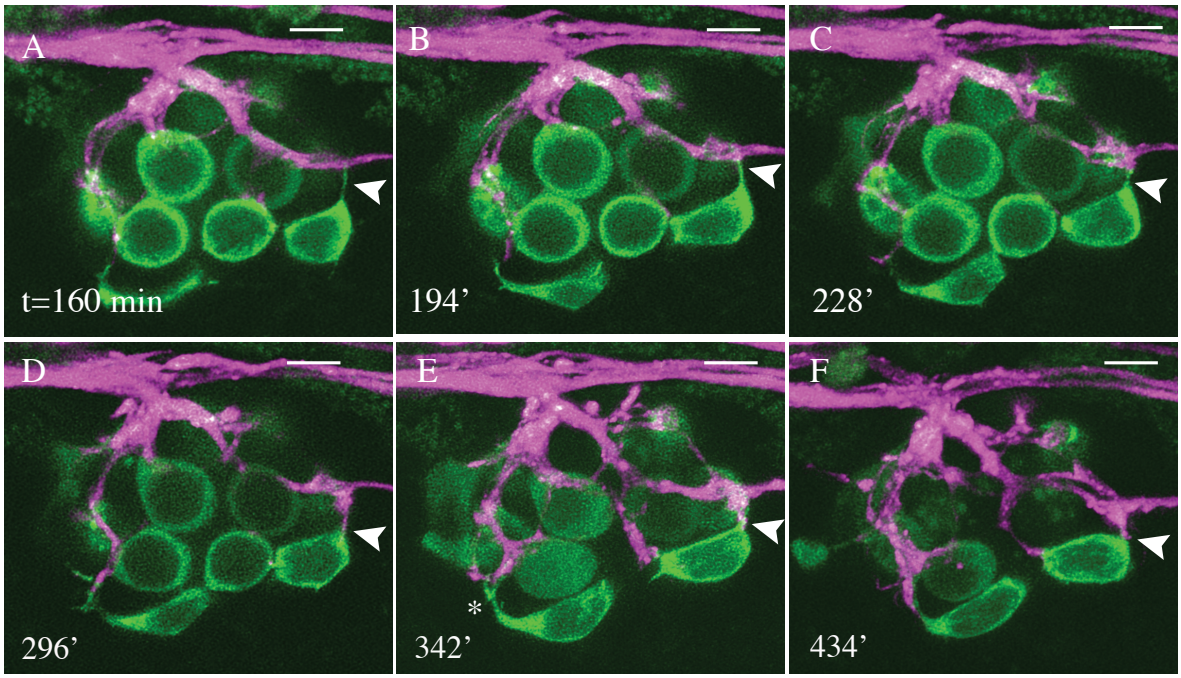
A
t=160 min
B
194’
C
228’
D
296’
E
342’
*
F
434’

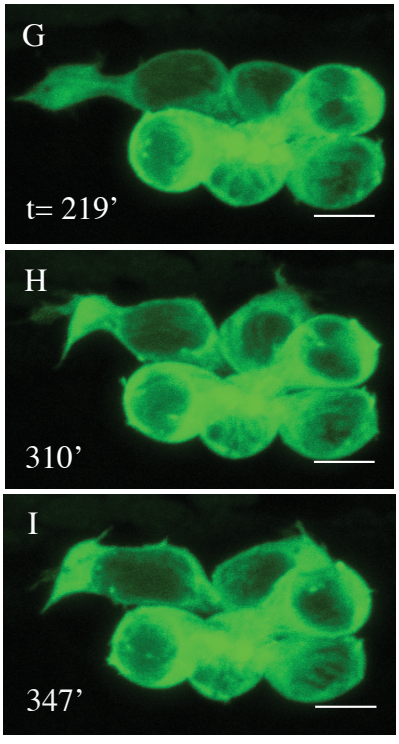
G
t= 219’
H
310’
I
347’

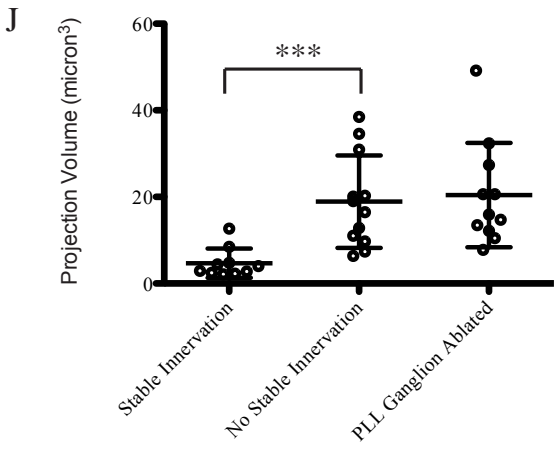
J
Projection Volume (micron3)
60
40
20
0
***
Stable Innervation
No Stable Innervation
PLL Ganglion Ablated

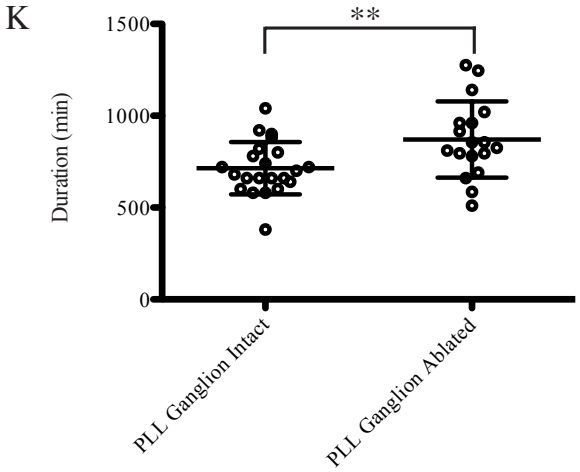
K
Duration (min)
1500
1000
500
0
**
PLL Ganglion Intact
PLL Ganglion Ablated

Presynaptic components reside near and within projections.

I investigated the ultrastructure of hair-cell projections imaged by SBEM. All of the projections contained immature ribbons at or near their sites of origin on the hair-cell somata (Fig. 4-13, E). The immature ribbons shared the same structure and labeling pattern as mature ribbon synapses but were one-third to half the diameter. Ribbons within cells in either stage of development were surrounded by synaptic vesicles. Additionally, clouds of vesicles similar to those surrounding the immature ribbons were abundant throughout the projections but were nearly absent elsewhere in the hair cell (Fig. 4-13, A-D).

I checked for the presence of the ribbon synapse protein ribeye in hair cells using the transgenic zebrafish line *Tg(pvalb3:ribeye-mCherry; myo6b:actin-GFP)* (Uthaiah and Hudspeth, 2010). In this transgenic line, the parvalbumin 3 promoter, expressed early in hair-cell development, drives the expression of the ribeye protein fused to mCherry (West and McDermott, 2011). Hair cells were judged as rearranging, early in differentiation, late in differentiation, or mature based upon their somatic and hair-bundle morphology (Kindt et al., 2012; Mirković et al., 2012) (see Materials and Methods).

Rearranging hair cells contained no ribeye-positive puncta nor did hair cells early in differentiation (Fig. 4-14, A and C). However, hair cells late in differentiation contained ribeye puncta, although they were less numerous, less densely stained, and smaller than ribeye-positive puncta in mature hair cells (Fig. 4-14, B-E). I also performed antibody labeling against the protein MAGUK, a post-synaptic density component of the glutamatergic hair-cell synapse (Sheets et al., 2012; Sheets et al., 2011). Similar to the staining pattern observed for ribeye, I did not observed MAGUK puncta in hair cells that

were rearranging or early in differentiation but did observed labeled puncta in hair cells late in differentiation (Fig. 4-15, A-C). Also, the puncta within hair cells late in differentiation were fewer in number, less densely labeled, and smaller in diameter than MAGUK puncta within mature hair cells (Fig. 4-15, C-E). Altogether these results indicate that ribbon synapses and synaptic vesicles are localized to the bases of hair-cell projections. Furthermore, the maturation of the hair-cell synapse is contemporaneous with the presence of hair-cell projections from early to late stages of hair-cell differentiation.

Figure 4-13

Hair-cell projections contain presynaptic components

A-B. SBEM image data shows that hair cell projections (outlined in green and blue) contained immature ribbon synapses and putative synaptic vesicles. Scale bars are 200 nm. C-D. Neither of these presynaptic components is present elsewhere in the immature hair cells. All scale bars are 500 nm. E. Reconstruction of the immature hair cells from SBEM data shows the sequestration of immature synaptic ribbons (red puncta) at the base of hair-cell projections.

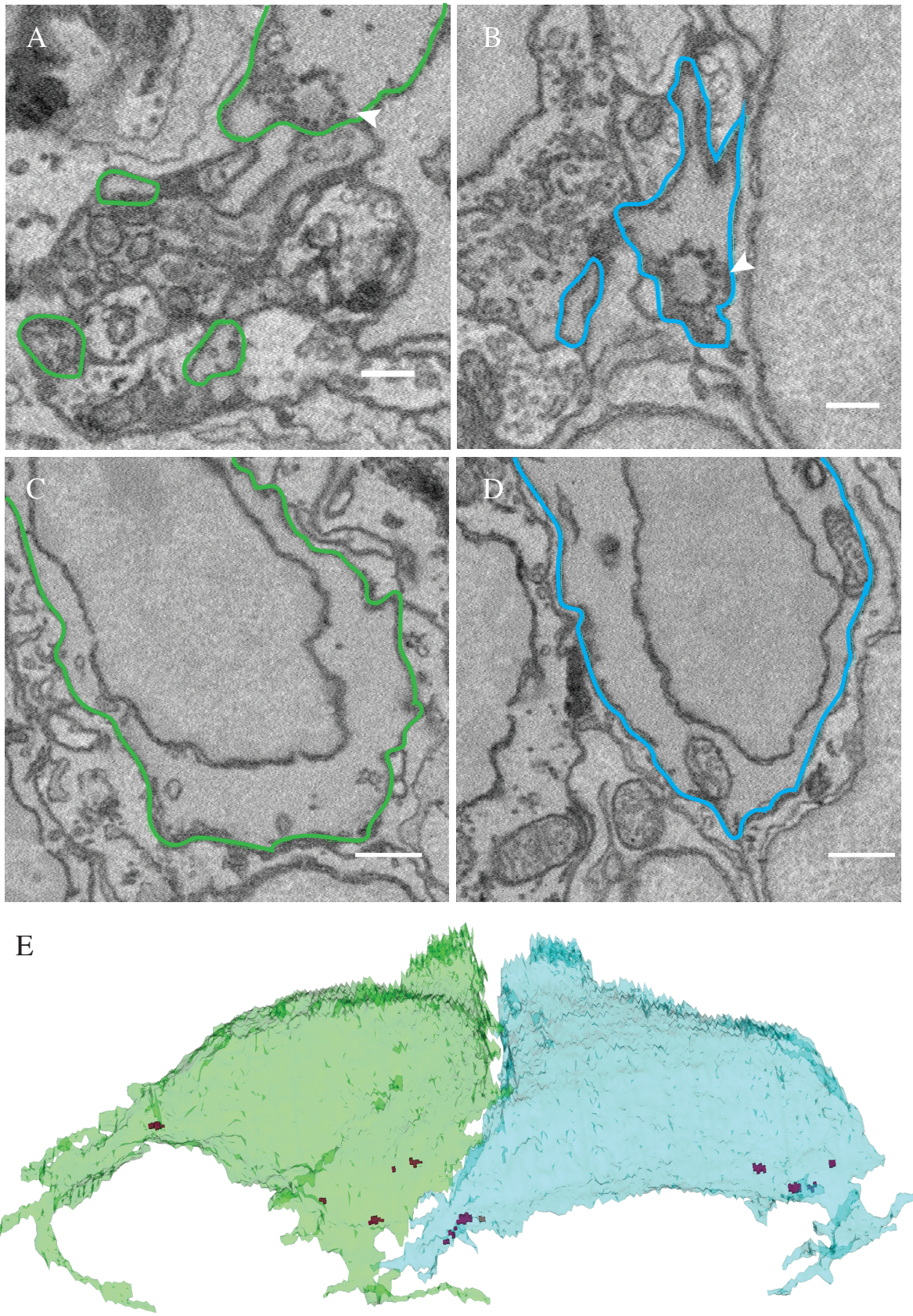
A
B
C
D
E

Figure 4-14

The presynaptic protein ribeye is present in late differentiating hair cells but not early differentiating or rearranging hair cells

A. A representative neuromast from a *Tg(pvalb8:Ribeye-mCherry;myo6b:actin-GFP)* zebrafish. Ribeye puncta (magenta) are present in mature hair cells (green) but not the projecting hair cell in early differentiation (asterisk). B. An immature punctum (arrowhead) in a late differentiating hair cells that is lacking projections. Both scale bars are 5 μm. C-D. Ribeye puncta were counted and their size and fluorescence intensity were measured in hair cells in four stages of differentiation. $p<0.0001$ for all three graphs.

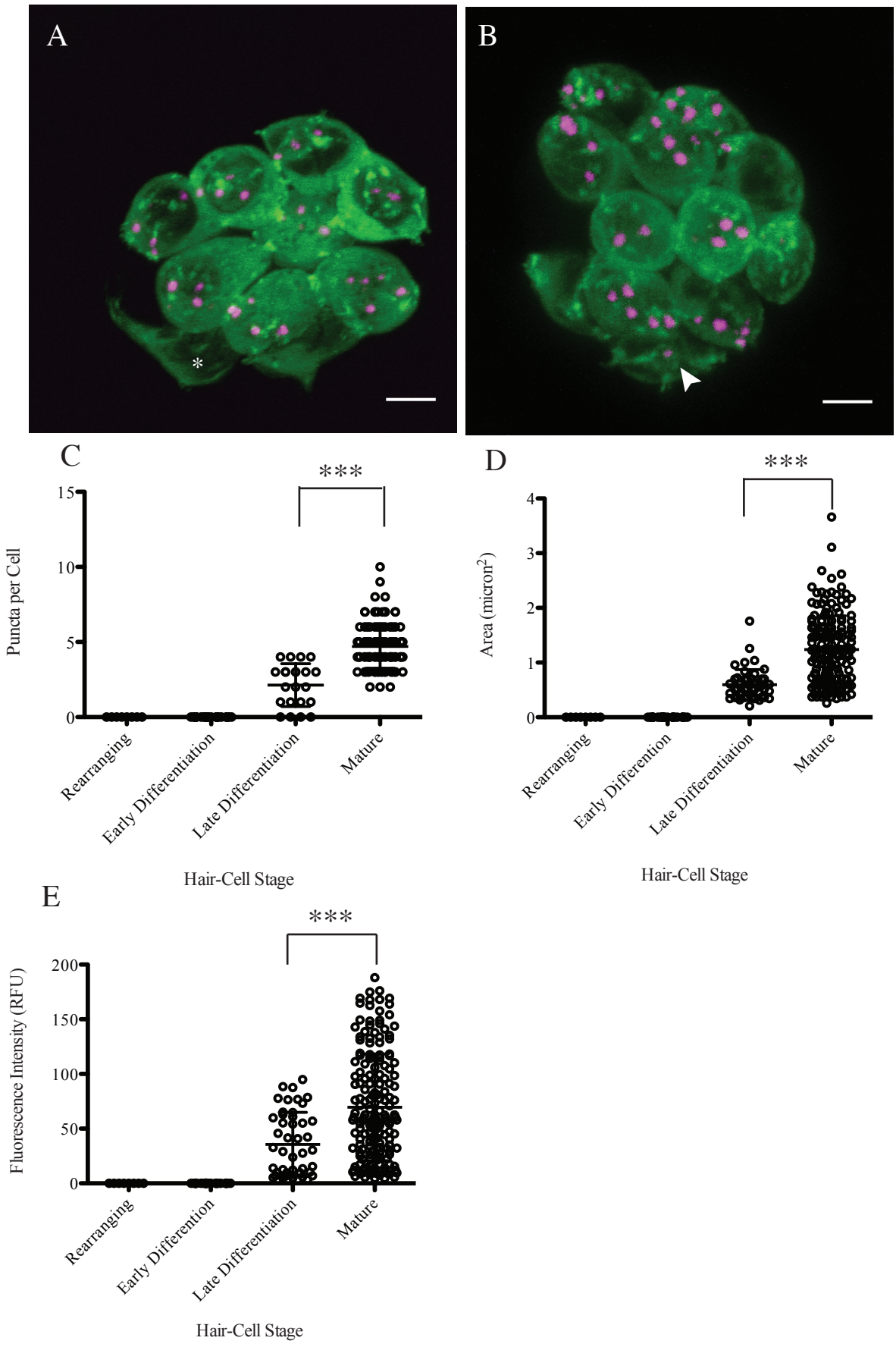
A
B
C
D
E
***
Puncta per Cell
Area (micron²)
Fluorescence Intensity (RFU)
Rearranging
Early Differentiation
Late Differentiation
Mature
Hair-Cell Stage

Figure 4-15

The postsynaptic protein MAGUK is present in late differentiating hair cells but not early differentiating or rearranging hair cells

A. A representative neuromast from a *Tg(myo6b:actin-GFP)* zebrafish labeled with an antibody against MAGUK, a postsynaptic density protein. MAGUK puncta (magenta) are present in mature hair cells (green) but not the projecting hair cell in early differentiation (asterisk). B. An immature puncta (arrowhead) within a late differentiating hair cell that is absent projections. Both scale bars are 5 μm. C-D. MAGUK puncta were counted and their size and fluorescence intensity were measured in hair cells in four stages of differentiation. $P<0.0003$ for graph C, and $P<0.0001$ for D and E.

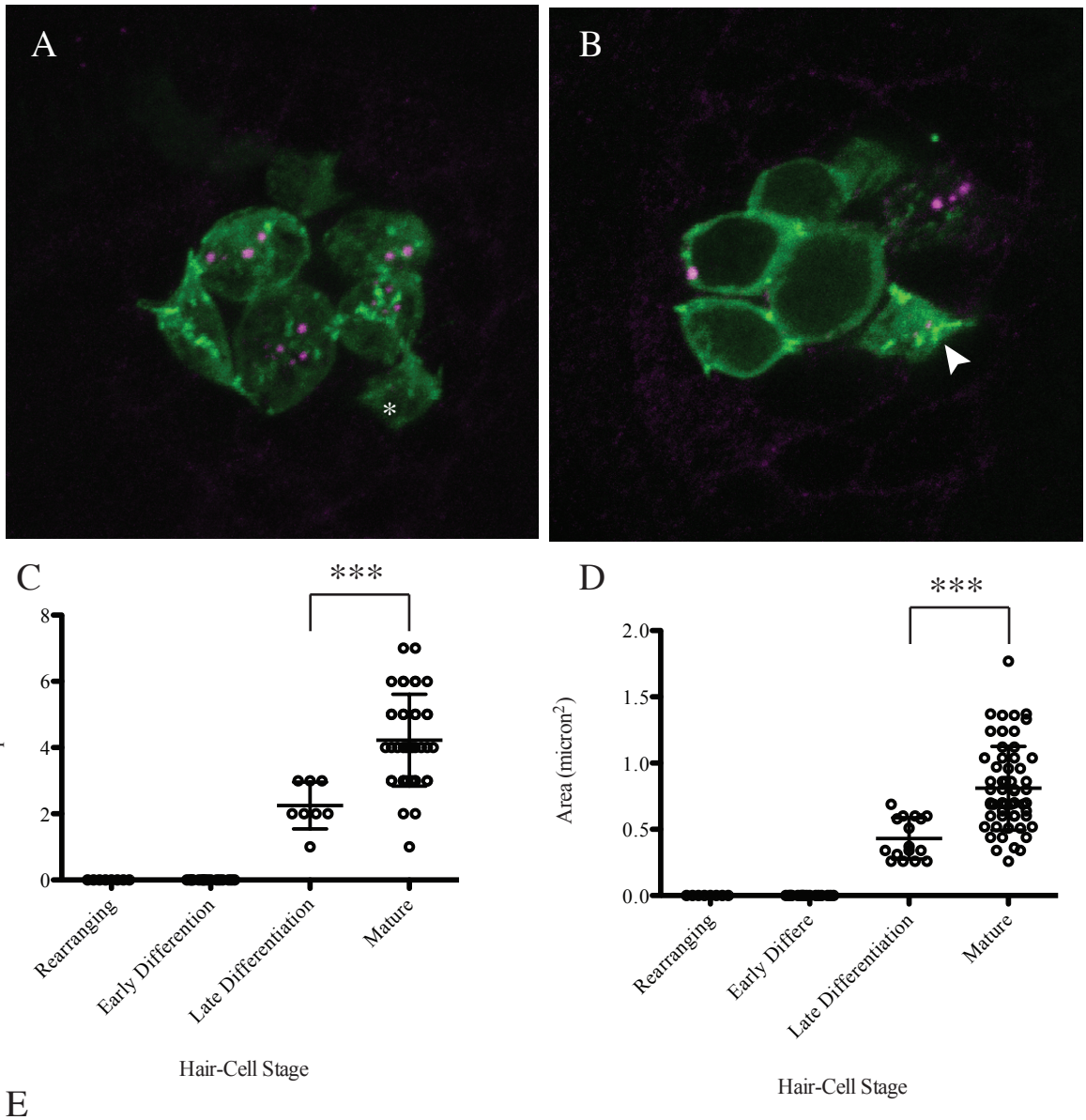
A
B
C
***
Puncta per Cell
8
6
4
2
0
Rearranging
Early Differention
Late Differentiation
Mature
Hair-Cell Stage
D
***
Area (micron^2)
2.0
1.5
1.0
0.5
0.0
Rearranging
Early Differe
Late Differentiation
Mature
Hair-Cell Stage
E
***
Fluorescence Intensity (RFU)
200
150
100
50
0
Rearranging
Early Differentiation
Late Differentiation
Mature
Hair-Cell Stage

Afferent terminals stabilize at the bases of nascent hair cells resulting in the retraction of projections.

I wondered whether afferent terminals might be traversing hair-cell projections in search of the available sites for synaptogenesis that reside at the projection base. I found that more than half of the immature ribbons at the base of the projections were juxtaposed to afferent terminals. Additionally, each terminal associated with a ribbon synapse had extended along a hair-cell projection to reach the ribbon. Moreover, each terminal was of the same functional polarity as the nascent hair cell. At several of the more developed immature ribbons, a flap of hair-cell membrane overlaid the afferent terminal as if to stabilize it (Fig. 4-16, A-B). I also observed a similar morphological feature at several afferent terminals juxtaposed with mature ribbons (Fig. 4-16, C). The portions of the afferent terminals juxtaposed to the immature synaptic ribbons were expanded similar to the morphology observed at mature ribbons synapses (Fig. 4-16, A-B). Finally, I found that the volumes of the four projections in the SBEM data was directly related to the number of uninnervated ribbons, suggesting that innervation of the immature ribbons acts as negative feedback to extension of hair-cell projections (Fig. 4-16, D).

Figure 4-16

Polarity-appropriate afferent neurons juxtapose immature synaptic ribbons at the base of hair-cell projections

A-B. Two reconstruction of hair-cell projections (light blue and green) show immature synaptic ribbons (yellow) at the base of the projections. Ribbon puncta are juxtaposed by polarity-appropriate neurons and are covered over by small cytoplasmic protrusions from the hair cell (arrowheads). C. An afferent neuron (dark blue) beneath a mature hair cell (orange) appears to be held in place at the ribbon synapse by cytoplasmic protrusions. D. The volume of hair-cell projections in SBEM reconstruction increases with the number of synaptic ribbons not juxtaposed by a neuron.

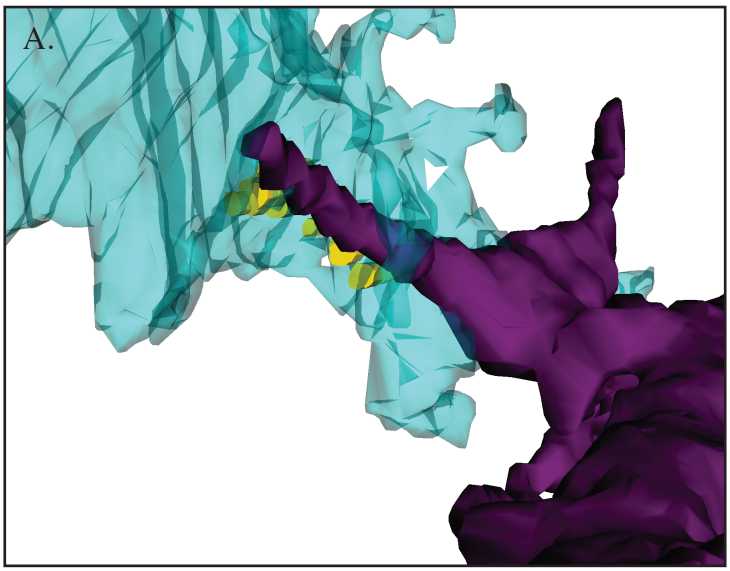

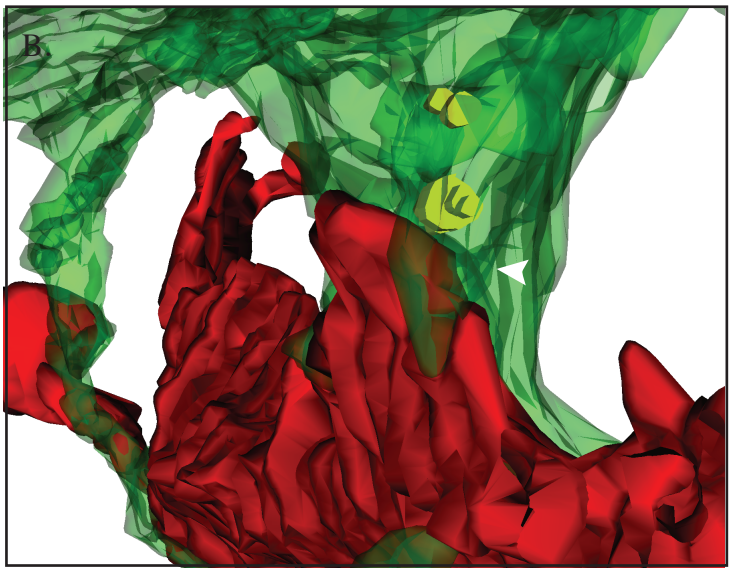

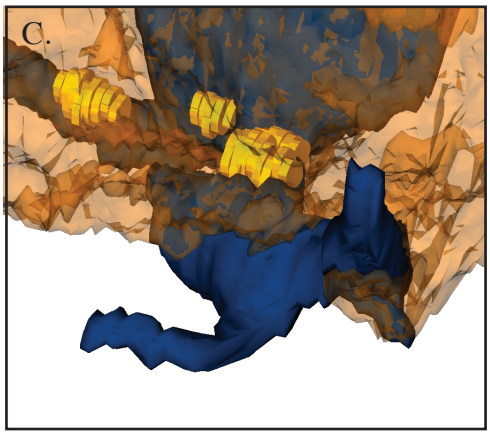

D.

Projection	Volume (cubic microns)	Number of uninnervated ribbons
AP-1	0.23	0
PP-1	0.43	1
AP-2	0.51	2
PP-2	0.62	3

DISCUSSION

Hair-cell projections act as scaffolds for a biased subpopulation of afferent neurons during ribbon synaptogenesis.

New hair cells arise in the neuromast throughout the life of a zebrafish (Williams and Holder, 2000). The afferent and efferent terminals innervating a neuromast incorporate these new cells while receiving mechanosensory input from the existing hair cells. Dynamic filopodia arising from afferent terminals appear to initiate contact with nascent hair cells. However, the foregoing results suggest that the hair cell also extends cellular projections that mediate innervation. By this mechanism, the hair cell is an active participant in its own innervation rather than a passive recipient.

Hair-cell projections appear in nascent hair cells immediately after rearrangement, a period during which the hair cells possess no stable innervation and are seldom contacted by afferent terminals. Contact between the hair cell and afferent terminals increases significantly upon the appearance of hair-cell projections, and the vast majority of the contact occurs across sites from which projections emerge. Afferent filopodia extend directly along the hair-cell projection and some of the filopodia stabilize at the base of the projection where presynaptic components reside. Both contact with the projection and juxtaposition of the immature ribbons is biased toward afferent terminals of the same functional polarity as the hair cell. Finally, stable afferent innervation of the hair-cell base correlates with the diminution of hair-cell projections, an event that correlates with the appearance of pre- and postsynaptic markers of ribbon synapses. Altogether, the data suggest that hair-cell projections mediate polarity-specific afferent synaptogenesis in nascent hair cells of the PLL (Fig. 4-17).

Because dendritic arbors possess dynamic filopodia that appear to scavenge the neuromast for new targets of innervation, the question arises of why the hair cell extends projections of its own. There are several possible advantages to this cellular behavior. First, whereas afferent filopodia are always present, hair-cell projections form only in immature cells, providing a transient signal that synaptic sites are available. Moreover, rather than confining such a signal to the local patch of membrane surrounding the synaptic ribbon, the hair-cell projection acts as an antenna to significantly increase the likelihood that a postsynaptic filopodium will encounter the hair cell. A projection also offers an afferent terminal a linear path to synaptic ribbons effectively reducing the terminal's search for available sites of synaptogenesis from three dimensions to one.

Pioneer axons provide a similar means of guidance in the developing nervous system (Goodman and Shatz, 1993). These neurons are often the first to innervate a target structure and provide a linear track upon which subsequent neurons can extend. It is likely that the existence of a preexisting path toward a target of innervation greatly accelerates the migration of a developing neuron and conserves its resources. Hair-cell projections may provide both gains to neurons within the developing nervous system

Hair-cell projections may additionally aid in neuronal target selection. Innervation within the neuromast is highly specific to both functional polarity and to size of the dendritic arbor. The hair-cell projection could serve as a substrate for upon which neurons compete for binding strength or speed of extension. Such a mechanism would better avoid the risk of an inappropriate neuron preciously innervating an available synaptic site and consequently sequestering the binding site from a more appropriate competitor.

Figure 4-17

Hair-cell projections mediate synaptogenesis in nascent hair cells

A diagram showing the interactions of hair-cell projections and afferent neurons across time, suggesting that hair cell projections act as cytoplasmic scaffolds for the guidance of polarity-appropriate afferent neurons to new sites for ribbon synaptogenesis.

a.

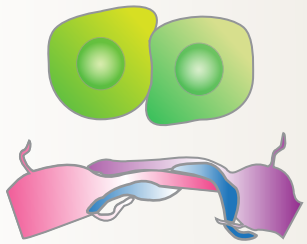

New hair cells lack contact with afferent neurons during rearrangement.

b.

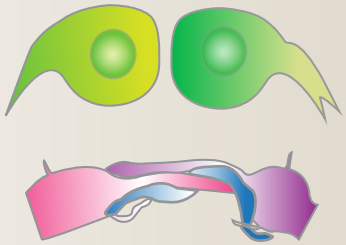

Projections emerge immediately after hair cells' final rearrangement.

c.

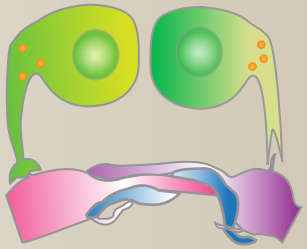

Projections extend to and contact aggregations of afferent neurons at nearby hair cells synapses. Immature ribbon synapses reside at the projection base.

d.

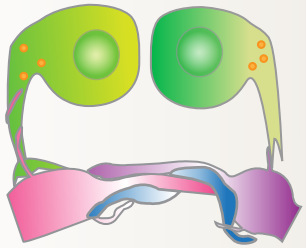

Offshoots from afferent neurons fasciculate along the projections toward the soma.

e.

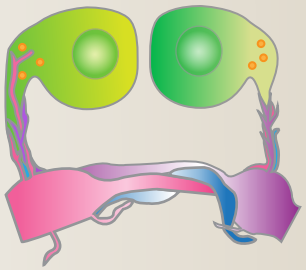

Afferent neurons increasingly extend along the hair-cell projections and do so in a subpopulation-biased manner.

f.

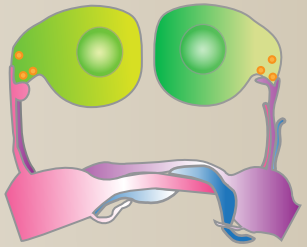

Afferent neurons of the polarity-appropriate subpopulation stabilize at the immature ribbons. Projections diminish and subside.

Expanding the understanding of hair-cell projections.

The proposed model needs to be further evaluated in a variety of ways. First, if projections are suppressed in immature cells it is unknown whether hair-cell synapses form at all, and if so, whether they are morphologically normal, polarity-specific, and assemble at a normal rate. It may be possible to eliminate projections by treating neuromasts with actin-disrupting agents like cytochalasin D or latrunculin B. However, given the importance of actin in afferent filopodia as well as mitosis, observing a defect in synapse formation would not conclusively determine the necessity of hair-cell projections for synaptogenesis. Instead, the experiments would use knowledge of the factors underlying the projections to exert temporal and cell-type specific control. Second, by inducing the formation of projections from inappropriate locations in immature hair cells or in inappropriate cell types such as mature hair cells, one could determine whether projections are sufficient to induce terminals to extend toward and stabilize on the cell. These experiments would also be best performed by the manipulations of factors directly involved in the formation of hair-cell projections.

An additional feature of the model that would benefit from closer examination is the biased association of hair-cell projections with afferent terminals of the same functional polarity. This preferential contact could involve a set of adhesion molecules unique to the projections arising from each hair-cell polarity and complementary to receptors on afferent terminals of the same functional polarity. These adhesion molecules could be the same or different from those that are presumed to mediate innervation of synaptic bodies in polarity-specific hair cells. Eliminating or ectopically expressing the

underlying molecules, which at present are unknown, would reveal their role in mediating polarity-specific synapse formation.

Another aspect of hair-cell projections to explore is whether there are signals that attract hair-cell projections and afferent terminals to one another. For instance, hair-cell projections may be attracted to the base of mature hair cells because of a factor released at the synapse. This hypothesis could be tested in zebrafish that lack activity-induced synaptic release due to inactivating mutations in the voltage-dependent L-type calcium channel Cav1.3. Similarly, the seeming attraction of afferent terminals to hair-cell projections could be mediated by an attractive signal released from the projections. For instance, the synaptic vesicles observed in hair-cell projections could undergo early spontaneous neurotransmitter release that is detected by afferent terminals. It would be interesting to determine whether the close association between nerve and projection is retained in zebrafish mutants defective in the glutamate transporter vGlut3.

There are other ways in which the current research could be improved. Reconstruction from SBEM image data, although highly informative, is labor-intensive. As a consequence, the current study was limited to examining four projections arising from two immature hair cells in a single neuromast. Because of the certitude of relationships between cellular structures provided by such a high-resolution method, perhaps the results can be trusted without requiring a large sample size. Nevertheless, I have prepared, imaged, and reconstructed additional neuromast samples, which should corroborate the findings described in the original sample.

Second, efferent neurons appeared to interact with hair-cell projections in the SBEM sample and had significant direct contact with projections. However, in the

confocal imaging of *Tg(myo6b:actin-GFP;hspGFF4A;UAS:nfsb-mCherry)* zebrafish, efferent neurons went undocumented. It would be interesting to examine whether the interaction of efferent neurons with the hair-cell projections is similar to that of afferent neurons. Unfortunately, I did not observe any presynaptic vesicle clusters, postsynaptic densities, or other ultrastructure in the areas of contact between efferent neurons and hair-cell projections that would be indicative of synapses.

Finally, with the confocal and SBEM imaging methods used in the study, the presence of synapses had to be inferred. In the case of confocal microscopy, stable association of a nerve fiber at the hair cell was used as a surrogate of innervation. In the SBEM data, postsynaptic densities were not apparent at afferent ribbon synapses of mature or immature hair cells, so it was assumed that nerve fibers juxtaposed to ribbons had formed synapses or were undergoing synaptogenesis. It would be informative to use antibody labeling to examine in fixed tissue whether projections indeed contain presynaptic markers of synaptogenesis or active synapse function.

Cytoplasmic Extensions in Other Systems and Species

Hair-cell projections may be better understood and investigated by comparing them to other well-characterized cellular processes. At least three types of cellular process bear mentioning. First, the searching behavior, dynamism, and morphology of hair-cell projections are reminiscent of neuronal growth cones. A major function of growth cones is the detection of and orientation toward nearby guidance cues. Hair-cell projections also seem to orient toward particular targets, namely afferent terminals beneath mature hair cells of the same polarity as the immature cell from which it

originates. A growth cone can be divided into three domains. The core domain contains tightly bundled microtubules whose polymerization drives the growth cone forward. Dynamic filopodia and lamellipodia driven by bundles or branched networks of filamentous actin make up the peripheral domain. Here lie the adhesion proteins as well as signaling receptors that mediate the growth cone's binding to a substrate and guidance. Finally, there is a transitional zone composed of contractile actomyosin structures oriented perpendicular to the filamentous actin of the peripheral domain (Lowery and Van Vactor, 2009; Pak et al., 2008). It is conceivable that the machinery of the axonal growth cone has been reappropriated in the nascent hair cell. I was not able to establish that microtubules extend throughout all regions of the hair-cell projection, so it is possible that three regions analogous to those within the growth cone exist in the hair-cell projection. Several significant differences separate growths cones from hair cell projections including the transience of projections as well as a lack of motility or migration.

Cytonemes are other intriguing filopodial structures that may share characteristics with hair-cell projections. Cytonemes are long, actin-filled structures that appear to transport signaling molecules during development in a variety of tissues (Hsiung et al., 2005; Ramirez-Weber and Kornberg, 1999; Roy et al., 2011; Roy et al., 2014). One well-characterized type of cytoneme arises from the *Drosophila* wing disc to extend to cells producing the morphogen decapentaplegic, which it binds with the receptor thickveins. Like hair-cell projections, the cytonemes are transient structures that do not mediate cell migration. Additionally, just as synaptogenesis appears to occur at the base of hair-cell projections, receptor-ligand endocytosis and signal processing seem to occur at its point

of origin on the soma rather than at the tip of the process (Roy et al., 2014). Cytonemes have been identified in developing vertebrates and include those that transport the hedgehog signaling factor in the chick limb bud (Sanders et al., 2013). Cytonemes are hypothesized to create gradients of morphogens as an alternative to Wolpert's model of molecular diffusion (Wolpert, 1969; Wolpert, 2009). An alternative mechanism to diffusion may also be necessary for new hair cells to attract innervation in the neuromast since a guiding gradient may be untenable due to the numerous presynaptic puncta that emerge simultaneously as well as the tortuous paths of diffusion created by neighboring cells.

However, there are a number of differences between the two types of projections. Although the 0.1-0.5 μm diameter of the cytonemes is similar to that of hair-cell projections, cytonemes can extend as much as 700 μm, a far greater length than the longest hair-cell projections. Additionally, unlike hair-cell projections, cytonemes are often straight and unbranched. Cytonemes may growth rapidly (>15 μm per minute) but remain stable thereafter until later in development when they disappear (Kornberg and Roy, 2014; Ramirez-Weber and Kornberg, 1999). Finally, it is not clear whether hair-cell projections in fact mediate signaling with PLL neurons. Although I made several observations that suggest that new postsynaptic filopodia are induced at locations where a hair-cell projection has contacted the dendritic arbor, this interaction has not been rigorously supported.

A third type of cytoplasmic processes for comparison is the filopodia that form from epithelial cells during *Drosophila* dorsal closure as well as wound healing (Jacinto et al., 2000; Wood et al., 2002). These actin-filled filopodia extend approximately 10 μm,

or sometimes grow much farther, to dynamically sample the cellular environment on the opposite edge of the epithelial gap. Filopodia associate preferentially with epithelia of their same engrailed or patched subtype (Millard and Martin, 2008). Upon stable association with cellular partners, lamellipodia emerge from between the filopodia (Jacinto et al., 2000).

Although the foregoing behavior resembles some aspects of hair-cell projections, the net effect of the filopodia is to bind the two edges of the wound and exert mechanical force to close the epithelial gap. The force is generated by an actinomyosin band that lies at the edge of the epithelium (Martin and Parkhurst, 2004). Although hair-cell projections do appear to shorten as the afferent neurons get closer to the soma, there is no evidence that this occurs through mechanical towing rather than neuron-autonomous climbing behavior. Additionally, there is no current evidence of an actinomyosin band residing at the base of the projections. Finally, it is plausible that the mechanism of bringing together epithelial sheets differ from those that unite focal portions of sensory epithelium and neuronal tissue.

CHAPTER FIVE

Hair-cell gene expression reveals candidate genes for polarity-specific synapse formation in the neuromast

Previous research indicates that polarity-specific synapse formation is independent of hair-cell activity. The foregoing work additionally proposes that the synaptic specificity arises early in hair-cell maturity through the interaction of hair-cell projections with PLL afferent terminals of the same functional polarity. Nanometer-scale reconstruction of the neuromast using SBEM demonstrates that polarity-appropriate afferent terminals juxtapose synaptic ribbons by directly displacing adjacent afferent terminals of the opposite functional polarity. Finally, no other cell type apart from afferent terminals and hair cells appears to directly mediate synapse formation or maintenance. Altogether, these observations provide strong support for the hypothesis that beginning shortly after mitosis anteriorly and posteriorly polarized hair cells express distinct sets of adhesion molecules that are complementary to synaptic adhesion molecules expressed by distinct classes of PLL afferent neurons.

One approach for identifying the molecular differences between hair cells of the two polarities is to compare the transcriptomes of anteriorly and posteriorly polarized hair cells. To do so, I developed a novel method that relied on kaede-based photoconversion and fluorescence-activated cell sorting to obtain pure samples of RNA from anteriorly and posteriorly polarized hair cells for next-generation sequencing. Additionally, I performed next-generation sequencing on RNA from tens of thousands of double-labeled

hair cells of both polarities collected by fluorescence-activated cell sorting in order to construct a reliable library of transcripts to which to compare the sequence data. The data sets yielded candidate genes for polarity-specific synapse formation.

RESULTS

Individual kaede-expressing hair cells in the neuromast can be marked and collected for next-generation sequencing.

I wished to collect pure samples of anteriorly and posteriorly polarized hair cells for next-generation sequencing. Hair cells are closely entwined at their apices eliminating the possibility of collecting samples by laser-capture microdissection. Additionally, there are no known gene-expression differences between anteriorly and posteriorly polarized hair cells that could be employed for transgenic marking of the subpopulations.

Therefore, I developed a protocol for collecting hair cells of a single polarity in a line of zebrafish, *Tg(s1097t;s1999t),* that express the kaede protein in lateral-line hair cells beginning immediately after mitosis as well as in various epidermal, spinal, and central-nervous-system tissues (Fig. 5-1 A). Kaede is a photoconvertible protein that undergoes a permanent change from emitting green fluorescence to red fluorescence upon brief exposure to ultraviolet light (Ando et al., 2002). Using an ultraviolet laser focused through a laser-scanning confocal microscope, I was able to elicit a 200-fold increase in the ratio of red-to-green in individual hair cells of 4 dpf zebrafish without significantly altering the fluorescence ratio of the neighboring cells (Fig. 5-1 B and C). Hair cells survive the exposure to ultraviolet light, and in the case of immature hair cells, proceed normally through differentiation.

In 3-4 dpf embryos, hair-cell polarity can be determined *in vivo* by the pairwise positioning of hair cells in two columns within the neuromast (Fig. 5-1 B and C). Additionally, the asymmetric positioning of the kinocilium can often be appreciated under laser excitation of the kaede-green protein in *Tg(s1097t;s1999t)* zebrafish (Fig 5-1

B inset). Therefore, using confocal microscopy I could target hair cells of a single polarity for photoconversion. During each round of the experimental procedure, I photoconverted all of the hair cells of a single polarity in 50-100 zebrafish.

Following photoconversion, I enriched the tissue sample for the marked hair cells using a microdissection technique in which the periderm is removed from the zebrafish with fine forceps. The dissected periderm contains the intact lateral-line organ with no apparent damage to hair cells. The tissue sample was dissociated to a single-cell suspension using proteolytic enzymes and EDTA as well as mechanical trituration. Then the solution was filtered through a polycarbonate membrane with 8 μm pores, which improved both the efficacy of dissociation as well as the enrichment of hair cells in the solution. Viewing the cell suspension by widefield fluorescence microscopy showed that hair cells tended to be unattached to other cellular material and retained the characteristics of a healthy cell including a hair bundle and goblet shape (Fig5-1 D).

Upon examining the dissociated sample with fluorescence-activated cell sorting, a distinct event population appeared that was not present in samples from kaede-expressing zebrafish that had not been exposed to ultraviolet light (Fig. 5-2 A and B). The new population had an approximately 100-fold higher signal in the red-fluorescence channel and 10-fold lower signal in the green-fluorescence channel than the event population in the unexposed sample. Events of this population clustered on a graph of forward- and side-scatter, parameters that assess the size and internal density of cells (Fig. 5-2 C). Moreover, the subpopulation was eliminated by one-hour exposure of photoconverted zebrafish to copper sulfate, an agent that induces apoptosis in lateral-line hair cells (Fig. 5-2 D). Finally, when the cell population was sorted into phosphate-buffered saline, I

could identify kaede-red hair cells under fluorescence microscopy by their characteristic goblet shapes and kinocilia (Fig. 5-2 E).

Events from this population were collected by fluorescence-activated cell sorting directly into a cell-lysing buffer. The photoconversion and collection protocol routinely resulted in a 30-35% yield of the marked cells. After numerous repetitions of this procedure, I accumulated four samples of approximately 1000 anteriorly polarized and four samples of 1000 posteriorly polarized hair cells. RNA was isolated from the cells and the eluted volume was concentrated two-fold by evaporation. RNA collected by this method showed two distinct peaks and an RNA integrity number above 8.0 when measured on the Agilent Bioanalyzer 2100, indicating that the genetic material was of high quality and had suffered little degradation (Fig. 5-2 F). The RNA was converted into cDNA, the cDNA was amplified using a commercial kit based on Ribo-SPIA priming across the full transcript, and finally, the amplified cDNA was prepared as a library for next-generation sequencing (Kurn et al., 2005).

Given the small number of hair cells contained in each sample, contaminating RNA from non-hair cells could represent a significant source of transcripts in the sequencing data that would be falsely attributed to hair cells. In order to guard against this possibility, I generated a more reliable hair-cell transcriptome with which to compare the single-polarity samples. To do so, I collected 50,000 hair cells from a transgenic line of zebrafish, *Tg(Brn3c:GFP;myo6b:mCherry)*, which expresses GFP and mCherry under two different hair-cell specific promoters (Fig. 5-3 D). Tissue samples from these zebrafish were dissected, dissociated, and filtered under the same protocol as the kaede-derived samples. When these samples were analyzed by fluorescence-associated cell

sorting, they showed a distinct population of events with high green fluorescence and high red fluorescence (Fig. 5-3 A). The population disappeared in samples treated with copper sulfate (Fig 5-3 B).

I collected approximately 50,000 hair cells from the double-positive population. Additionally, I collected events from three other portions of the fluorescence-activated cell sorting scatterplot comprising periderm, blood cells, fin cells, and neuromast supporting cells but lacking hair cells (Fig. 5-3 C). Hair cells were divided into triplicate samples of 500, 1000, 5000, and 10,000 cells, and processed by next-generation sequencing in the same manner as described for the kaede-derived samples. The resulting data was treated as a reliable reference of the hair-cell transcriptome. All resultant sequencing data were aligned to the Zv9 zebrafish genome (Sanger Institute Zebrafish Genome Project) using BowTie software, and transcript assembly and abundance measurements were performed by CuffLinks software (Langmead et al., 2009; Trapnell et al., 2012).

Figure 5-1

Subpopulations of hair cells can be marked and dissociated in kaede-expressing zebrafish

A. Whole body imaging of 4 dpf *Tg(s1097t;s1999t)* zebrafish line reveals kaede expression in the PLL hair cells, spinal neurons, distal fin, and central nervous system. B. Mature and immature PLL hair cells express kaede. Their columnar arrangement denotes their polarity with posteriorly polarized cells occupying the left column and anteriorly polarized cells occupying the right column. These polarity identities can often be confirmed by viewing the bright dot of the kinocilium asymmetrically positioned on the hair-cell apex (*inset*). Anterior is to the left, dorsal is toward the top. C. Brief exposure to ultraviolet laser light focused through a confocal microscopy can induce a significant, permanent photoconversion in individual hair cells without significantly altering neighboring cells. D. A specialized dissociation protocol isolated healthy PLL hair cells in single-cell suspension.

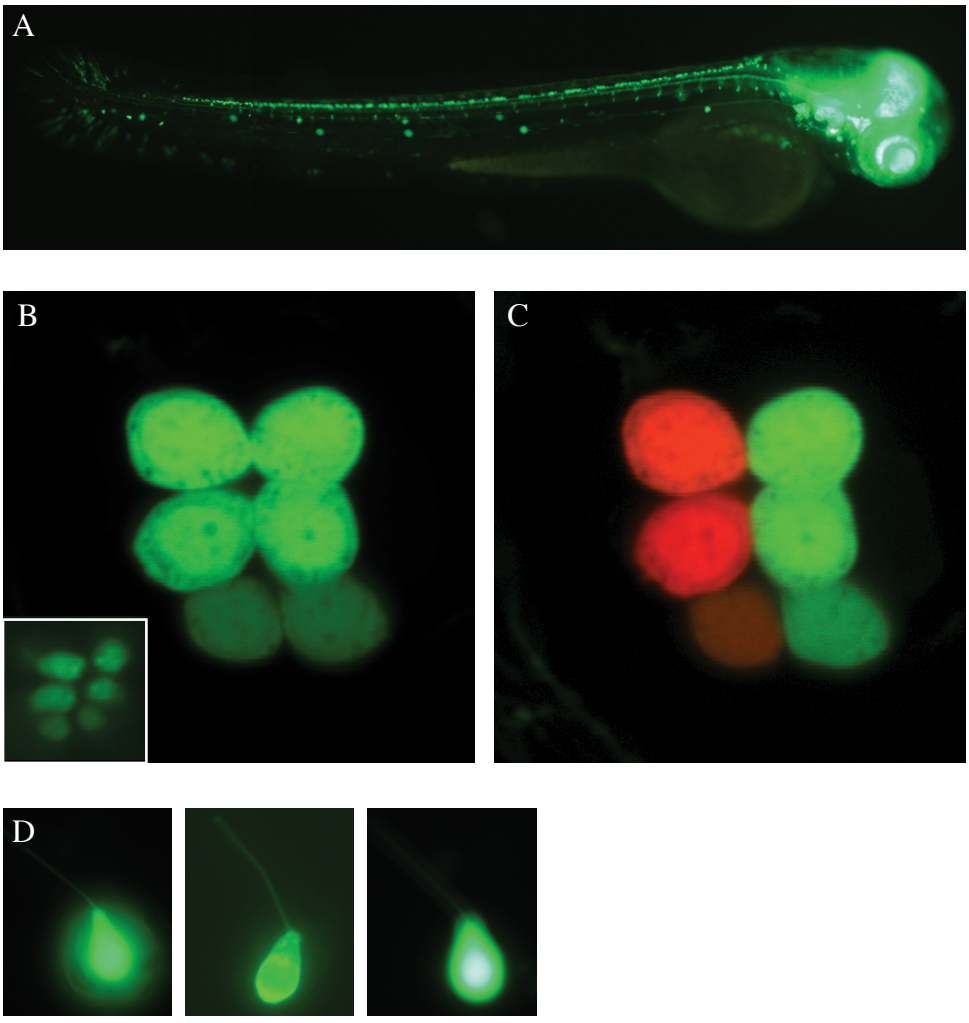
A
B
C
D

Figure 5-2

Photoconverted hair cells can be distinguished and collected using fluorescent-activated cell sorting

A. Cells from 4 dpf *Tg(s1097t;s1999t)* larvae not exposed to ultraviolet light show a population of events (P1) that is high in green fluorescence but low in red fluorescence. B. When PLL hair cells are briefly exposed to ultraviolet light, the P1 population shifts to P2 with events showing one tenth the green fluorescence and 100-fold more red fluorescence. C. Events in P2 are clustered on the forward- and side-scatter plot suggesting homogeneity in size and internal composition. D. In photoconverted kaede samples, the P2 population disappears after treatment with copper sulfate. E. Events collected from the P2 population in (B) were confirmed by morphology and fluorescence as photoconverted hair cells. F. Photoconverted hair cells collected by fluorescence-activated cell sorting yielded high-quality RNA when analyzed on the Agilent Bioanalyzer 2100.

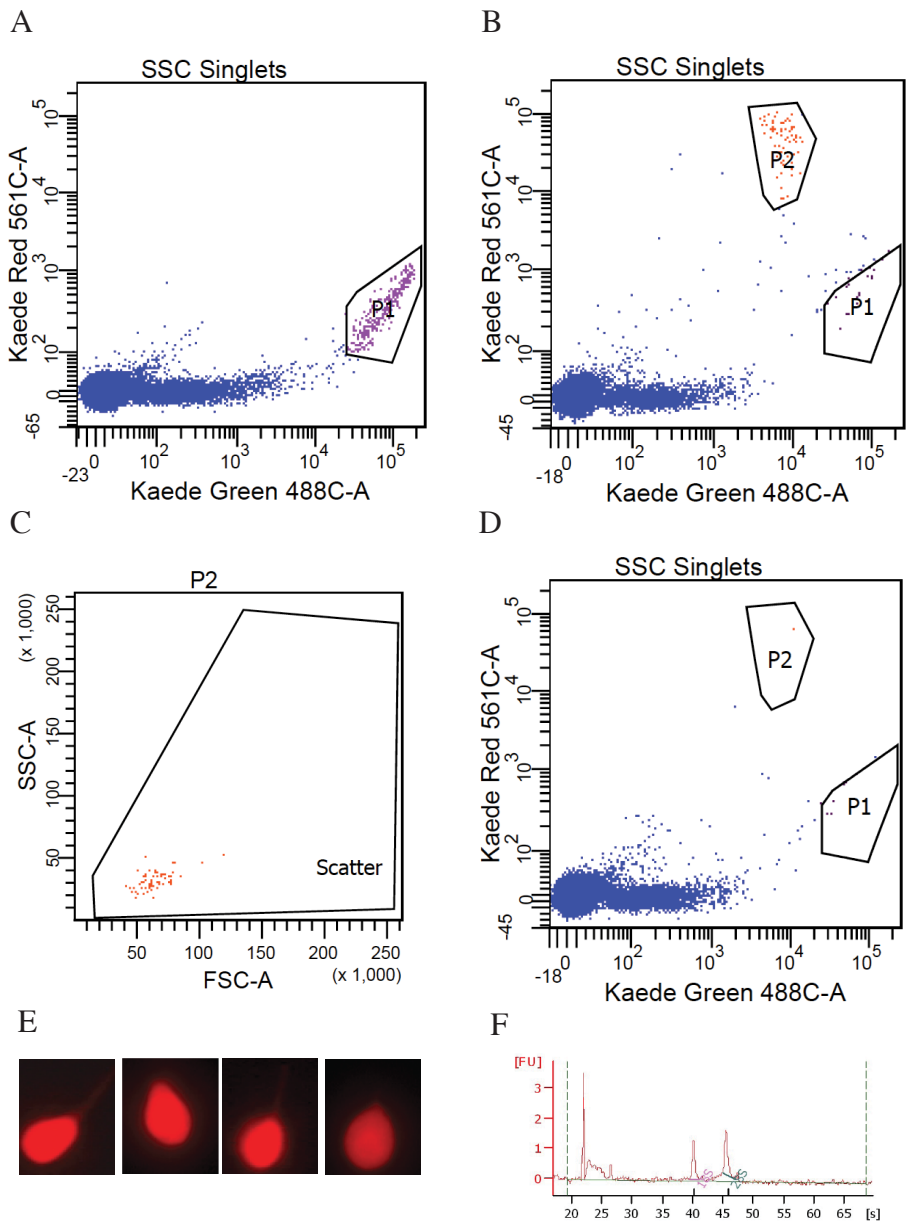
A
SSC Singlets
Kaede Red 561C-A
Kaede Green 488C-A
P1
B
SSC Singlets
Kaede Red 561C-A
Kaede Green 488C-A
P2
P1
C
P2
SSC-A
(x 1,000)
FSC-A
(x 1,000)
Scatter
D
SSC Singlets
Kaede Red 561C-A
Kaede Green 488C-A
P2
P1
E
F
[FU]
[s]

Figure 5-3

Tens of thousands of hair cells were collected by fluorescence-activated cell sorting

A. Tissue from 4 dpf *Tg(Brn3c:mGFP;myo6b:mCherry)* zebrafish processed to a single-cell suspension shows a population of events (P1) that is high in green fluorescence and red fluorescence on fluorescence-activated cell sorting. B. The P1 population disappears when zebrafish were treated with copper sulfate for one hour prior to tissue processing. C. In addition to putative hair cells collected from P1, cell events from three other portions of the scatter plot were collected for comparison. D. GFP and mCherry are both expressed in PLL hair cells in zebrafish of the *Tg(Brn3c:mGFP;myo6b:mCherry)* line.

A

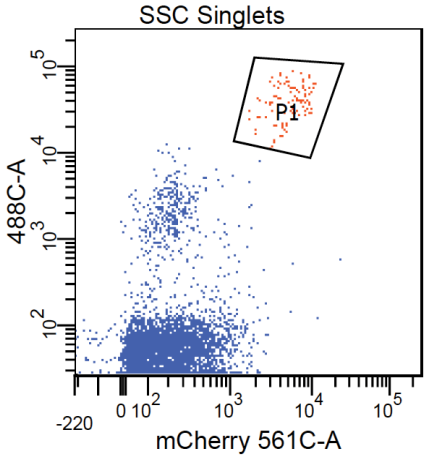
SSC Singlets
P1
488C-A
-220
mCherry 561C-A

B

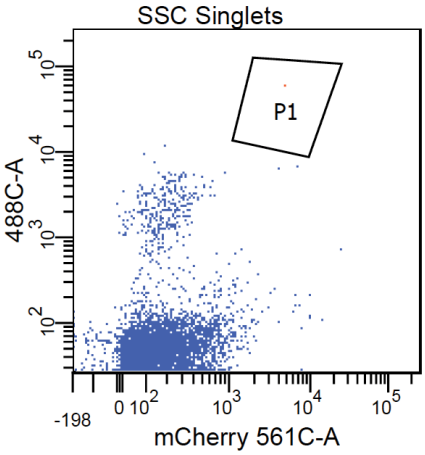
SSC Singlets
P1
488C-A
-198
mCherry 561C-A

C

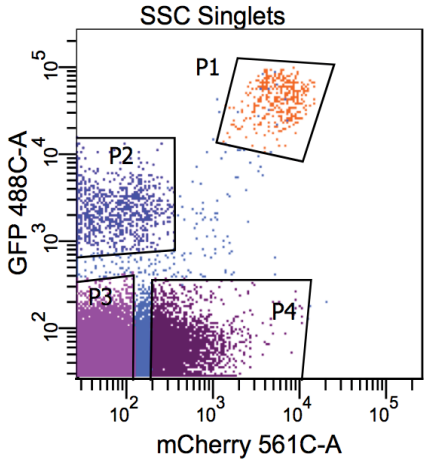
SSC Singlets
P1
P2
P3
P4
GFP 488C-A
mCherry 561C-A

D

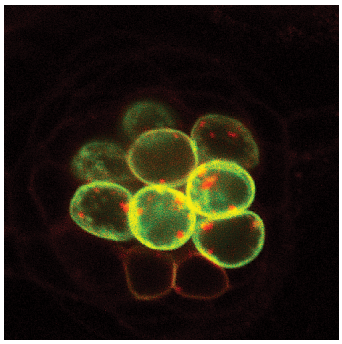

Next-generation RNA sequencing reveals the hair-cell transcriptome.

I analyzed the next-generation sequencing results in several ways. First, I wanted to determine the extent to which I had indeed collected a pure population of hair cells. I searched the literature to identify a set of genes with published evidence of expression in PLL hair cells, PLL supporting cells, PLL neurons, periderm cells, fin cells, or blood cells (Appendix 1). Fourty-four of forty-five hair-cell gene markers were presented above FPKM (Fragments Per Kilobase Of Exon Per Million Fragments Mapped) of one in the single-polarity samples, and all 45 genes were detected in the all-polarity samples (Fig. 5-4). Their gene-expression levels spanned more than four orders of magnitude, and the genes were diverse in function including synaptic and signaling molecules.

Gene expression levels of supporting-cell or neuronal markers were minimal to absent in both single-polarity and all-polarity samples suggesting that contamination by neurons or supporting cells was insignificant (Fig. 5-6). However, periderm, blood, and fin cells, which constitute the majority of cells in the tissue sample, showed greater levels of their markers in the samples including keratin, collagen, and hemoglobin (Fig. 5-4). Gene expression levels for skin, blood, and fin markers were typically 10-100 fold lower in the all-polarity samples compared to the single-polarity samples suggesting that contamination by non-hair cell transcripts had an excessive effect in samples with fewer numbers of cells.

To further confirm the validity of the hair-cell transcriptome, I selected several transcripts that showed moderate levels of gene expression in the hair-cell sequencing results but had not been previously identified in PLL hair cells. The five genes, Clasp2, Igsf9a, Ulk1a, Amigo1, and Diaph1 all showed results from *in situ* hybridization that

confirmed their expression in the PLL hair cells (Fig. 5-7). Altogether, this data shows that the single-polarity and all-polarity samples indeed collected PLL hair cells. Although there was mild contamination by transcripts presumably originating from periderm and fin cell transcripts, many of the false positive genes could be identified by comparing the single-polarity samples to the all-polarity samples.

Next, I sought to determine how much of the hair-cell transcriptome was represented in the samples. I found that the *Tg(Brn3c:GFP;myo6b:mCherry)* samples that were comprised of 10000 hair cells expressed, on average, 10,800 genes above an FPKM of 1.0, whereas the single-polarity hair-cell samples expressed nearly 10,500 genes (Fig. 5-7 A). Both numbers fall within the estimated range of 10,000-15,000 genes expressed by the typical differentiated cell (Jongeneel et al., 2003). Additionally the non-hair-cell samples, which likely contain transcripts pooled from numerous cell types, expressed 11,000-14,000 genes (Fig. 5-7 A). The results suggest that a significant proportion of the hair-cell transcriptome is represented in my samples, and additionally, that 1000 hair cells obtained by Kaede photoconversion and fluorescence-activated cell sorting yields nearly the same coverage of the transcriptome as a 10-fold greater amount of starting material.

To determine the reliability of the measurements across samples, I compared the gene expression values of several sample groups. Because there may be biological differences between the population of cells collected from the *Tg(Brn3c:GFP;myo6b:mCherry)* specimens and the *Tg(s1097t;s1999t)* specimens, I first plotted gene expression values for samples of 10000 all-polarity hair cell against those of samples of 1000 hair cells. This comparison showed a Pearson correlational coefficient of

0.92 (Fig. 5-7 B). Next, I compared the same samples of 10000 all-polarity hair cells to the averaged single-polarity samples, which unexpectedly showed a Pearson correlation coefficient of 0.93 (Fig. 5-7 C). The higher coefficient may be due to the fact that eight single-polarity samples were averaged compared to three all-polarity samples.

Finally, I compared the gene expression values of anteriorly polarized hair-cell samples to posteriorly polarized hair-cell samples. I anticipated that anteriorly and posteriorly polarized hair cells would have almost identical transcriptomes except for the those genes underlying their two identified phenotypic differences, namely polarity-specific synapse formation and opposite hair bundle orientation. However, when the gene expression values of anteriorly and posteriorly polarized hair cells were compared, the Pearson coefficient was 0.90 indicating that a significant number of genes differed between the two samples (Fig. 5-7 D). On the other hand, when I compared gene expression values for the list of hair-cell markers the Pearson coefficient was 0.99 (Fig. 5-7 E). This suggests that the hair-cell transcriptomes were reliably represented in the data, but either non-hair-cell transcripts were unequally distributed among the samples or there are a significant number of gene expression differences between anteriorly and posteriorly polarized hair cells. Intriguingly, the anteriorly polarized hair cells routinely showed fewer expressed genes than posteriorly polarized cells.

Single-polarity hair cell samples showed some variation between sample pairs, which may be attributed to the fact that pairs of samples were collected over the same period of time but each pair was obtained over the course of two years. Although the cell-collection procedure remained mostly consistent during this time, there were minor alterations to the protocol as well as potential operator differences across the two years.

Additionally, aging of the breeding adult zebrafish may have also caused developmental alterations in their offspring. Consequently, I worked with a bioinformatician, Dr. Deyou Zheng, to produce a list of genes with significantly different gene expression values between anteriorly and posteriorly polarized hair cells. Dr. Zheng produced a list of differentially expressed genes by using the fold change for a given gene within each sample pair as a test statistic and evaluating the fold-change distribution of the four sample pairs. From a list of 13,323 genes, 472 showed a fold change across the four samples pairs that was statistically significant for a p-value of less than 0.05.

Figure 5-4

Hair-cell markers are detected in single-polarity and all-polarity hair-cell samples

Hair-cell expression was confirmed for 45 genes based on evidence reported in the literature and performed in the Hudspeth lab. Gene expression for averaged single-polarity hair-cell samples and averaged all-polarity hair-cell samples is displayed as $\log_{10}$ of FPKM (fragment per kilobase of gene per million fragments), a standard unit for next-generation sequencing data.

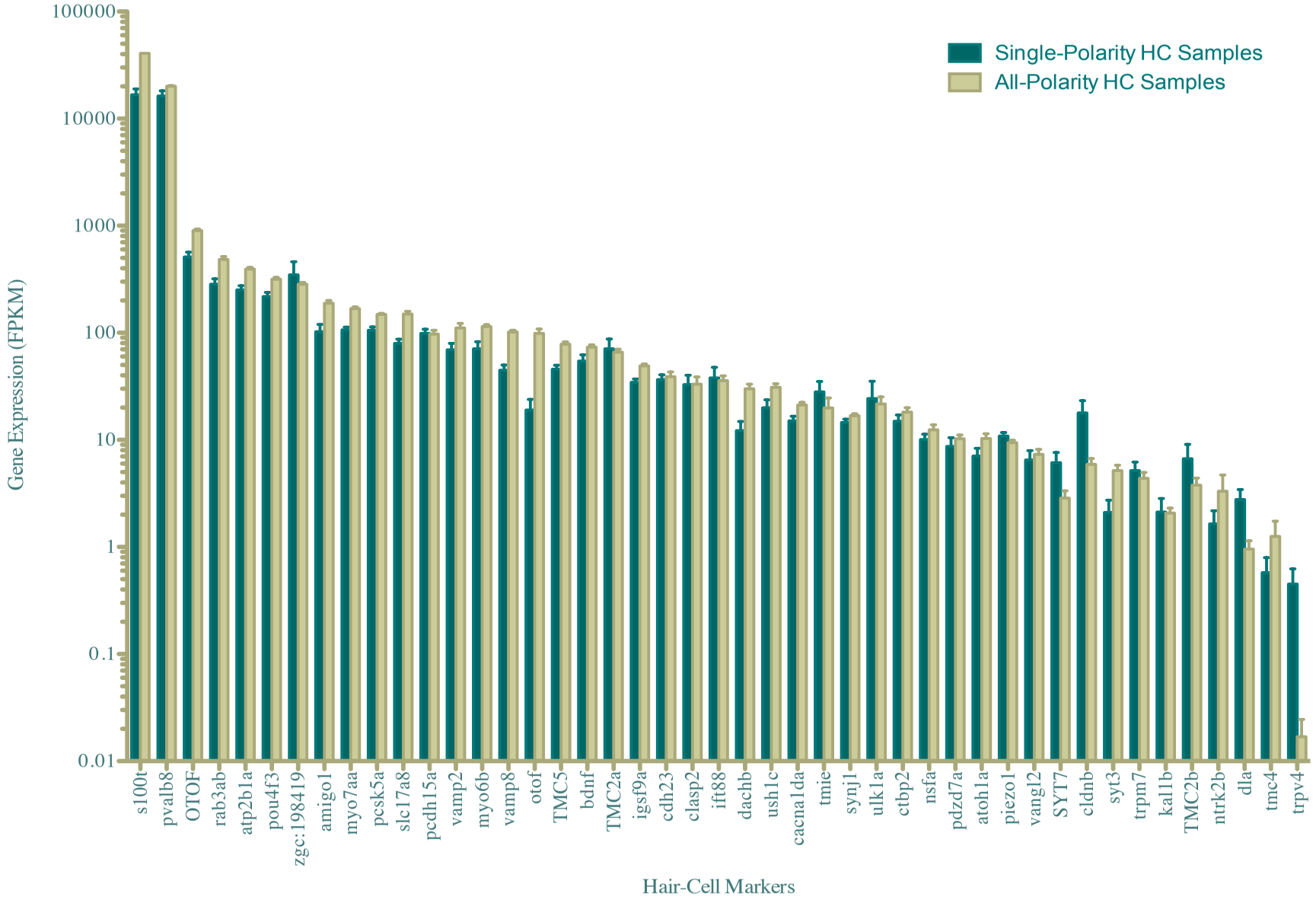
Single-Polarity HC Samples
All-Polarity HC Samples
Gene Expression (FPKM)
100000
10000
1000
100
10
1
0.1
0.01
s100t
pvalb8
OTOF
rab3ab
atp2b1a
pou4f3
zgc:198419
amigo1
myo7aa
pcsk5a
slc17a8
pcdh15a
vamp2
myo6b
vamp8
otof
TMC5
bdnf
TMC2a
igsf9a
cdh23
clasp2
ift88
dachb
ush1c
cacna1da
tmie
synj1
ulk1a
ctbp2
nsfa
pdzd7a
atoh1a
piezo1
vangl2
SYT7
cldnb
syt3
trpm7
kal1b
TMC2b
ntrk2b
dla
tmc4
trpv4
Hair-Cell Markers

Figure 5-5

Periderm and fin-cell markers are highly expressed in non-hair-cell samples, moderately expressed in single-polarity hair cell samples, and minimally expressed in all-polarity hair-cell samples

Periderm and fin-cell gene expression was confirmed by evidence reported in the literature. Gene expression for averaged single-polarity hair-cell samples, averaged all-polarity hair-cell samples, and three groups of averaged non-hair-cell samples.

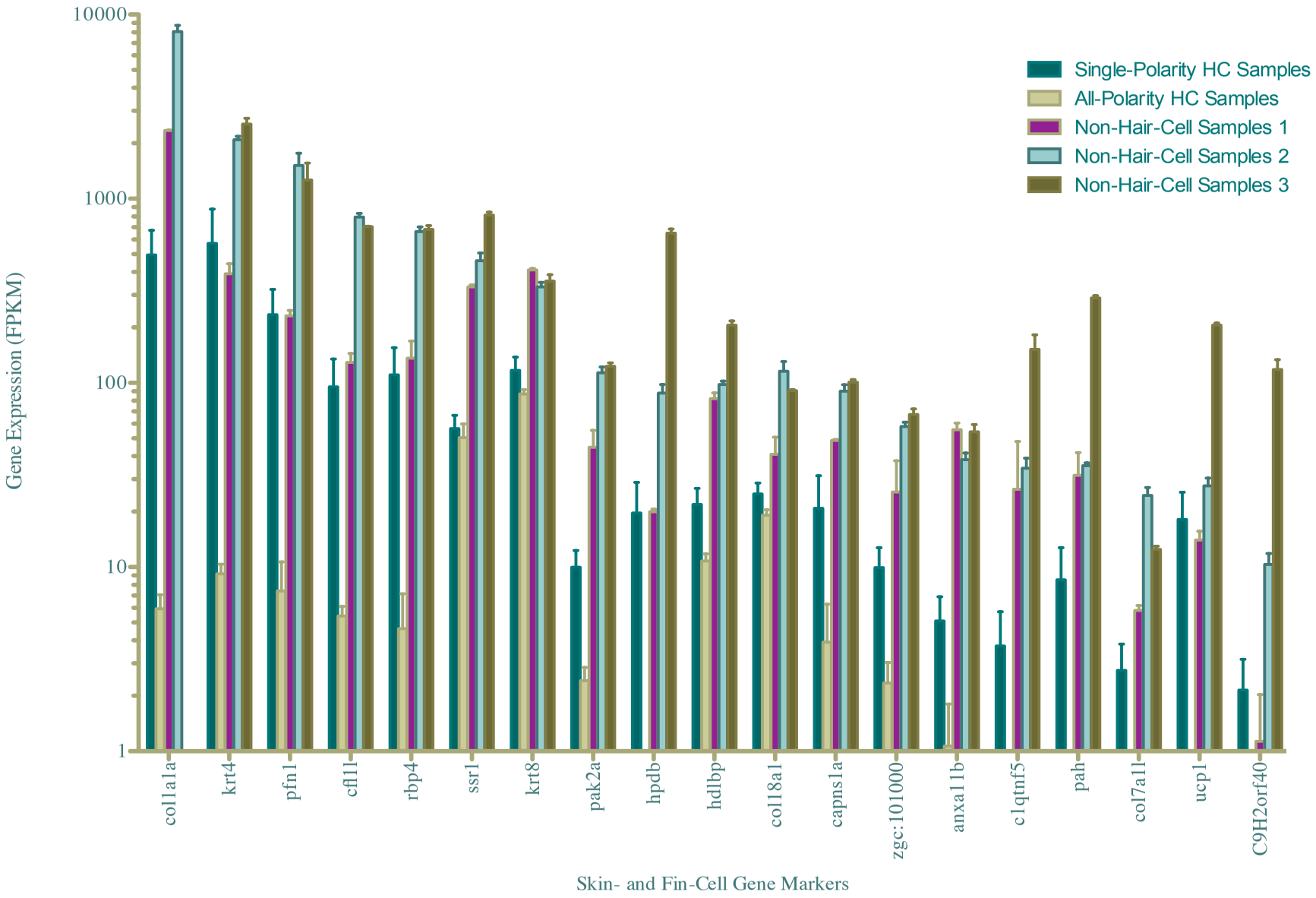
Single-Polarity HC Samples
All-Polarity HC Samples
Non-Hair-Cell Samples 1
Non-Hair-Cell Samples 2
Non-Hair-Cell Samples 3
Gene Expression (FPKM)
10000
1000
100
10
1
col1a1a
krt4
pfn1
cfl1l
rbp4
ssr1
krt8
pak2a
hpdb
hdlbp
col18a1
capns1a
zgc:101000
anxa11b
c1qtnf5
pah
col7a1l
ucp1
C9H2orf40
Skin- and Fin-Cell Gene Markers

Figure 5-6

PLL neuron, PLL supporting cell, and blood cell markers show variable expression across samples

PLL neuron, supporting cell, and blood cell gene expression was confirmed by evidence reported in the literature. Gene expression for averaged single-polarity hair-cell samples, averaged all-polarity hair-cell samples, and three groups of averaged non-hair-cell samples.

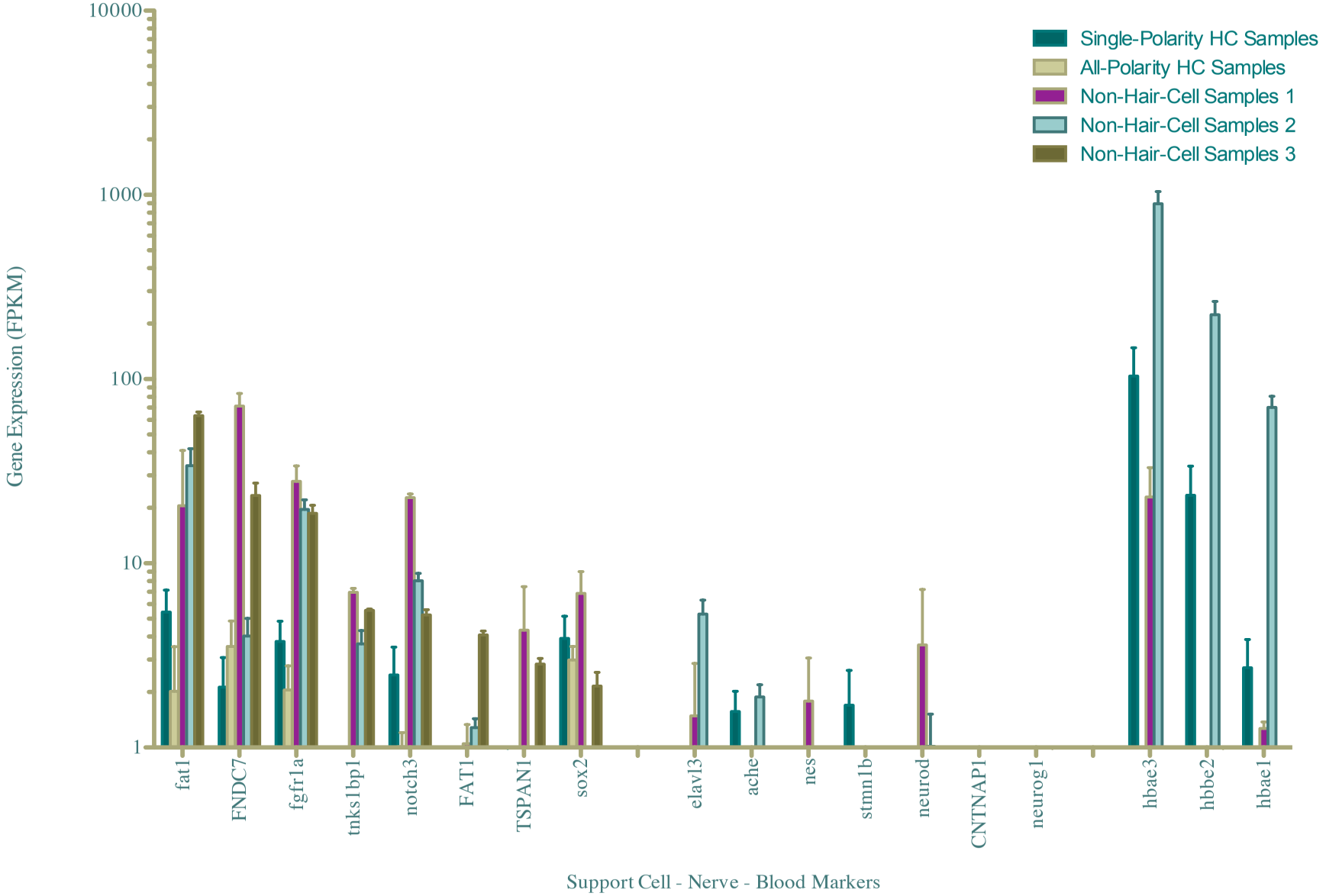
Single-Polarity HC Samples
All-Polarity HC Samples
Non-Hair-Cell Samples 1
Non-Hair-Cell Samples 2
Non-Hair-Cell Samples 3
Gene Expression (FPKM)
10000
1000
100
10
1
fat1
FNDC7
fgfr1a
tnks1bp1
notch3
FAT1
TSPAN1
sox2
elavl3
ache
nes
stmn1b
neurod
CNTNAP1
neurog1
hbae3
hbbe2
hbae1
Support Cell - Nerve - Blood Markers

Figure 5-7

In situ hybridization confirms hair-cell gene expression in next-generation sequencing data

In situ hybridization results in the whole body and neuromast for Igsf9a (A, B), Amigo1 (C, D), Clasp2 (E, F), and Diaph1 (G, H). Zebrafish were 4 dpf *Tg(myo6b:actin-GFP)* embryos. Left is anterior and up is dorsal in all panels.

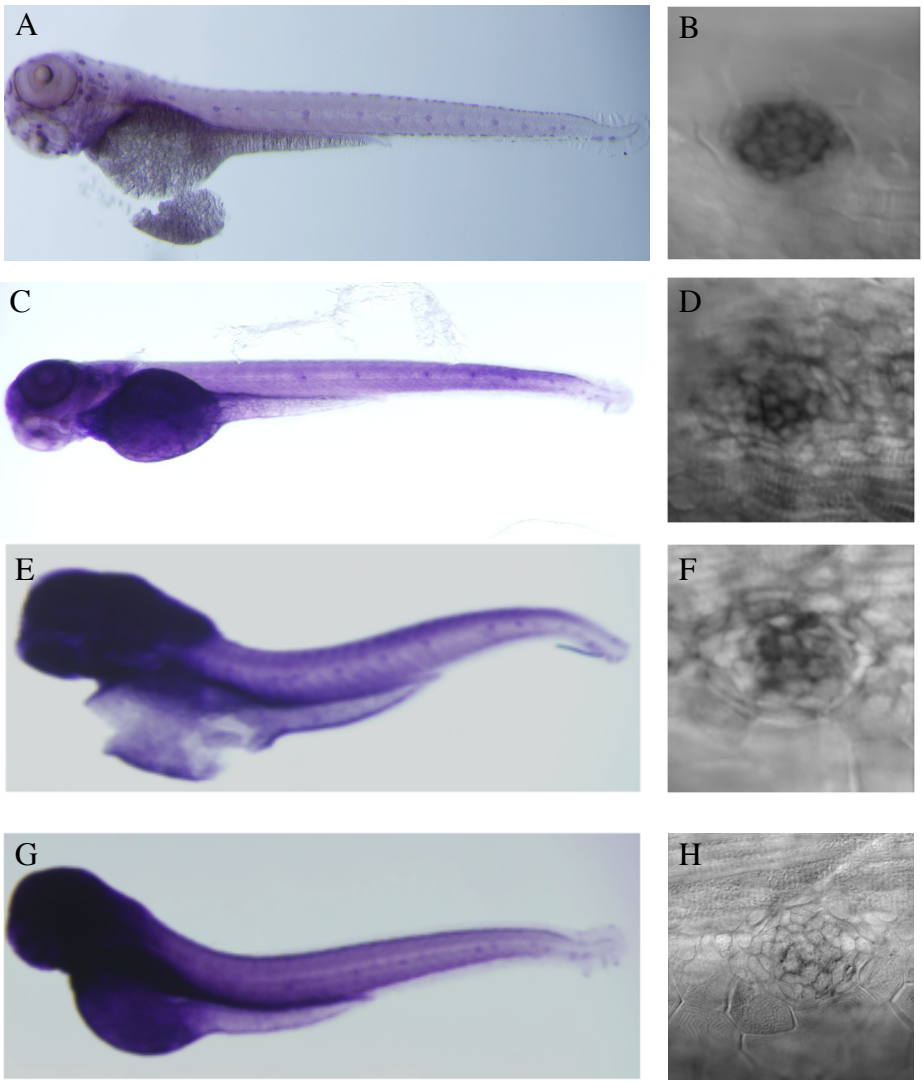
A
B
C
D
E
F
G
H

Figure 5-8

Next-generation sequencing samples show reliability in gene expression

A. Number of genes expressed above FPKM of 1.0 for averaged sample groups. B. Log_2(FPKM) comparison of all-hair-cell polarity samples of 9000 hair cells or 1000 hair cells. Pearson r = 0.9241. C. Log_2(FPKM) comparison of all-hair-cell polarity samples of 9000 hair cells or averaged Kaede-capture single-polarity hair cells. Pearson r = 0.9345. D. Log_2(FPKM) comparison of averaged Kaede-capture anteriorly polarized hair-cell samples and posteriorly polarized hair-cell samples. Pearson r = 0.9006. E. Log_2(FPKM) comparison of averaged Kaede-capture anteriorly polarized hair-cell samples and posteriorly polarized hair-cell samples for 45 hair-cell gene markers. Pearson r = 0.9878.

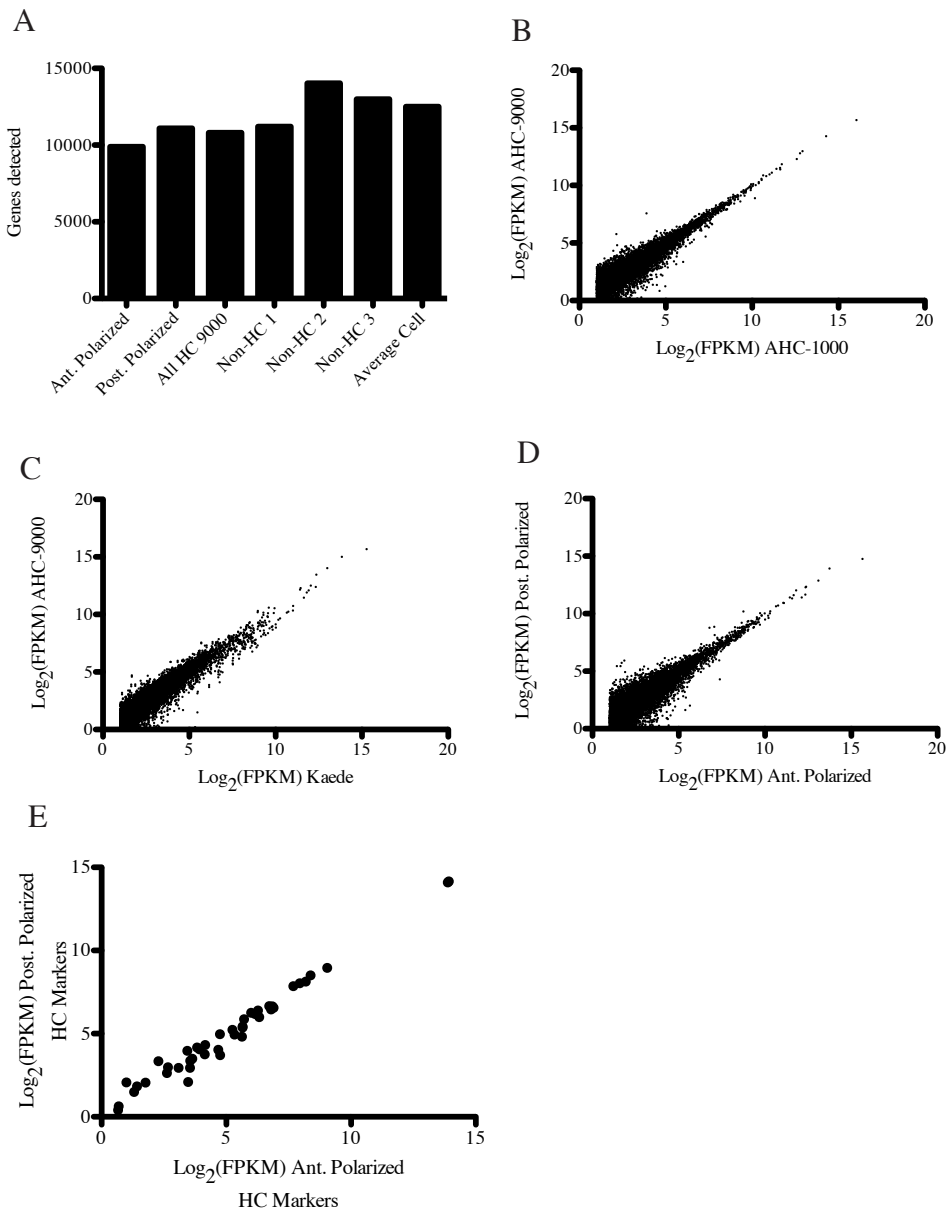
A
15000
10000
5000
0
Genes detected
Ant. Polarized
Post. Polarized
All HC 9000
Non-HC 1
Non-HC 2
Non-HC 3
Average Cell
B
Log2(FPKM) AHC-9000
Log2(FPKM) AHC-1000
C
Log2(FPKM) AHC-9000
Log2(FPKM) Kaede
D
Log2(FPKM) Post. Polarized
Log2(FPKM) Ant. Polarized
E
Log2(FPKM) Post. Polarized HC Markers
Log2(FPKM) Ant. Polarized HC Markers

Comparison of anteriorly and posteriorly polarized hair-cell transcriptomes revealed differential gene expression.

I investigated the list of 472 differentially expressed genes for candidates that may mediate polarity-specific synapse targeting in hair cells. I identified six such molecules, all of which were expressed in the all-polarity hair-cell samples (Table 1). Two of the candidate genes, *nrcamA* and *zgc:153911*, contain immunoglobulin domains. NrcamA, or neuronal cell adhesion molecule A, in particular, has accumulated strong evidence as a synapse-adhesion molecule (Dai et al., 2013; Demyanenko et al., 2014). Four other candidate genes, *lrrc23, phlpp1, fbxl7,* and *lrrc57*, contained leucine-rich repeated domains, which mediate synapse targeting in a number of neuronal systems (Hong et al., 2012; Shinza-Kameda et al., 2006). Interestingly, fbxl7 has been implicated in planar-cell polarity signaling in *Drosophila* via direct interactions with the molecules Hippo and Fat (Bosch et al., 2014). Additionally, leucine-rich repeat proteins have been identified as mediating target adhesion in cytonemes (Roy et al., 2014).

Two more candidate molecules, neuropilin 2b and agrin, are not adhesion molecules themselves but may act as co-receptors to influence the binding properties of other synaptic molecules. The neuropilins are receptors for semaphoring molecules and have a documented role in neural circuit assembly (Yoshida, 2012). In the neuromuscular junction, the secretion of agrin by presynaptic motor neurons alters receptor properties of their postsynaptic targets (Sanes and Lichtman, 2001). The molecule has also been documented to induce filopodia formation during synaptogenesis (Uhm et al., 2001).

In addition to the molecular cues that mediate polarity-specific hair-cell innervation, I also sought to identify candidate genes responsible for the opposing hair bundle orientation of anteriorly and posteriorly polarized hair cells. In other areas of the

nervous system, the unique fates of two cells arising from an asymmetric cell division appears to be conferred by the inheritance of the mother or daughter centriole (Wang et al., 2009). The close relationship of the centriole to the hair bundle offers the possibility that it serves as an instructive cue for hair-cell polarity. Therefore, I identified three genes, *b9d2, sdccag8,* and *cep70,* involved in ciliogenesis that are each 6-8 fold upregulated in posteriorly polarized hair cells (Dowdle et al., 2011; Insolera et al., 2014; Wilkinson et al., 2009). No such genes were found in anteriorly polarized hair cells. The gene ligand of numb protein X 2b (*Lnx2b*) was also upregulated in posteriorly polarized hair cells. Numb is a factor mediating asymmetric cell division in *Drosophila* and *C. elegans*, and Lnx2b acts as a scaffold for Numb and may mediate its degradation (Rice et al., 2001).

Figure 5-9

Candidate molecules for polarity-specific synapse targeting and hair-cell polarization

Table 1. Eight molecules with differential expression between anteriorly polarized and posteriorly polarized hair cells were identified as possible candidates for mediating afferent target selection. Table 2. Four differentially expressed molecules were associated with centriole formation or asymmetric cell division.

Table 1

Function	Gene Name	Anteriorly Polarized Hair Cells (FPKM)	Posteriorly Polarized Hair Cells (FPKM)	Fold Change	P-value	All Hair Cells (FPKM)	Full Name	Gene Ontology
Immunoglobulin adhesion domain	nrcamA	5.63	2.94	1.92	0.026	2.45	neuronal cell adhesion molecule	protein binding; protein binding; protein binding; protein binding
	zgc:153911	87.55	64.39	1.36	0.002	56.33	zgc:153911	biological_process; membrane; integral to membrane; molecular_function; protein binding
Leucine rich repeat adhesion domain	lrrc23	4.81	14.63	0.33	0.008	33.76	leucine rich repeat containing 23	biological_process; protein binding
	PHLPP1	3.56	1.72	2.07	0.040	2.03	PH domain and leucine rich repeat protein phosphatase 1	catalytic activity; protein binding
	FBXL7	0.75	2.17	0.34	0.038	1.49	F-box and leucine-rich repeat protein 7	protein ubiquitination; cytoskeleton; cytoplasm; microtubule organizing center; protein binding
	lrrc57	2.93	2.10	1.39	0.000	2.41	leucine rich repeat containing 57	biological_process; cellular_component; protein binding
Synapse targeting co-receptors	nrp2b	8.17	3.59	2.27	0.001	4.16	neuropilin 2b	cell adhesion; axon guidance; axonal fasciculation; regulation of vascular endothelial growth factor receptor signaling pathway; semaphorin receptor activity
	agrn	22.00	15.73	1.40	0.012	14.70	agrin	peripheral nervous system development; receptor clustering; G-protein coupled acetylcholine receptor signaling pathway; central nervous system development; anterior/posterior pattern specification; axonogenesis

Table 2

Function	Gene Name	Anteriorly Polarized Hair Cells (FPKM)	Posteriorly Polarized Hair Cells (FPKM)	Fold Change	P-value	All Hair Cells (FPKM)	Full Name	Gene Ontology
Cilium assembly	b9d2	0.26	1.94	0.13	0.027	1.42	B9 protein domain 2	cilium assembly; cell projection organization; cytoskeleton; cytoplasm; centrosome; cilium; cell projection; microtubule basal body; cilium axoneme; TCTN-B9D complex; gamma-tubulin binding
	sdccag8	1.13	6.30	0.18	0.035	5.07	serologically defined colon cancer antigen 8	embryo development; cytoskeleton; cytoplasm; cell junction; centriole
	cep70	0.29	2.35	0.12	0.021	7.29	centrosomal protein 70	cilium morphogenesis; epithelial cilium movement involved in determination of left/right asymmetry
Asymmetric Cell Division	lnx2b	3.32	10.01	0.33	0.012	5.63	ligand of numb-protein X 2b	protein ubiquitination; protein K48-linked ubiquitination; cellular_component; ubiquitin-protein ligase activity; zinc ion binding; metal ion binding; protein binding;

DISCUSSION

A method for targeting cell subpopulations for transcriptome analysis.

Transcriptome analysis is routinely used to discover new genes involved in cellular processes, but obtaining pure populations of cell subpopulations from an *in vivo* tissue environment is challenging. Laser-capture microdissection is one option for recovering cells of interest from an intact tissue. However, the method is laborious, requires special equipment and training, and often results in material nearby to the target cells being included in the sample. Additionally, staining, fixing, and sectioning tissue can lead to a loss of cell morphology and other phenotypic information used to identify cells (Decarlo et al., 2011).

When the desired cell type expresses a gene whose transcription is absent elsewhere in the organism, the gene's promoter may be employed to drive the production of fluorescence thereby marking the cell type for collection by fluorescence-activated cell sorting. However, cell subpopulations often lack an identified gene marker, and when they are known, the time involved in creating a line of transgenic organism is significant. Although transgenic zebrafish created by enhancer-trap screening are not reliant upon *a priori* knowledge of gene markers, their resultant patterns of transgenic expression are rarely isolated to a single cell subpopulation (Kawakami et al., 2010; Scott et al., 2007).

The kaede-based cell-collection procedure described above offers the ability to rapidly and specifically collect cell subpopulations that can be identified based on location, morphology, and other characteristics observable with a fluorescence microscope. Kaede-expressing cells undergo permanent photoconversion in response to brief exposure to ultraviolet light and a laser-scanning microscope allows single cells to

be photoconverted without significantly affecting neighboring cells. The dosage of ultraviolet light required for photoconversion does not compromise the health of the cell, alter the integrity of the RNA, or induce significant changes to the transcriptome. The thousands of available Gal4 enhancer-trap transgenic zebrafish lines and a freely available *Tg(UAS:Kaede)* line allows one to target nearly any cell in the larval zebrafish for collection and next-generation sequencing (Kawakami et al., 2010; Scott et al., 2007).

Evaluating transcriptome differences in anteriorly and posteriorly polarized hair cells.

The primary goal in analyzing the transcriptomes of anteriorly and posteriorly polarized hair cells was to identify the molecular differences that mediate polarity-specific synapse formation by afferent neurons. Specifically, I hypothesized that anteriorly and posteriorly polarized hair cells would possess markedly different levels of two or more synaptic adhesion molecules similar to the expression patterns of sidekick-1, sidekick-2, dscam, and dscamL in cell subpopulations of the chick retina (Yamagata and Sanes, 2008). I also anticipated that the transcriptomes of the two subtypes of hair cells would show few differences aside from a small set of genes mediating synapse formation and hair-bundle polarization.

However, I found hundreds of putative differences in gene expression between anteriorly and posteriorly polarized hair cells that I observed in the next-generation sequencing data. Although it is possible that these differences arose from biological or technical noise, the high reliability of hair-cell gene markers in the single-polarity data suggests instead that the data reveals true differences in their transcriptomes. This raises the possibility that the two hair-cell polarities are less mirror symmetrical than they

appear at first glance. In addition to the polarity-specific differences that have already been mentioned, I have also observed polarity-specific differences in terms of volume, shape, and orientation of the soma, as well as number of ribbon synapses, kinocilium length, and stereocilia number. In other sensory epithelia, like the murine utricle, hair cells exist as two distinct populations, type I and II, which have markedly different somatic morphologies, positions within the sensory epithelia, synaptic function, and hair bundle structure (Eatock and Songer, 2011). Likewise, the two subpopulations of PLL hair cells may also diverge significantly in their structure and function. After all, it is plausible that mechanical stimuli directed from the anterior-to-posterior of the zebrafish could have frequencies, strengths, locations, or durations that differ from mechanical stimuli traveling from posterior-to-anterior. On evolutionary timescales, the two subpopulations of sensory receptors may become tuned to their respective stimuli.

Additionally, among the synapse-targeting candidate genes, none show binary expression differences between the two types of hair cells. Instead the genes have a 1.4-3.0 fold difference. One explanation is that each hair-cell polarity bears different amounts of two or more synapse adhesion molecules, and it is the ratio of these molecules that confers biased innervation. This hypothesis is supported by the observation that afferent neurons are able to form contacts with hair cells of both polarities, including their hair-cell projections, and in a few cases, ribbon synapses.

Alternatively, the differences in adhesion protein levels on the cell membrane could arise from post-transcriptional or post-translational regulation. In this case, minimal or absent differences in gene expression could coexist with large differences in the presentation of its protein. Another possibility is that differentially expressed co-receptors

alter the binding properties of similarly expressed adhesion molecule. Therefore, determining the genes underlying selection synapse formation may require the assembly of a more exhaustive list of synapse adhesion molecules identified in the hair-cell transcriptome. Since many synapse adhesion molecules are homodimeric and other heterodimeric binding partners have been identified, the search may be narrowed down by analyzing the transcriptome of PLL afferent neurons. Published protocols allow ready access to afferent neurons for gene expression experiments by dissecting and dissociating the PLL ganglion (Sato and Takeda, 2013).

In any case, follow-up work should be performed on the identified candidate genes. As a first step, *in situ* hybridization should be used to confirm each gene's expression in hair cells and to confirm the polarity-biased expression. Zebrafish offer a cadre of genetic tools for the further evaluation of candidate genes. Morpholinos, anti-sense oligomers that bind to specific RNA sequences inhibiting their translation, provide a rapid, simple method for identifying gene loss-of-function phenotypes (Nasevicius and Ekker, 2000). Similarly, DNA constructs can be engineered and injected into zebrafish eggs for the over-expression of a gene or a dominant-negative gene isoform. Finally, there has been success in using the CRISPR-CAS system to create germline transgenic zebrafish (Hwang et al., 2013).

CHAPTER SIX
Conclusions and future directions

The foregoing research has provided novel descriptive, methodological, and experimental findings about synapse formation in the zebrafish posterior lateral line. This work includes a description of the neuromast at nanometer resolution by serial block-face electron microscopy; identifying and characterizing a previously unreported cellular behavior that may mediate hair-cell synaptogenesis; and identifying candidate molecules involved in synapse adhesion using a novel technique for performing comparative transcriptomics. Additional work remains in order to fully understand synapse formation in the lateral line and follow up on new areas of investigation identified by the research.

Serial block-face electron microscopy for the neuromast.

Serial block-face electron microscopy has recently been applied to the central nervous system, but the research described herein is the first to apply it to the zebrafish neuromast, and moreover, the first study to densely reconstruct a complete sensory unit. A number of characteristics make the neuromast highly amenable to serial block-face electron microscopy. First, the target neuromast can be readily imaged *in vivo* prior to tissue processing; I have performed up to 30 hr of multi-channel timelapse confocal imaging prior to successful SBEM imaging of the sample thus documenting the stage of differentiation of each hair cell. Second, the myotomes in the larval zebrafish serve as fiducials to facilitate homing-in on the region of interest. Third, the neuromasts' functions including sensory processing, hair-cell regeneration, synapse targeting, and planar cell polarization are confined to the approximately 70 cells contained within it. Finally, its

small diameter allows it to be captured with a half day of imaging and only a few hundred sections. Consequently, total reconstruction of the neuromast can be completed with around 1000 hours of labor, a small amount compared to other efforts.

There are numerous ways that serial block-face electron microscopy can be applied to understand various biological processes within the neuromast. First, cell contact partners are fundamental to a cell's identity and function, for instance, transmembrane delta-notch signaling between supporting cells and hair cells is essential for regulating mitosis. Subjecting neuromast samples to timelapse confocal preimaging followed by SBEM and dense reconstruction of the cell membranes would produce an exhaustive description of the neuromast cells throughout differentiation. Additionally, it may reveal previously unrecognized subpopulations of cells. Furthermore, it may reveal additional phenotypic differences between anteriorly and posteriorly polarized hair cells such as somatic volume or shape, synapse structure, or hair bundle morphology.

In terms of synapse formation, serial block-face electron microscopy could be performed in zebrafish lacking PLL afferent neurons to characterize at finer detail the structure and ultrastructure of hair-cell projections in these preparations. Additionally, should a gene candidate be identified that allows one to manipulate the presence or absence of hair-cell projections, serial block-face electron microscopy would provide an ideal method for investigating the resultant samples for a breadth of phenotypes not easily determined at the light-microscope level, including the hair cell-afferent terminal adhesion partners, detailed morphology of the ribbon synapse, and interrelationship of neuronal arbors.

Serial block-face electron microscopy can also be used to investigate the relationship of polarity-specific innervation and hair-bundle polarization. One possibility is that canonical planar-cell polarity proteins dictate the synapse-targeting phenotype of a hair cell in addition to their role in orienting the hair bundle. On the other hand, a different cell-fate determinant could mediate polarity-specific synapse formation independently of the molecular pathway controlling hair-bundle polarization. A detailed investigation of innervation in the planar-cell-polarity mutant *trilobite* could answer this question. Hair cells in this mutant zebrafish line have hair bundles that are randomly oriented with respect to the anterior-posterior axis. However, it is unknown whether each sibling cell nonetheless is innervated by different subpopulations of afferent terminals. This experiment is challenging to perform at the light-microscope level because of severe morphological defects in the mutants that make assessing innervation and carrying out mosaic neuron labeling extremely difficult. However, one could use longterm fluorescence confocal preimaging of the *trilobite* neuromast to determine hair-cell sibling pairs, and then use SBEM reconstruction to evaluate ribbon synapse innervation across siblings.

Finally, progress is being made in carrying out serial block-face electron microscopy elsewhere in the zebrafish. A relatively achievable and highly informative data set would involve performing serial block-face electron microscopy imaging from the two most anterior neuromasts to the hindbrain. Tracking the neurons from the neuromasts to the hindbrain may reveal the neuroanatomy underlying how the lateral-line organ computes the direction and rate of water currents. This would also reveal how PLL

afferent neurons, which are known to possess somatotopic organization in the hindbrain, are organized with respect to functional polarity.

Do structures analogous to hair-cell projections exist elsewhere in the nervous system?

Many cells throughout the central and peripheral nervous system face a similar challenge of matching postsynaptic partners to available presynaptic sites. The foregoing work suggests that the presynaptic site is not a passive recipient of innervation but rather is an active participant in its own partner matching. If the model that hair-cell projections act as short-range scaffolds for synapse formation is upheld, it would interesting to explore whether a similar mechanism is at work elsewhere in the nervous system. A first step is to determine whether hair cells of the zebrafish inner ear also develop transient projections following mitosis. Furthermore, cellular projections may contribute to innervation of other sensory epithelial tissue including photoreceptors of the retina and cutaneous mechanoreceptors.

Additionally, cytoplasmic extensions have previously been observed in inner-ear hair cells of higher vertebrates and mammalians. For instance, in the developing chick basilar papilla, epithelial cells committed to differentiate directly into sensory hair cells have elongations of the basal somata that extend to the basal lamina. When afferent neurons cross the basal lamina to innervate the developing organ, these basal extensions recede in tandem with the migrating nerve fibers (Whitehead and Morest, 1985). In the chick basilar papilla, regenerated hair cells also extend basal processes, which appear 2-4 hours after the cell had differentiated but not 14-24 hours or 7 days afterward (Stone and Rubel, 2000).

Other work identified basal extensions in type II hair cells of the developing and adult mouse utricle with morphological similarity to PLL hair-cell projections (Pujol et al., 2014). These utricular hair-cell processes originate from the basal soma and extend laterally above the supporting cell nuclei. Additionally, electron microscopy imaging and antibody staining experiments showed that afferent and efferent neurons form synapses on the projections. However, unlike lateral-line hair cells, the projections are present in nearly all type II hair cells, and they persist into adulthood (Pujol et al., 2014). In regenerated hair cells of the mouse utricle, processes were observed for at least 180 days after mitosis suggesting that they are stable structures (Golub et al., 2012).

The role of mouse utricular hair-cell processes has not been determined. Some work suggests that ribbon synapses increase in number into adulthood in the mouse utricle (Lysakowski, 1999), and at least in the case of the guinea pig, hair cells may also be persistently added to the mature mammalian utricle. This suggests that the axonal terminal arbor incorporates new cells throughout adulthood (Forge et al., 1993; Lambert et al., 1997; Rubel et al., 1995). It would be interesting to observe whether the utricular hair-cell processes undergo morphological change if innervation of the utricle were disrupted similar to that observed in the lateral line.

Finally, Sobkiewicz has observed what he termed spinous synapses at the bases of hair cells in the murine cochlea. The spinous synapses consisted of several micrometer-long cytoplasmic extensions from the inner hair cell bases onto which afferent and efferent neurons formed synapses. The cytoplasmic extensions emerged from the inner hair cells around postnatal day 9-10, but it is not clear whether they persisted into adulthood (Sobkowicz et al., 2002, 2003). Altogether, the previous research suggests that

zebrafish hair-cell projections are unique cellular components but that related structures are present in other hair-cell bearing sensory epithelia.

The neuromast is a model system for synapse targeting during development and homeostasis.

Previous research has shown that anteriorly and posteriorly polarized hair cells of the PLL are innervated by distinct subpopulations of afferent neurons, and furthermore, that this specificity is independent of activity across the hair-cell synapse. The present work enhances the understanding of how polarity-specific innervation arises.

First, polarity-specific synapse formation may be mediated by supporting cells or other accessory cells, which bear the guidance factors that direct partner matching to adjacent hair cells. However, a nanometer-resolution reconstruction of the cellular environment surrounding mature and immature hair-cell synapses showed that there is no intervening cell type, apart from the neuronal terminals, at the ribbon synapse. Additionally, the area directly juxtaposing the ribbon synapse showed greater specificity for polarity-appropriate neurons than did other areas of the hair cell. This suggests that polarity-specific innervation is mediated by a competitive process among neurons for access to the synaptic ribbons.

Second, polarity-specific synapses could arise if hair cells were indiscriminately innervated during immaturity and then subsequent synaptic pruning during maturity refined innervation. However, I identified the 6-14 hours following hair cell rearrangement as being a critical time for hair-cell innervation and that polarity-appropriate afferent neurons juxtapose afferent synapses at the earliest stages of contact.

Additionally, during this early stage of innervation, hair-cell projections appear to mediate synapse formation.

Finally, I have identified a variety of plausible candidate molecules that are differentially expressed in anteriorly and posteriorly polarized hair cells and may mediate polarity-specific synaptogenesis. These candidate genes will serve as a starting point for the loss-of-function and gain-of-function experiments necessary to confirm a chemoaffinity-based mechanism of synapse targeting. The hair-cell transcriptome data may also provide a means for identifying the genes underlying hair-cell projections, which are likely to be similar to factors involved in filopodia formation in other systems including nWASP, cdc42, and FAK kinase. Altogether, this work expands the repertoire of tools available for investigations of the neuromast and enhances the understanding of synapse formation in the zebrafish lateral-line organ.

APPENDIX ONE

Hair-cell markers

Gene	Cell Type Marker	Tg Line	In situ	IHC	qPCR	Other	Source
piezo1	Hair Cell		+				Low and Hudspeth (personal communication)
tmc2a	Hair Cell		+				Low and Hudspeth (personal communication)
tmc2b	Hair Cell		+				Low and Hudspeth (personal communication)
tmc4	Hair Cell		+				Low and Hudspeth (personal communication)
tmc5	Hair Cell		+				Low and Hudspeth (personal communication)
Rab3ab	Hair Cell		+	+		+	Low and Hudspeth (personal communication)
VAMP2	Hair Cell		+	+		+	Low and Hudspeth (personal communication)
VAMP8	Hair Cell		+				Low and Hudspeth (personal communication)
Syt3	Hair Cell		+				Low and Hudspeth (personal communication)
Syt7	Hair Cell		+				Low and Hudspeth (personal communication)
OTOF	Hair Cell		+	+		+	Low and Hudspeth (personal communication)
otof	Hair Cell		+	+		+	Low and Hudspeth (personal communication)
trpm7	Hair Cell		+				Low and Hudspeth (personal communication)
clasp2	Hair Cell		+				Dow and Hudspeth
amigo1	Hair Cell		+				Dow and Hudspeth
lgsf9a	Hair Cell		+				Dow and Hudspeth
Ulk1a	Hair Cell		+				Dow and Hudspeth
dachB	Hair Cell		+				Hammond et al. 2002
pvalb8	Hair Cell	+					McDermott 2010; Hsiao 2002
s100t	Hair Cell	+		+			Sandulescu 2011
cldnB	Hair Cell	+	+				Haas 2006
pou4f3	Hair Cell	+	+				DeCarvalho 2004
myo6b	Hair Cell	+	+	+			Kappler 2004; Seiler 2004
atp2b1a	Hair Cell	+	+				Thisse 2001; Go 2010
ntrk2b	Hair Cell			+			Germana 2010
bdnf	Hair Cell			+			Germana 2010
ctbp2	Hair Cell		+	+			Sheets 2011
pcdh15a	Hair Cell		+			+	Seiler 2005
slc17a8	Hair Cell		+				Obholzer 2008
NSFa	Hair Cell			+			Mo 2011

CDH23	Hair Cell			+			Blanco-Sanchez 2014
cacna1da	Hair Cell			+			Sheets 2011
synj1	Hair Cell		+				Trapani 2009
trpv4	Hair Cell		+				Mangos 2004
kal1b	Hair Cell			+		+	Ernest 2007
pcsk5a	Hair Cell		+				Babykumari 2010
pdzd7a	Hair Cell			+			Ebermann 2010
tmie	Hair Cell					+	Gleason 2009
ush1c	Hair Cell			+			Blanco-Sanchez 2014
vangl2	Hair Cell		+			+	Lopez-Schier 2006
zgc:198419	Hair Cell		+				Behra 2012
atoh1a	Hair Cell	+	+				Wibowo 2011; Ma 2008
ift88	Hair Cell			+			Blanco-Sanchez 2014
myo7aa	Hair Cell			+			Blanco-Sanchez 2014
dla	Hair Cell		+				Wibowo 2011
fat1a	Support Cell		+				Steiner 2014
fat1b	Support Cell		+				Steiner 2014
fgfr1a	Support Cell		+				Steiner 2014
fndc7	Support Cell		+				Steiner 2014
robo3	Support Cell		+				Steiner 2014
tspan1	Support Cell		+				Steiner 2014
tnks1bp1	Support Cell	+					Behra 2012
notch3	Support Cell		+				Wibowo 2011
sox2	Support Cell		+	+			Hernandez 2007; Germana 2009
c1qtnf5	Skin/Fin Cells		+				Steiner 2014
C9H2orf40	Skin/Fin Cells		+				Steiner 2014
hpdb	Skin/Fin Cells		+				Steiner 2014
pah	Skin/Fin Cells		+				Steiner 2014
ptx3b	Skin/Fin Cells		+				Steiner 2014
ucp1	Skin/Fin Cells		+				Steiner 2014
col1a1a	Skin/Fin Cells		+				Duran 2011

krt4	Skin/Fin Cells	+					Rieger 2011
cfl1l	Skin/Fin Cells		+				Thisse 2001
krt8	Skin/Fin Cells	+					Gong 2002
zgc:101000	Skin/Fin Cells		+				Thisse 2001
pak2a	Skin/Fin Cells		+				Buchner 2007
col7a1l	Skin/Fin Cells		+				Thisse 2001
col18a1	Skin/Fin Cells		+				Haftek 2003
capns1a	Skin/Fin Cells		+				Lepage 2003
anxa11b	Skin/Fin Cells		+				Thisse 2001
ssr1	Skin/Fin Cells		+				Thisse 2001
hdlbp	Skin/Fin Cells		+				Chen 2003
pfn1	Skin/Fin Cells		+				Thisse 2001
rbp4	Skin/Fin Cells		+				Tingaud-Sequeira 2006
hbbe2	Blood		+				Thisse 2001
hbae3	Blood		+				Thisse 2001
hbae1	Blood		+				Thisse 2001
elavl3	PLL Nerve Cells	+			+	+	Sato 2013
ache	PLL Nerve Cells		+				Bertrand 2001
cntnap1	PLL Nerve Cells	+					Pujol-Marti 2012
neuroD	PLL Nerve Cells				+	+	Sato 2013
stmn1b	PLL Nerve Cells				+		Sato 2013
nes	PLL Nerve Cells				+		Sato 2013
neurog1	PLL Nerve Cells				+		Sato 2013

APPENDIX TWO

Cellular projections from sensory hair cells form polarity-specific scaffolds during synaptogenesis

Eliot Dow, Kimberly Siletti, and A. J. Hudspeth

(Manuscript submitted)

Cellular projections from sensory hair cells form polarity-specific scaffolds during synaptogenesis

Eliot Dow, Kimberly Siletti, and A. J. Hudspeth

Howard Hughes Medical Institute and Laboratory of Sensory Neuroscience, The Rockefeller University, 1230 York Avenue, New York, NY 10065, USA

Running title: Hair-cell projections

Keywords: auditory system, filopodium, lateral line, ribbon synapse, vestibular system, zebrafish

Abstract

The assembly of a nervous system requires the extension of axons and dendrites to specific regions where they are matched with appropriate synaptic targets. Although the cues that guide long-range outgrowth have been characterized extensively, additional mechanisms are required to explain short-range guidance in neural development [Tessier-Lavigne and Goodman 1996]. Using a complementary combination of timelapse imaging by fluorescence confocal microscopy and serial block-face electron microscopy, we have identified a novel type of presynaptic projection that participates in the assembly of the vertebrate nervous system. Synapse formation by each hair cell of the zebrafish's lateral line occurs during a particular interval after the cell's birth. During the same period projections emerge from the cellular soma, extending toward a specific subpopulation of mature hair cells and interacting with polarity-specific afferent nerve terminals. The terminals then extend along the projections to reach appropriately matched presynaptic sites, after which the projections recede. Our results suggest that presynaptic projections act as transient scaffolds for short-range partner matching, a mechanism that may occur elsewhere in the nervous system.

Introduction

Like many other aquatic vertebrates, zebrafish possess lateral-line organs that sense water currents [Metcalf et al. 1985]. The posterior lateral line on each side of a 3-day-old larva initially comprises seven neuromasts, each of which is a compact cluster of mechanosensitive hair cells separated by supporting cells and surrounded by mantle cells [Ghysen and Dambly-Chaudiere 2004]. Hair cells occur in two oppositely polarized subpopulations, half of them sensitive to mechanical stimulation in the anterior direction and half responsive in the posterior direction [Flock and Wersäll 1962; López-Schier et al. 2004]. New hair cells arise throughout a fish's life by mitosis of precursor cells, each

of which yields one anteriorly and one posteriorly polarized hair cell [López-Schier and Hudspeth 2006]. Two hours after mitosis, the daughter cells undergo a characteristic rearrangement of their somata [Wibowo et al. 2011; Mirković et al. 2012] before passing through early, intermediate, and late stages of differentiation defined by their morphology and physiology [Wibowo et al. 2011; Kindt et al. 2012]. By 18 hr after mitosis the hair cells are functionally mature (Fig. 1f). From the posterior lateral-line ganglion, which lies immediately caudal to the ear, several bipolar neurons extend sensory axons to contact a neuromast [Metcalf et al. 1985]. Each afferent fiber receives synaptic input from hair cells of only one polarity, a specificity that occurs independently of hair-cell activity [Nagiel et al. 2008, 2009]. To learn how this synaptic pattern arises, we studied synapse formation by newly differentiated hair cells in larvae two to four days after fertilization.

Results

We first sought to determine when differentiating hair cells form synapses. By using fluorescence confocal microscopy to observe newly arisen hair cells and afferent fibers during the 20 hr following mitosis, we found that hair cells made minimal contacts with axons during rearrangement and completed the process without stably associating with afferent terminals. Immediately following rearrangement, however, contacts between hair cells and afferents increased significantly, and by 15 hr after mitosis hair cells had associated stably with terminals (Fig. 1a). We additionally confirmed that the pre- and post-synaptic markers of functional ribbon synapses, ribeye and membrane-associated guanylate kinase (MAGUK) [Sheets et al. 2011], were absent from hair cells at early maturity but appeared by late maturity (Fig. 1b-f).

Although confocal microscopy provided a useful means of assessing the period of synaptogenesis, we were unable to identify the functional polarities of the axonal terminals by that means. In order to determine whether hair cells make polarity-specific

synapses from the outset, we investigated three-dimensional reconstructions of neuromasts by serial block-face electron microscopy (SBEM; Fig. S1 and Video 1) [Denk and Horstmann 2004]. A neuronal arbor was classified as an afferent terminal if it was juxtaposed to one or more hair-cell synaptic ribbons. In contrast, an efferent terminal made extensive contact with all hair cells in a neuromast without apposition to any synaptic ribbons. An afferent terminal's functional polarity was assigned on the basis of the polarity of the mature hair cells to whose synaptic ribbons it was juxtaposed, which could be determined by the orientation of the relevant hair bundles.

We found that by early maturity only half (6/12) of the synaptic ribbons in hair cells were juxtaposed with afferent nerve fibers, indicating that synapse formation continued during this period. By late maturity nearly all synaptic ribbons (21/22) were juxtaposed with afferent terminals. At all stages of differentiation the afferent terminals at synaptic ribbons represented the polarity-appropriate subpopulation (early maturity, 6/6; late maturity, 20/21). These results indicate that synapses form 2-15 hr after mitosis and that polarity specificity commences early in this process.

Timelapse imaging of nascent hair cells during the period of synaptogenesis revealed striking projections that protruded from the base of each soma (Fig. 2a and Videos 2,3). Originating 41 ± 25 min ($N = 12$) after rearrangement and extending up to 15 μm, the projections were variously filamentous, branched, or clavate. The projections extended and retracted dynamically, but arose consistently from the same two or three sites on each soma. Fluorescent labeling revealed that the projections contained numerous actin filaments as well as Map1b indicating the presence of microtubules (Fig. 2b). Projections from nascent hair cells extended toward neighboring mature hair cells in a biased manner: the projections originating from hair cells of each polarity generally approached the vicinity of mature hair cells of the same polarity (Fig. 2c).

The neuromast is a useful model system for mechanosensory epithelia owing to its small size, microscopic accessibility, well-characterized development, and polarity-

specific innervation. To ensure that our findings with this preparation are of more general relevance, however, we also conducted timelapse imaging of the developing inner ear of the zebrafish. Hair cells in the utricle extended from their basal surfaces projections whose morphology and behavior matched those of lateral-line hair cells (Video 4). For the reasons noted above, we focused our remaining investigations on the projections of lateral-line hair cells.

Intrigued by the appearance of hair-cell projections during the period of synapse formation, we investigated more closely the interactions between projections and afferent terminals. The SBEM data, which afforded a view of the projections and their interaction partners on a nanometer scale, confirmed that hair cells extended projections during early maturity but not thereafter (Fig. 2d). Projections were observed in neither supporting cells nor mantle cells. The projections formed extensive areas of contact with afferent terminals, less contact with efferent fibers, and almost no contact with other hair cells (afferent terminals, $20.0 \pm 9.6\ \mu m^2$; efferent terminals, $3.9 \pm 3.1\ \mu m^2$; mature hair cells, $0.5 \pm 0.5\ \mu m^2$; sibling hair cells, $0.4 \pm 0.4\ \mu m^2$; $N = 4$). Although in timelapse videos we frequently observed projections extending to aggregations of afferent terminals beneath mature hair cells, SBEM reconstruction revealed that the projections were prevented from making direct contact with those cells by the intervening nerve fibers (Fig. 3a,b). Exhaustive SBEM reconstruction of other cell types did not reveal any structures that appeared to play a role in the genesis or structure of the projections (Video 5).

The terminal arbors of lateral-line afferents include immobile portions that reside beneath mature hair cells as well as thin filopodia that roam throughout the neuromast and initiate contact with nascent hair cells [Faucherre and López-Schier 2014]. These filopodia frequently extended along a hair-cell projection toward the associated soma (Fig. 3c). The SBEM reconstructions provided several examples of afferent filopodia passing directly along a projection (Fig. 3d). In fact, 94 % of the afferent filopodia that co-localized with the somata of nascent hair cells in the timelapse videos did so at sites

from which projections extended ($N = 77$ instances of co-localization at ten hair cells). The SBEM data revealed that all the contacts of early mature hair cells with afferent fibers occurred along projections (Fig. 3e). Moreover, the projections from hair cells of a given polarity contributed significantly greater areas of contact to terminals of the same functional polarity than to those of the opposite polarity (Fig. 3f). This preferential contact occurred even when the projections from hair cells of opposite polarity extended into the same aggregation of afferent neurons (Fig. S2).

Because the appearance of projections coincided with the onset of abundant contacts between hair cells and afferent terminals, we wondered whether afferent nerve fibers are necessary for the formation of projections. To address this question, we performed timelapse imaging of neuromasts in larvae whose afferent neurons had been ablated by ultraviolet irradiation of the lateral-line ganglia. SBEM data revealed a complete absence of nerve terminals in the neuromast of a treated specimen and demonstrated that the foramen in the basal lamina through which neurons normally extend from the posterior lateral-line nerve into the neuromast was closed. Projections nevertheless arose as usual shortly after the conclusion of cellular rearrangement (Fig. 3g,h). Furthermore, the projections in specimens that underwent ablation were less stable than those in samples that retained afferent terminals (Fig. 3i).

In timelapse images we often observed afferent terminals halting near the bases of projections. Upon investigating the ultrastructure of such regions by SBEM we discovered clusters of vesicles as well as immature synaptic ribbons with associated synaptic vesicles, structures nearly absent elsewhere in the cell (Fig. 4a,b). Half of the immature synaptic ribbons (6/12) were juxtaposed with afferent nerve terminals, which in each case belonged to the subpopulation of appropriate polarity. In two instances we observed sheets of hair-cell membrane embracing the juxtaposed nerve terminals as if they were clamping them in place (Fig. 4c).

The sizes of the projections varied through the course of timelapse imaging. In hair cells whose bases were stably associated with afferent terminals the projections were significantly smaller than in those without stably associated afferents (Fig. 4d). Projections also tended to be larger in specimens lacking lateral-line neurons (Fig. 4d and Video 6). In the SBEM data, projections associated at their bases with a greater number of unpaired synaptic ribbons had larger volumes. Finally, we observed that hair cells in specimens without lateral-line neurons continued to extend projections later than those in normal neuromasts (Fig. 4e). Nevertheless, mature hair cells in specimens lacking lateral-line neurons contained synaptic ribbons and vesicles.

Discussion

This study used a combination of timelapse microscopy and SBEM to identify novel cellular projections involved in innervation during the period 2-12 hr after hair-cell birth. The data suggest the following model of hair-cell innervation (Fig. 5). A nascent hair cell extends projections from its soma into the vicinity of mature hair-cell synapses nearby. Polarity-appropriate axonal terminals interact with these projections, growing along them to reach synaptic sites on the soma. Finally, after afferent terminals have reached the synaptic sites and become apposed to synaptic ribbons, the hair-cell projections retract.

Although the somata of hair cells are generally regarded as stable structures, the present evidence indicates that they participate actively in synaptogenesis. The involvement of hair-cell projections as transient scaffolds that mediate polarity-specific innervation at new synaptic sites might offer several advantages. First, the length of the projections makes them large targets for attracting contacts from afferent filopodia. Next, the presence of projections only when prospective synaptic sites are available economizes the process of innervation. Third, their linear structure provides a suitable substrate for directing afferent terminals, which fasciculate extensively with other neurites, to their

targets. Finally, the extension of projections toward nearby afferent terminals reduces a terminal's search for new synaptic sites from three dimensions to only one.

Because polarity-specific innervation of lateral-line hair cells occurs in the absence of hair-cell activity, a chemoaffinity mechanism may be responsible for partner matching (Nagiel et al., 2009). Although hair-cell projections are more likely to extend into the vicinity of mature hair cells of the same polarity, this predilection alone is unlikely to confer specific innervation inasmuch as afferent terminals of both functional polarities reside beneath mature hair cells. The chemoaffinity mechanism may instead be based in part on the preferential association of hair-cell projections with afferent terminals of the same functional polarity.

It remains to be determined whether projections mediate innervation by the homologous hair cells of the mammalian inner ear as well. Protuberances containing ribbon synapses extend from the bases of type II hair cells in the murine utricle, but unlike the cellular projections reported here they persist through life [Pujol et al. 2014]. The transient processes described here resemble the filopodia that establish morphogen gradients and exchange signaling molecules with distant targets [Hsiung et al. 2005; Ramirez-Weber and Kornberg 2011; Sanders et al. 2013; Kornberg and Roy 2014; Roy et al. 2014]. Hair-cell projections may likewise bear proteins that mediate their interactions with nerve terminals in order to achieve polarity-specific innervation.

Materials and Methods

Animal care and breeding

Experiments were conducted in accordance with the standards of Rockefeller University's Institutional Animal Care and Use Committee. Zebrafish were maintained under standard conditions [Westerfield 2000]. Embryos were raised at 28 ˚C in E3 medium (5 mM NaCl,

0.17 mM KCl, 0.33 mM $CaCl_2$, and 0.33 mM $MgSO_4$) containing 1 μg/mL methylene blue. All experiments used larvae at 2-4 days post fertilization (dpf).

The transgenic zebrafish lines included *ET4*, *Tg*(*pvalb3:Ribeye-mCherry*), *Tg*(*myo6b:actin-GFP*), *Tg(myo6b:Map1b-GFP)* and *Tg*(*hspGFF4A;UAS:nfsb-mCherry*) [Faucherre et al. 2009; Kawakami et al. 2010; West and McDermott 2011; Kindt et al. 2012].

Classification of hair cells and afferent terminals

The stage of differentiation of each hair cell was determined on the basis of morphological characteristics of the soma, apical surface, and hair bundle, fluorescence expression, and observable cellular behavior [Kindt et al. 2012]. A rearranging hair cell is tightly apposed to its sibling cell and occasionally changes position with it, fluoresces dimly in *Tg*(*myo6b:actin-GFP*) larvae, and lacks basal projections and a discernible kinocilium. An early-maturity hair cell may display anterior-posterior elongation of the soma, expresses an intermediate level of fluorescence in *Tg*(*myo6b:actin-GFP*) larvae, possesses basal projections, and has a small apical surface with a centrally situated kinocilium. A late-maturity hair cell has a soma of intermediate size, fluoresces strongly in *Tg*(*myo6b:actin-GFP*) larvae, may retain regressed basal projections, and possesses a small apical surface with a polarized kinocilium. Finally, a mature hair cell has a rotund soma with a convex base and a large apical surface with a strongly polarized kinocilium. Additional characteristics of hair-bundle morphology have been described at various stages [Kindt et al. 2012].

Live imaging of larvae

A larva at 2-4 dpf was anesthetized in 600 μM 3-aminobenzoic acid ethyl ester methanesulfonate in E3 medium and mounted in a 35 mm glass-bottomed dish in 1% low-melting-point agarose. Laser-scanning confocal imaging was performed with an

inverted Zeiss Axio Observer Z1 with an LSM 780 system equipped with a 60X oil-immersion objective lens. Neuromasts were imaged at 20 min intervals as Z-stacks acquired with 0.7 μm steps under laser excitation at 488 nm and 561 nm. Images were deconvolved with AutoQuant X3 software (Media Cybernetics), processed into maximum-intensity Z-projections or movies, and analyzed with FIJI (National Institutes of Health). Imaging of the utricule in the inner ear was performed identically to that of neuromasts. Spinning-disk confocal imaging was conducted on an inverted Zeiss Axiovert 200 with a Perkin-Elmer scanning unit and 63X water-immersion objective lens. Neuromasts were imaged as above under laser excitation at 491 nm and 561 nm. Images were processed and analyzed using FIJI. Each image depicts a plane of view tangential to the animal's surface and is oriented with anterior to the left and dorsal upward.

Image quantification

Contact between afferent terminals and nascent hair cells was judged by their colocalization in image stacks acquired by spinning-disc confocal microscopy. Ribeye and MAGUK puncta were segmented manually and their areas measured in FIJI. A projection was considered stable if between successive time points it did not retract more than 50% of its length or shift in azimuthal position by more than 30˚ as viewed along the apicobasal axis. A projection was considered for analysis only if it was clearly distinguishable from neighboring GFP-positive hair cells. As a result, approximately one-third of the projections analyzed by confocal microscopy extended toward the center of a neuromast whereas two-thirds extended toward the periphery. The epoch of projection was considered complete when the hair cell no longer extended projections exceeding 1 μm in length.

The contact areas of projections were calculated by multiplying the contact lengths measured through SBEM by the sectioning interval. Hair-cell projections were segmented and measured in deconvolved image stacks imported into Imaris (Bitplane).

Each projection was measured beginning at the dilatation of the soma that departed from the smooth contour of the cell membrane. A technician with no knowledge of the sample's identity performed the segmentation.

Ablation of posterior lateral-line ganglia

A zebrafish of the *Tg*(*hspGFF4A;UAS:nfsb-mCherry;myo6b:actin-GFP*) line was anesthetized at 2 dpf in 600 μM 3-aminobenzoic acid ethyl ester methanesulfonate in E3 medium and mounted in a 35 mm glass-bottomed dish in 1% low-melting-point agarose. The red-fluorescent posterior lateral-line ganglion was identified in a Nikon Eclipse Ti inverted widefield fluorescence microscope with a Micropoint laser-ablation system (Andor). Five high-powered shots from a coumarin 440 dye laser obliterated the ganglion. The absence of mCherry-fluorescent neurons was confirmed immediately after laser firing and 24 hr later. Efferent neurons, which pass through the ganglion, were assumed to have been ablated as well, a supposition that was confirmed by fluorescence microscopy in *Tg*(*HuC:GFP*) zebrafish and by SBEM.

Antibody labeling

For antibody labeling, 3.5 dpf *Tg*(*myo6b:actin-GFP*) larvae were fixed overnight at 4 ˚C in 4 % aqueous formaldehyde and washed in phosphate-buffered saline solution with 0.1 % Tween-20 (PBST). Nonspecific labeling was blocked for 1 hr at room temperature with 2 mg/mL bovine serum albumin in PBST before exposure to the primary antibody overnight at 4 ˚C. After a wash, an AlexaFluor 568 anti-mouse secondary antibody was applied for 4 hr at room temperature. Pan-MAGUK antibody (NeuroMab) was used at a dilution of 1:500, mouse anti-acetylated tubulin (Sigma-Aldrich) at 1:500, and AlexaFluor 568-conjugated anti-mouse secondary antibody (Life Technologies) at 1:500. Imaging was performed on an Olympus IX81 confocal microscope with a Fluoview FV1000 laser-scanning system.

Tissue preparation for electron microscopy

Serial blockface electron microscopy of an entire larval neuromast requires that sectioning commence at one margin of the structure and continue through its complete extent of about 40 μm. The data-acquisition procedure is time-consuming and expensive, however, so it is useful to have a means of restricting the sectioning as much as possible. As it progresses from behind the otic vesicle to the tail, the primary lateral-line primordium of the larval zebrafish typically deposits seven neuromasts on each side of the body. Our studies generally involved the third through sixth of these receptor organs, which could readily be identified and studied at the level of compound and confocal microscopy. All but one of the serial blockface electron microscopy specimens underwent timelapse fluorescence confocal microscopy imaging of the neuromast for lengths of time ranging from 4-28 hr. Within minutes after the conclusion of confocal imaging of a 4 dpf *Tg*(*myo6b:actin-GFP*) larva, we removed the animal from 1% low melting-point agarose and anesthetized it in a 600 μM solution of 3-aminobenzoic acid ethyl ester methanesulfonate. The fish was fixed for 18 hr at 4 ˚C in 200 mM glutaraldehyde, 400 mM formaldehyde, 75 mM sodium cacodylate, 10 mM sucrose, and 1 mM $CaCl_2$. To facilitate the subsequent localization of the cells of interest we photographed the preparation at a magnification great enough to reveal the relevant neuromast, but low enough to include several myomeres and landmarks such as melanocytes. The tail was cut transversely 200 μm posterior to the target neuromast and washed in 75 mM sodium cacodylate, 10 mM sucrose, and 1 mM $CaCl_2$.

To enhance the contrast of the specimen, it was postfixed for 1.5 hr at 4 ˚C in 80 mM OsO_4, 75 mM sodium cacodylate, 10 mM sucrose, 35 mM K^+ ferrocyanide, and 1 mM $CaCl_2$. Following a wash in distilled water and treatment for 30 min at 60 ˚C with 100 mM thiocarbohydrazide, the specimen was again washed in distilled water and treated with 80 mM OsO_4 for 1 hr at room temperature. After the sample had been rinsed

in distilled water, it was incubated for 16 hr at 4 ˚C in 25 mM uranyl acetate. Washes in distilled water were followed by treatment for 30 min at 60 ˚C in 20 mM lead (II) nitrate dissolved in 30 mM L-aspartic acid adjusted to pH 3.5 with 25 mM KOH. After washing, the specimen was dehydrated in a graded series of ethanol concentrations culminating in immersion in 100 % ethanol twice for 45 min at room temperature. The sample was then transferred to propylene oxide twice for 45 min.

Each specimen was placed for 24 hr in an isovolumetric mixture of propylene oxide and embedding plastic, then transferred to pure plastic mixture and gently stirred for 24 hr before being placed into a 2 mm layer of plastic and cured in a vacuum oven for 48 hr at 60 ˚C. The embedded sample was trimmed and glued onto a stub for sectioning. Owing to the flat surface of the preparation, it was readily possible to image an embedded specimen. Because of the intense metal deposition, however, transillumination was not possible. It was therefore necessary to locate the appropriate neuromast by use of landmarks such as the ends of fins prior to the heavy-metal treatments. The specimen was transected two or three myomeres caudal to the relevant neuromast and secured at its rostral end with epoxy glue to an epoxy specimen capsule held in a microtome chuck.

We next sectioned the face of the mounted plastic block at 1 μm intervals and stained the semithin sections with ethanolic toluidine blue and basic fuchsin. Three techniques helped to determine when sectioning had proceeded to the point at which serial blockface electron microscopy should commence. First, cellular landmarks such as melanocytes were apparent in sections, and their positions and shapes could be compared with the images of live or fixed specimens before metal impregnation. Next, owing to the volcano-like shape of a neuromast, it was sometimes possible to see a slight bulging of the skin as the target was neared. Finally, and most importantly, the chevrons of successive myomeres provided a quantitative metric of the progress of sectioning.

In most semithin transverse sections, two myomeres are apparent on each side of the body. Because the myomeres are arranged in a forward-pointing arrowhead

configuration, sectioning in a caudal-to-rostral direction first encounters the barbed ends of each myomere at the dorsal and ventral larval margins. As sectioning progresses, the cross-sectional area of that myomere grows as its boundaries extend toward the horizontal midline. The adjacent but more caudal myomere meanwhile displays a complementray decrease in area, and at some level the pointed end of that myomere shrinks to nothing along the horizontal midline. At that point the more rostral myomere reaches its maximal cross-sectional area and the first traces of the next more rostral myomere appear at the dorsal and ventral edges of the specimen. As sectioning continues, the sequence commences anew.

We made use of the progression of myomere boundaries by noting in the live and aldehyde-fixed specimen at what level the caudal edge of a neuromast lay with respect to the underlying myomeres. Semithin sectioning could then continue until the cross-sectional profile of the myomere posterior to the neuromast had reached the appropriate size, halting approximately 5 μm posterior to the target neuromast. Finally, the block face was trimmed to approximately 200 μm x 200 μm to exclude extraneous tissue and submitted for serial blockface electron microscopy.

Serial block-face electron microscopy

Four initial samples embedded in EMbed-812 were imaged by Renovo Neural, Inc. on a Zeiss Sigma VP scanning electron microscope with a Gatan 3View high-precision ultramicrotome. As the ultramicrotome cut the block face at 50-60 nm increments, images were acquired in high-vacuum mode with a lateral resolution of 5 nm x 5 nm per pixel. Overnight imaging resulting in 700-1000 consecutive images of the tissue sample, which were aligned using the SIFT algorithm of FIJI. Five additional samples embedded in Durcapan were imaged at The Rockefeller University Electron Microscopy Resource Center with a Zeiss Merlin high-vacuum scanning electron microscope with a Gatan 3View2XP camera. The ultramicrotome cut the block face at 30 nm increments with a

lateral resolution of 6 nm X 6 nm per pixel. Alignment was performed with Digital Micrograph software.

One data set that included a nearly complete neuromast was chosen for complete reconstruction of the cell membranes. Data-annotation technicians were identified through Craigslist and passed a work-sample test before being hired. Each cell in the neuromast was given a unique identification number and the annotator responsible was provided a set of starting coordinates. The cell was reconstructed on the user's computer by outlining its plasmalemma across serial sections with the free software Reconstruct [Fiala 2004]. Challenging areas for annotation were noted and evaluated by the first author, leaving no areas of significant ambiguity. Cell contours were compiled into a master file that was twice checked independently for accuracy. Surfaces of the cells were rendered from contours in Reconstruct, after which additional rendering and post-production were performed in MeshLab and Blender [Blender Foundation 2014]. Volume and distance measurements were performed in Reconstruct and measurements of contact areas were conducted in FIJI.

Statistical analysis

The significance of pairwise differences between groups of samples was computed by Student's two-tailed *t*-tests. Significance is denoted in graphs as follows: ***, $p < 0.001$; **, $p < 0.01$; *, $p < 0.05$.

Acknowledgments

We thank K. Kawakami for the *Tg*(*hspGFF4A*) zebrafish line, Nadine Soplop of the Electron Microscopy Resource Center for the careful conduct of SBEM, and the members of our research group for comments on the manuscript. Zebrafish care was provided by Adedeji Afolalu and Nathan McKenney. Confocal microscopy experiments

were conducted at the Bio-Imaging Resource Center. The annotation of SBEM data was capably performed by Nate Aiken, Kattya Gibbs, Dinara Guliyeva, Sajjad Hossain, David Kahler, and Anh Ung. Kattya Gibbs and Dinara Guliyeva additionally contributed to making figures and Sajjad Hossain helped make figures and performed data analysis. ED was supported by the NINDS through a Ruth L. Kirschstein National Research Service Award (DC013468) and by the NIGMS through the Medical Scientist Training Program (GM07739) and KS by a grant (DC014212) from the National Institutes of Health. AJH is an Investigator of Howard Hughes Medical Institute.

References

Blender Foundation. 2014. Blender - a 3D modeling and rendering package v. 2.72b (Blender Institute, Amsterdam).

Denk W, Horstmann H. 2004. Serial block-face scanning electron microscopy to reconstruct three-dimensional tissue nanostructure. *PLoS Biol* **2:** e329.

Faucherre A. Lopez-Schier H. 2014. Dynamic neuroanatomy at subcellular resolution in the zebrafish. *Meth Mol Biol* **1082:** 187-195.

Faucherre A, Pujol-Marti J, Kawakami K, Lopez-Schier H. 2009. Afferent neurons of the zebrafish lateral line are strict selectors of hair-cell orientation. *PLoS One* **4:** e4477.

Fiala JC. Reconstuct: a free editor for serial section microscopy. 2004. *J Microsc* **218:** 52-61.

Flock Å, Wersäll J. 1962. A study of the orientation of the sensory hairs of the receptor cells in the lateral line organ of fish, with special reference to the function of the receptors. *J Cell Bio* **15:** 19-27.

Ghysen A, Dambly-Chaudiere C. 2004. Development of the zebrafish lateral line. *Curr Opin Neurobiol* **14:** 67-73.

Hsiung F, Ramirez-Weber Fa, Iwaki DD, Kornberg TB. 2005. Dependence of *Drosophila* wing imaginal disc cytonemes on Decapentaplegic. *Nature* **437:** 560-563.

Kawakami, K. *et al*. 2010. zTrap: zebrafish gene trap and enhancer trap database. *BMC Dev Biol* **10:** 105 (2010).

Kindt KS, Finch G, Nicolson T. 2012. Kinocilia mediate mechanosensitivity in developing zebrafish hair cells. *Develop Cell* **23:** 329-341.

Kornberg TB, Roy S. 2014. Cytonemes as specialized signaling filopodia. *Development* **141:** 729-736.

López-Schier H, Starr CJ, Kappler JA, Kollmar R, Hudspeth AJ. 2004. Directional cell migration establishes the axes of planar polarity in the posterior lateral-line organ of the zebrafish. *Develop Cell* **7:** 401-412.

López-Schier H, Hudspeth AJ. 2006. A two-step mechanism underlies the planar polarization of regenerating sensory hair cells. *Proc Natl Acad Sci USA* **103:** 18615-18620.

Metcalfe W, Kimmel C, Schabtach, E. 1985. Anatomy of the posterior lateral line system in young larvae of the zebrafish. *J. Comp. Neurol.* **233:** 377-389.

Mirković I, Pylawka, S, Hudspeth AJ. 2012. Rearrangements between differentiating hair cells coordinate planar polarity and the establishment of mirror symmetry in lateral-line neuromasts. *Biol Open* **1:** 498-505.

Nagiel A, Andor-Ardó D, Hudspeth AJ. 2008. Specificity of afferent synapses onto plane-polarized hair cells in the posterior lateral line of the zebrafish. *J Neurosci* **28:** 8442-8453.

Nagiel A, Patel SH, Andor-Ardó D, Hudspeth AJ. 2009. Activity-independent specification of synaptic targets in the posterior lateral line of the larval zebrafish. *Proc Natl Acad Sci USA* **106:** 21948-21953.

Pujol R, Pickett SB, Nguyen TB, Stone JS. 2014. Large basolateral processes on type II hair cells are novel processing units in mammalian vestibular organs. *J Compe Neurol* **522:** 3141-3159.

Ramirez-Weber FA, Kornberg TB. 1999. Cytonemes: cellular processes that project to the principal signaling center in *Drosophila* imaginal discs. *Cell* **97:** 599-607.

Roy S, Hsiung F, Kornberg TB. 2011. Specificity of *Drosophila* cytonemes for distinct signaling pathways. *Science* **332:** 354-358.

Roy S, Huang H, Liu S, Kornberg TB. 2014. Cytoneme-mediated contact-dependent transport of the *Drosophila* decapentaplegic signaling protein. *Science* **343:** 1244624 (2014).

Sanders TA, Llagostera E, Barna M. 2013. Specialized filopodia direct long-range transport of SHH during vertebrate tissue patterning. *Nature* **497:** 628-632.

Sheets L, Trapani JG, Mo W, Obholzer N, Nicolson T. 2011. Ribeye is required for presynaptic Ca(V)1.3a channel localization and afferent innervation of sensory hair cells. *Development* **138:** 1309-1319.

Tessier-Lavigne M, Goodman CS. 1996. The molecular biology of axon guidance. *Science* **274:** 1123-1132.

West, MC, McDermott BM Jr. 2011. Ribeye a-mCherry fusion protein: a novel tool for labeling synaptic ribbons of the hair cell. *J Neurosci Meth* **197:** 274-278.

Westerfield M. 2000. *The Zebrafish Book: A Guide for the Laboratory Use of Zebrafish (Danio rerio)*, Fourth Edition. (University of Oregon Press).

Wibowo I, Pinto-Teixeira F, Satou C, Higashijima S, López-Schier H. 2011. Compartmentalized Notch signaling sustains epithelial mirror symmetry. *Development* **138:** 1143-1152.

Figures

Figure 1. Hair cells form synapses 2-15 hr after mitosis. (*A*) The fraction of nascent hair cells making contact with afferent terminals (blue) rises briskly following cellular rearrangement. Although the contacts are transitory at the outset, their duration increases progressively until by 15 hrs after mitosis the slope of the line approaches unity, indicating complete stability (red). Time is denoted in hours after mitosis. The grey band marks the period of cellular rearrangement and the vertical dashed line marks the emergence of projections ($N = 30$). (*B*-*E*) Ribeye (*B*,*D*) and MAGUK (*C*,*E*) puncta (arrowheads) appear in late-maturity and full-maturity hair cells (magenta), but are absent from rearranging cells and early-maturity cells (asterisks in *B*,*C*) ($p < 0.0001$ for *D* and *E*; for D, $N = 8$, 34, 47, and 176 measurements for the respective hair-cell stages; for *E*, $N = 8$, 16, 16, and 58 measurements). (*F*) A timeline of hair-cell differentiation. The magenta box denotes the extension of projections from nascent hair cells from shortly after their rearrangement until stable synapses have formed (see Figs. 2-4).

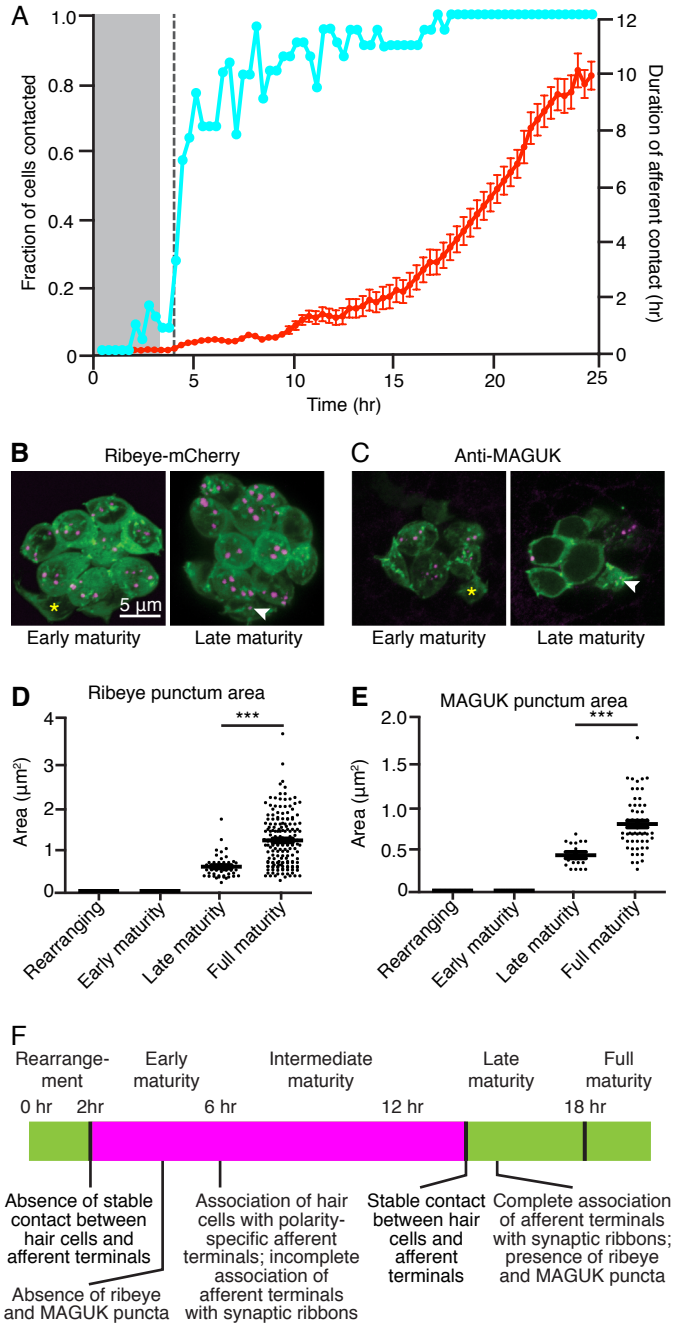
A
Fraction of cells contacted
Duration of afferent contact (hr)
Time (hr)
B
Ribeye-mCherry
5 µm
Early maturity
Late maturity
C
Anti-MAGUK
Early maturity
Late maturity
D
Ribeye punctum area
Area (µm²)
***
Rearranging
Early maturity
Late maturity
Full maturity
E
MAGUK punctum area
Area (µm²)
***
Rearranging
Early maturity
Late maturity
Full maturity
F
Rearrange-ment
Early maturity
Intermediate maturity
Late maturity
Full maturity
0 hr
2hr
6 hr
12 hr
18 hr
Absence of stable contact between hair cells and afferent terminals
Absence of ribeye and MAGUK puncta
Association of hair cells with polarity-specific afferent terminals; incomplete association of afferent terminals with synaptic ribbons
Stable contact between hair cells and afferent terminals
Complete association of afferent terminals with synaptic ribbons; presence of ribeye and MAGUK puncta

Figure 2. Nascent hair cells extend dynamic basal projections. (*A*) Timelapse imaging by fluorescence confocal microscopy of hair cells expressing GFP fused to actin shows the emergence of a basal projection (arrowheads) shortly after the completion of rearrangement. Times are denoted in minutes from the end of rearrangement. (*B*) In a cell expressing the actin-GFP fusion protein, hair-cell projections (arrowheads) contain Map1b (green) suggesting the presence of microtubules. The scale accords with that in panel *A*. (*C*) Projections extend predominantly toward mature hair cells of the same polarity and occasionally toward a sibling cell or a non-hair cell ($p < 0.0001$ for both group comparisons; $N = 9$ for anteriorly polarized hair cells and $N = 12$ for posteriorly polarized cells). (*D*) A basal view of an SBEM reconstruction of all the hair cells in one neuromast shows that early-maturity hair cells (asterisks) but not late-maturity or full-maturity hair cells bear projections. The plane of view is tangential to the larval surface.

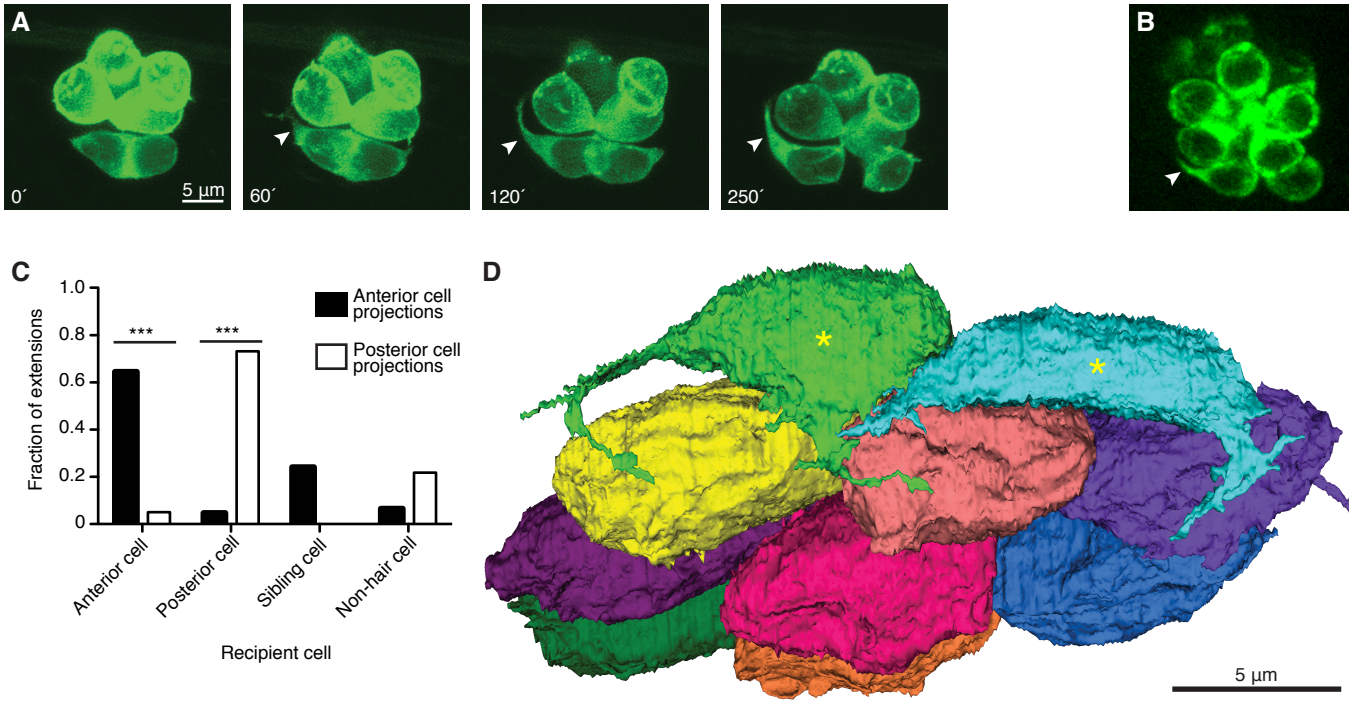
A
0´
5 µm
60´
120´
250´
B
C
1.0
0.8
0.6
0.4
0.2
0
Fraction of extensions
***
***
Anterior cell projections
Posterior cell projections
Anterior cell
Posterior cell
Sibling cell
Non-hair cell
Recipient cell
D
5 µm

Figure 3. Afferent neurons traverse projections that extend to mature synapses. (*A*) An SBEM reconstruction shows a hair-cell projection (green) extending into an aggregation of variously colored axonal terminals beneath mature ribbon synapses made by another hair cell (yellow). (*B*) In a frame from a timelapse sequence, a projection (arrowhead) extends toward a presumptive ribbon synapse (asterisk). (*C*) A series of timelapse confocal images shows extension of an afferent terminal along a projection (arrowheads). Times are denoted in minutes after rearrangement. (*D*) A reconstructed afferent terminal (magenta) traverses a hair-cell projection (cyan). (*E*) An SBEM reconstruction demonstrates that all neurons contact the nascent cell soma on its two projections (asterisks). (*F*) Projections arising from anteriorly and posteriorly polarized hair cells make the greatest areas of contact with afferent neurons of the same polarity ($p < 0.02$; $N = 4$). (*G*) An unusually large projection (arrowhead) forms in the absence of lateral-line neurons. (*H*) The reconstructed sibling hair cells from a larvae whose lateral-line ganglion had been ablated exhibit numerous and lengthy projections. (*I*) In the absence of lateral-line neurons, projections show reduced stability ($p < 0.01$; $N = 12$ and 11).

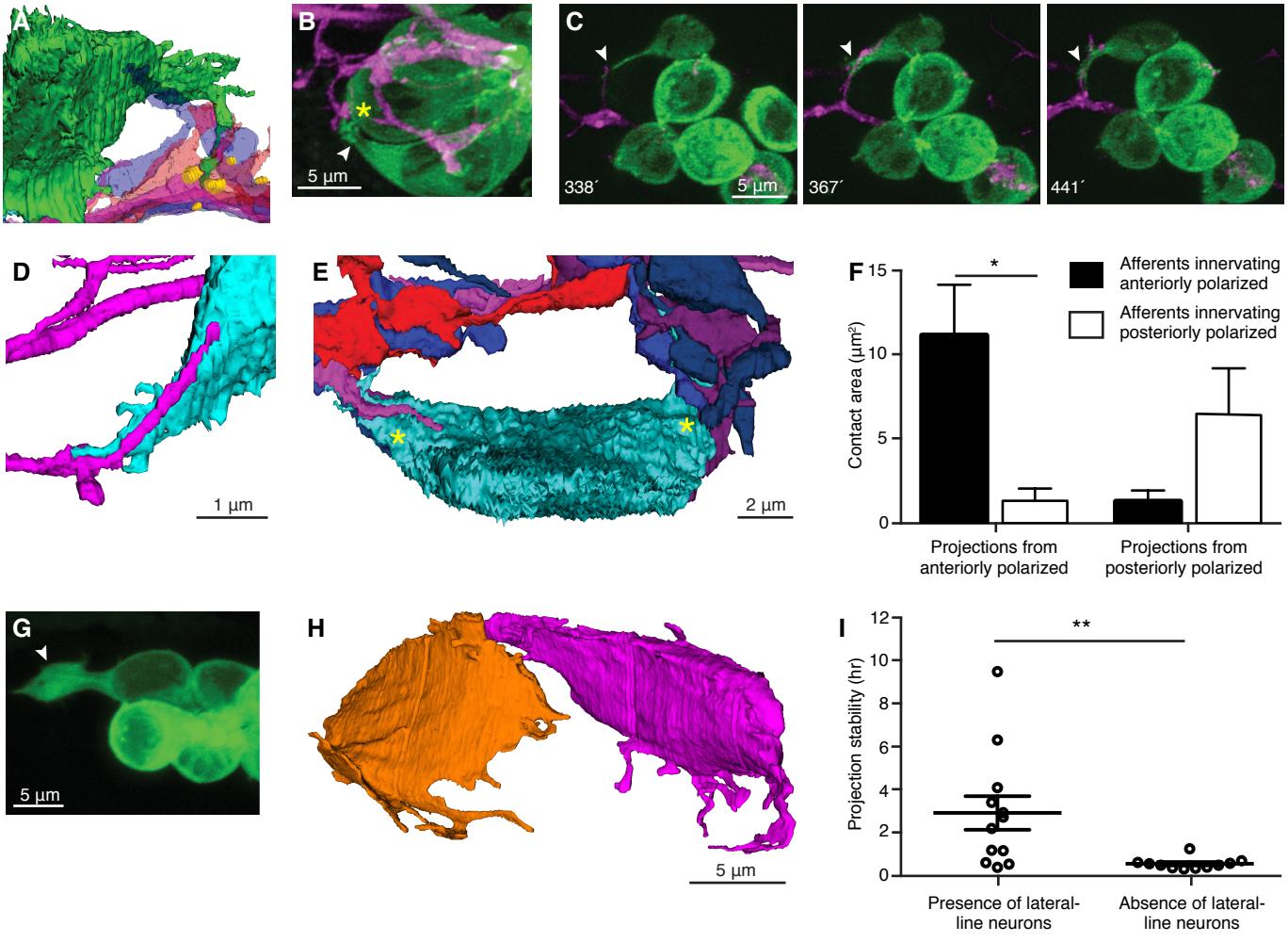
A
B
5 µm
C
338´
5 µm
367´
441´
D
1 µm
E
2 µm
F
15
10
5
0
Contact area (µm²)
*
Afferents innervating anteriorly polarized
Afferents innervating posteriorly polarized
Projections from anteriorly polarized
Projections from posteriorly polarized
G
5 µm
H
5 µm
I
12
10
8
6
4
2
0
Projection stability (hr)
**
Presence of lateral-line neurons
Absence of lateral-line neurons

Figure 4. Retraction of projections is associated with stable afferent contact. (*A*) An SBEM image shows an immature synaptic ribbon (arrowhead) within a hair-cell projection (blue outline). (*B*) In a reconstruction of the sibling hair cells from a recent division, synaptic ribbons (red) cluster at the sites from which projections emerge (N=10). In this basal view, the partially developed hair bundles are apparent at the cells' apical ends (asterisk). (*C*) An afferent terminal of the functionally appropriate subpopulation (green) contacts immature synaptic ribbons (red) on a hair-cell projection (blue). A sheet of hair-cell membrane (asterisk) folds over the afferent terminal. (*D*) Enlarged projections are associated with the absence of stable nerve contacts ($p < 0.001$) or of lateral-line neurons ($p < 0.0001$; $N = 10$, 12, and 11). (*E*) The total period during which projections emerge from hair cells increases in the absence of lateral-line neurons ($p < 0.01$; $N = 23$ and 18).

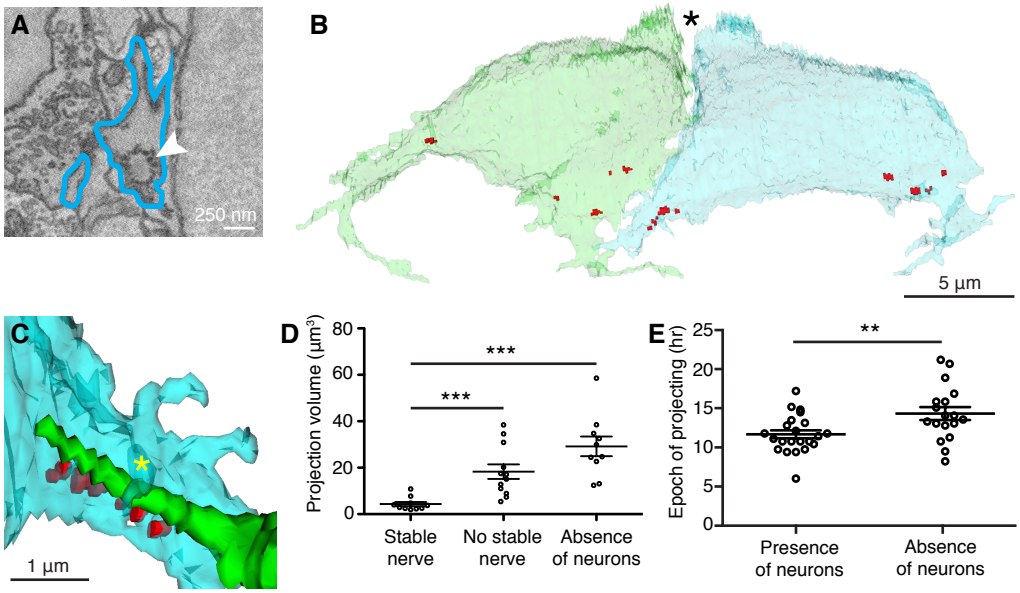
A
250 nm
B
*
5 µm
C
*
1 µm
D
Projection volume (µm³)
80
60
40
20
0
***
***
Stable nerve
No stable nerve
Absence of neurons
E
Epoch of projecting (hr)
25
20
15
10
5
0
**
Presence of neurons
Absence of neurons

Figure 5. Diagram of a projection-based model of hair-cell innervation. (*A*) During their rearrangement, hair cells make few transient contacts and no stable contacts with afferent terminals. (*B*) Following the completion of rearrangement, hair cells develop basal projections. (*C*) The projections extend toward aggregations of afferent neurons at neighboring hair-cell synapses. (*D*) Filopodia from afferent terminals extend along the projections toward the hair-cell somata. (*E*) Afferent filopodia reach the available presynaptic sites at the bases of the projections. (*F*) Afferent terminals form stable contacts at presynaptic sites and the hair-cell projections retract.

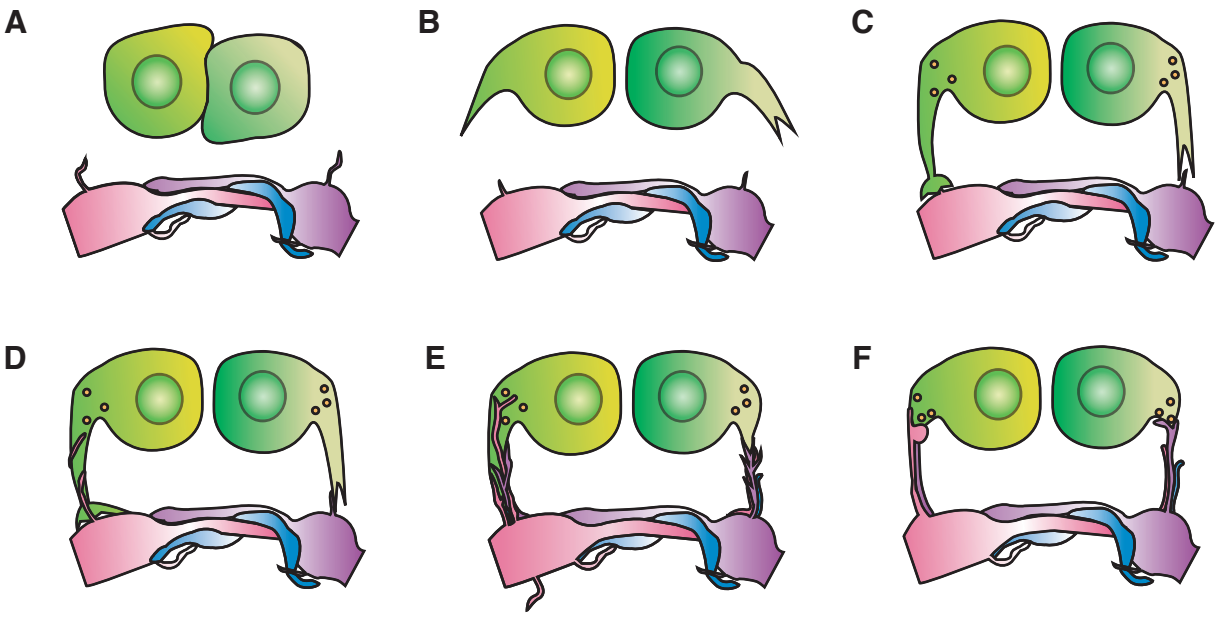
A
B
C
D
E
F

REFERENCES

Alexandre, D., and Ghysen, A. (1999). Somatotopy of the lateral line projection in larval zebrafish. Proceedings of the National Academy of Sciences of the United States of America *96*, 7558-7562.

Ando, R., Hama, H., Yamamoto-Hino, M., Mizuno, H., and Miyawaki, A. (2002). An optical marker based on the UV-induced green-to-red photoconversion of a fluorescent protein. Proceedings of the National Academy of Sciences of the United States of America *99*, 12651-12656.

Ango, F., Wu, C., Van der Want, J.J., Wu, P., Schachner, M., and Huang, Z.J. (2008). Bergmann Glia and the Recognition Molecule CHL1 Organize GABAergic Axons and Direct Innervation of Purkinje Cell Dendrites. PLoS Biology *6*, 739-756.

Azevedo, F.A., Carvalho, L.R., Grinberg, L.T., Farfel, J.M., Ferretti, R.E., Leite, R.E., Jacob Filho, W., Lent, R., and Herculano-Houzel, S. (2009). Equal numbers of neuronal and nonneuronal cells make the human brain an isometrically scaled-up primate brain. J Comp Neurol *513*, 532-541.

Batista-Brito, R., and Fishell, G. (2009). Chapter 3: The Developmental Integration of Cortical Interneurons into a Functional Network. *87*, 81-118.

Behra, M., Gallardo, V.E., Bradsher, J., Torrado, A., Elkahloun, A., Idol, J., Sheehy, J., Zonies, S., Xu, L., Shaw, K.M., *et al*. (2012). Transcriptional signature of accessory cells in the lateral line, using the Tnk1bp1:EGFP transgenic zebrafish line. BMC Developmental Biology *12*, 6.

Bertrand, C., Chatonnet, A., Takke, C., Yan, Y.L., Postlethwait, J., Toutant, J.P., and Cousin, X. (2001). Zebrafish acetylcholinesterase is encoded by a single gene localized on linkage group 7. The Journal of Biological Chemistry *276*, 464-474.

Blanco-Sanchez, B., Clement, A., Fierro, J., Jr., Washbourne, P., and Westerfield, M. (2014). Complexes of Usher proteins preassemble at the endoplasmic reticulum and are required for trafficking and ER homeostasis. Disease Models & Mechanisms *7*, 547-559.

Bosch, J.A., Sumabat, T.M., Hafezi, Y., Pellock, B.J., Gandhi, K.D., and Hariharan, I.K. (2014). The Drosophila F-box protein Fbxl7 binds to the protocadherin Fat and regulates Dachs localization and Hippo signaling. eLife *3*, e03383.

Bricaud, O., Chaar, V., Dambly-Chaudiere, C., and Ghysen, A. (2001). Early Efferent Innervation of the Zebrafish Lateral Line. The Journal of Comparative Neurology *434*, 253-261.

Briggman, K.L., Helmstaedter, M., and Denk, W. (2011). Wiring specificity in the direction-selectivity circuit of the retina. Nature *471*, 183-188.

Brose, K., Bland, K., Wang, K.H., Arnott, D., Henzel, W., Goodman, C.S., Tessier-Lavigne, M., and Kidd, T. (1999). Slit Proteins Bind Robo Receptors and Have an Evolutionarily Conserved Role in Repulsive Axon Guidance. Cell *96*, 795-806.

Buchner, D.A., Su, F., Yamaoka, J.S., Kamei, M., Shavit, J.A., Barthel, L.K., McGee, B., Amigo, J.D., Kim, S., Hanosh, A.W., *et al*. (2007). pak2a mutations cause cerebral hemorrhage in redhead zebrafish. Proceedings of the National Academy of Sciences of the United States of America *104*, 13996-14001.

Chan, S., Zheng, H., Su, M., Wilk, R., Killeen, M., Hedgecock, E., and Culotti, J. (1996). UNC-40, a C. elegans Homolog of DCC (Deleted in Colorectal Cancer) Is Required in Motile Cells Responding to UNC-6 Netrin Cues. Cell *87*, 187-195.

Chitramuthu, B.P., Baranowski, D.C., Cadieux, B., Rousselet, E., Seidah, N.G., and Bennett, H.P. (2010). Molecular cloning and embryonic expression of zebrafish PCSK5 co-orthologues: functional assessment during lateral line development. Developmental Dynamics *239*, 2933-2946.

Cruickshanks, K.J., Wiley, T.L., Tweed, T.S., Klein, B.E.K., Klein, R., Perlman, J.A., and Nondahl, D.M. (1998). Prevalence of Hearing Loss in Older Adults in Beaver Dam, Wisconsin. American Journal of Epidemiology *148*, 879-886.

Dai, J., Buhusi, M., Demyanenko, G.P., Brennaman, L.H., Hruska, M., Dalva, M.B., and Maness, P.F. (2013). Neuron glia-related cell adhesion molecule (NrCAM) promotes topographic retinocollicular mapping. PLoS One *8*, e73000.

De Felipe, J., Marco, P., Busturia, I., and Merchan-Perez, A. (1999). Estimation of the number of synapses in the cerebral cortex: methodological considerations. Cerebral Cortex *9*, 722-732.

Decarlo, K., Emley, A., Dadzie, O., and Mahalingam, M. (2011). Laser Capture Microdissection: Methods and Protocols. Methods in molecular biology *755*, 1-15.

DeCarvalho, A.C., Cappendijk, S.L., and Fadool, J.M. (2004). Developmental expression of the POU domain transcription factor Brn-3b (Pou4f2) in the lateral line and visual system of zebrafish. Developmental Dynamics *229*, 869-876.

Dell, A.L., Fried-Cassorla, E., Xu, H., and Raper, J.A. (2013). cAMP-induced expression of neuropilin1 promotes retinal axon crossing in the zebrafish optic chiasm. The Journal of Neuroscience *33*, 11076-11088.

Demyanenko, G.P., Mohan, V., Zhang, X., Brennaman, L.H., Dharbal, K.E., Tran, T.S., Manis, P.B., and Maness, P.F. (2014). Neural Cell Adhesion Molecule NrCAM

Regulates Semaphorin 3F-Induced Dendritic Spine Remodeling. The Journal of neuroscience : the official journal of the Society for Neuroscience *34*, 11274-11287.

Denk, W., and Horstmann, H. (2004). Serial block-face scanning electron microscopy to reconstruct three-dimensional tissue nanostructure. PLoS Biol *2*, e329.

Dickson, B.J., and Gilestro, G.F. (2006). Regulation of commissural axon pathfinding by slit and its Robo receptors. Annual Review of Cell and Developmental Biology *22*, 651-675.

Dowdle, W.E., Robinson, J.F., Kneist, A., Sirerol-Piquer, M.S., Frints, S.G., Corbit, K.C., Zaghloul, N.A., van Lijnschoten, G., Mulders, L., Verver, D.E., *et al*. (2011). Disruption of a ciliary B9 protein complex causes Meckel syndrome. American Journal of Human Genetics *89*, 94-110.

Duran, I., Mari-Beffa, M., Santamaria, J.A., Becerra, J., and Santos-Ruiz, L. (2011). Actinotrichia collagens and their role in fin formation. Developmental Biology *354*, 160-172.

Durand, C.M., Betancur, C., Boeckers, T.M., Bockmann, J., Chaste, P., Fauchereau, F., Nygren, G., Rastam, M., Gillberg, I.C., Anckarsater, H., *et al*. (2007). Mutations in the gene encoding the synaptic scaffolding protein SHANK3 are associated with autism spectrum disorders. Nat Genet *39*, 25-27.

Eatock, R.A., and Songer, J.E. (2011). Vestibular hair cells and afferents: two channels for head motion signals. Annual Review of Neuroscience *34*, 501-534.

Ebermann, I., Phillips, J.B., Liebau, M.C., Koenekoop, R.K., Schermer, B., Lopez, I., Schafer, E., Roux, A.F., Dafinger, C., Bernd, A., *et al*. (2010). PDZD7 is a modifier of retinal disease and a contributor to digenic Usher syndrome. The Journal of Clinical Investigation *120*, 1812-1823.

Egea, J., and Klein, R. (2007). Bidirectional Eph-ephrin signaling during axon guidance. Trends in Cell Biology *17*, 230-238.

Ernest, S., Guadagnini, S., Prevost, M.C., and Soussi-Yanicostas, N. (2007). Localization of anosmin-1a and anosmin-1b in the inner ear and neuromasts of zebrafish. Gene Expression Patterns *7*, 274-281.

Faucherre, A., Baudoin, J.P., Pujol-Marti, J., and Lopez-Schier, H. (2010). Multispectral four-dimensional imaging reveals that evoked activity modulates peripheral arborization and the selection of plane-polarized targets by sensory neurons. Development *137*, 1635-1643.

Faucherre, A., and Lopez-Schier, H. (2014). Dynamic neuroanatomy at subcellular resolution in the zebrafish. Methods in Molecular Biology *1082*, 187-195.

Faucherre, A., Pujol-Marti, J., Kawakami, K., and Lopez-Schier, H. (2009). Afferent neurons of the zebrafish lateral line are strict selectors of hair-cell orientation. PLoS One *4*, e4477.

Fiala, J.C. (2004). Reconstuct: a free editor for serial section microscopy. Journal of Microscopy *218*, 52-61.

Flock, A., and Wersall, J. (1962). A study of the orientation of the sensory hairs of the receptor cells in the lateral line organ of fish, with special reference to the function of the receptors. The Journal of Cell Biology *15*, 19-27.

Forge, A., Li, L., Corwin, J., and Nevill, G. (1993). Ultrastructural evidence for hair cell regeneration in the mammalian inner ear. Science *259*, 1616-1619.

Fox, M.A., and Umemori, H. (2006). Seeking long-term relationship: axon and target communicate to organize synaptic differentiation. Journal of Neurochemistry *97*, 1215-1231.

Frisen, J., Yates, McLaughlin, T., Friedman, G.C., O'Leary, D., and Barbacid, M. (1998). Ephrin-A5 (AL-1/RAGS) Is Essential for Proper Retinal Axon Guidance and Topographic Mapping in the Mammalian Visual System. Neuron *20*, 235-243.

Fuchs, P.A., Glowatzki, E., and Moser, T. (2003). The afferent synapse of cochlear hair cells. Current Opinion in Neurobiology *13*, 452-458.

Gauthier, J., Spiegelman, D., Piton, A., Lafreniere, R.G., Laurent, S., St-Onge, J., Lapointe, L., Hamdan, F.F., Cossette, P., Mottron, L., *et al*. (2009). Novel de novo SHANK3 mutation in autistic patients. American Journal of Medical Genetics *150B*, 421-424.

Germana, A., Laura, R., Montalbano, G., Guerrera, M.C., Amato, V., Zichichi, R., Campo, S., Ciriaco, E., and Vega, J.A. (2010). Expression of brain-derived neurotrophic factor and TrkB in the lateral line system of zebrafish during development. Cellular and Molecular Neurobiology *30*, 787-793.

Germana, A., Montalbano, G., Guerrera, M.C., Laura, R., Levanti, M., Abbate, F., de Carlos, F., Vega, J.A., and Ciriaco, E. (2009). Sox-2 in taste bud and lateral line system of zebrafish during development. Neuroscience Letters *467*, 36-39.

Ghysen, A., and Dambly-Chaudiere, C. (2007). The lateral line microcosmos. Genes & Development *21*, 2118-2130.

Gilmour, D., Knaut, H., Maischein, H.M., and Nusslein-Volhard, C. (2004). Towing of sensory axons by their migrating target cells in vivo. Nature Neuroscience *7*, 491-492.

Gleason, M.R., Nagiel, A., Jamet, S., Vologodskaia, M., Lopez-Schier, H., and Hudspeth, A.J. (2009). The transmembrane inner ear (Tmie) protein is essential for normal hearing and balance in the zebrafish. Proceedings of the National Academy of Sciences of the United States of America *106*, 21347-21352.

Go, W., Bessarab, D., and Korzh, V. (2010). atp2b1a regulates Ca(2+) export during differentiation and regeneration of mechanosensory hair cells in zebrafish. Cell Calcium *48*, 302-313.

Golub, J.S., Tong, L., Ngyuen, T.B., Hume, C.R., Palmiter, R.D., Rubel, E.W., and Stone, J.S. (2012). Hair cell replacement in adult mouse utricles after targeted ablation of hair cells with diphtheria toxin. The Journal of Neuroscience *32*, 15093-15105.

Gompel, N., Cubedo, N., Thisse, C., Thisse, B., Dambly-Chaudiere, C., and Ghysen, A. (2001a). Pattern formation in the lateral line of zebrafish. Mechanisms of Development *105*, 69-77.

Gompel, N., Dambly-Chaudiere, C., and Ghysen, A. (2001b). Neuronal differences prefigure somatotopy in the zebrafish lateral line. Development *128*, 387-393.

Gong, Z., Ju, B., Wang, X., He, J., Wan, H., Sudha, P.M., and Yan, T. (2002). Green fluorescent protein expression in germ-line transmitted transgenic zebrafish under a stratified epithelial promoter from keratin8. Developmental Dynamics *223*, 204-215.

Goodman, C.S., and Shatz, C.J. (1993). Developmental mechanisms that generate precise patterns of neuronal connectivity. Cell *72*, 77-98.

Gubbels, S.P., Woessner, D.W., Mitchell, J.C., Ricci, A.J., and Brigande, J.V. (2008). Functional auditory hair cells produced in the mammalian cochlea by in utero gene transfer. Nature *455*, 537-541.

Guilmatre, A., Huguet, G., Delorme, R., and Bourgeron, T. (2014). The emerging role of SHANK genes in neuropsychiatric disorders. Developmental Neurobiology *74*, 113-122.

Haas, P., and Gilmour, D. (2006). Chemokine signaling mediates self-organizing tissue migration in the zebrafish lateral line. Developmental Cell *10*, 673-680.

Haftek, Z., Morvan-Dubois, G., Thisse, B., Thisse, C., Garrone, R., and Le Guellec, D. (2003). Sequence and embryonic expression of collagen XVIII NC1 domain (endostatin) in the zebrafish. Gene Expression Patterns *3*, 351-354.

Hammond, K.L., Hill, R.E., Whitfield, T.T., and Currie, P.D. (2002). Isolation of three zebrafish dachshund homologues and their expression in sensory organs, the central nervous system and pectoral fin buds. Mechanisms of Development *112*, 183-189.

Han, K., Holder, J.L., Jr., Schaaf, C.P., Lu, H., Chen, H., Kang, H., Tang, J., Wu, Z., Hao, S., Cheung, S.W., *et al*. (2013). SHANK3 overexpression causes manic-like behaviour with unique pharmacogenetic properties. Nature *503*, 72-77.

He, Z., and Tessier-Lavigne, M. (1997). Neuropilin Is a Receptor for the Axonal Chemorepellent Semaphorin III. Cell *90*, 739-751.

Helmstaedter, M. (2013). Cellular-resolution connectomics: challenges of dense neural circuit reconstruction. Nature Methods *10*, 501-507.

Helmstaedter, M., Briggman, K.L., and Denk, W. (2011). High-accuracy neurite reconstruction for high-throughput neuroanatomy. Nature Neuroscience *14*, 1081-1088.

Helmstaedter, M., Briggman, K.L., Turaga, S.C., Jain, V., Seung, H.S., and Denk, W. (2013). Connectomic reconstruction of the inner plexiform layer in the mouse retina. Nature *500*, 168-174.

Helmstaedter, M., and Mitra, P.P. (2012). Computational methods and challenges for large-scale circuit mapping. Current Opinion in Neurobiology *22*, 162-169.

Herculano-Houzel, S. (2009). The human brain in numbers: a linearly scaled-up primate brain. Frontiers in Human Neuroscience *3*, 31.

Hernandez, P.P., Olivari, F.A., Sarrazin, A.F., Sandoval, P.C., and Allende, M.L. (2007). Regeneration in zebrafish lateral line neuromasts: expression of the neural progenitor cell marker sox2 and proliferation-dependent and-independent mechanisms of hair cell renewal. Developmental Neurobiology *67*, 637-654.

Hong, W., Mosca, T., and Luo, L. (2012). Teneurins instruct synaptic partner matching in an olfactory map. Nature *484*, 201-207.

Hsiao, C.-D., Tsai, W.-Y., and Tsai, H.-J. (2002). Isolation and expression of two zebrafish homologues of parvalbumin genes related to chicken CPV3 and mammalian oncomodulin. Mechanisms of Development *119S*, S161-S166.

Hsiung, F., Ramirez-Weber, F.A., Iwaki, D.D., and Kornberg, T.B. (2005). Dependence of Drosophila wing imaginal disc cytonemes on Decapentaplegic. Nature *437*, 560-563.

Hu, H.T., and Hsueh, Y.P. (2014). Calcium influx and postsynaptic proteins coordinate the dendritic filopodium-spine transition. Developmental Neurobiology *74*, 1011-1029.

Huang, Z.J., Di Cristo, G., and Ango, F. (2007). Development of GABA innervation in the cerebral and cerebellar cortices. Nature Reviews Neuroscience *8*, 673-686.

Hubel, D., and Wiesel, T. (1977a). Ferrier lecture. Functional architecture of macaque monkey visual cortex. Proceedings of the Royal Society of London *198*, 1-59.

Hubel, D., and Wiesel, T. (1977b). Plasticity of ocular dominance columns in monkey striate cortex. Philosophical Transactions of the Royal Society of London *278*, 377-409.

Hudspeth, A.J. (1989). How the ear's works work. Nature *341*, 397-404.

Hudspeth, A.J., and Jacobs, R. (1979). Stereocilia mediate transduction in vertebrate hair cells. Proceedings of the National Academy of Sciences of the United States of America *76*, 1506-1509.

Hwang, W.Y., Fu, Y., Reyon, D., Maeder, M.L., Tsai, S.Q., Sander, J.D., Peterson, R.T., Yeh, J.R., and Joung, J.K. (2013). Efficient genome editing in zebrafish using a CRISPR-Cas system. Nature Biotechnology *31*, 227-229.

Insolera, R., Shao, W., Airik, R., Hildebrandt, F., and Shi, S.H. (2014). SDCCAG8 Regulates Pericentriolar Material Recruitment and Neuronal Migration in the Developing Cortex. Neuron *83*, 805-822.

Jacinto, A., Wood, W., Balayo, T., Turmaine, M., Martinez-Arias, A., and Martin, P. (2000). Dynamic actin-based epithelial adhesion and cell matching during Drosophila dorsal closure. Current Biology *10*, 1420-1426.

Jacob, S., Landeros-Weisenberger, A., and Leckman, J.F. (2009). Autism spectrum and obsessive-compulsive disorders: OC behaviors, phenotypes and genetics. Autism Research *2*, 293-311.

Jamain, S., Quach, H., Betancur, C., Rastam, M., Colineaux, C., Gillberg, I.C., Soderstrom, H., Giros, B., Leboyer, M., Gillberg, C., *et al*. (2003). Mutations of the X-linked genes encoding neuroligins NLGN3 and NLGN4 are associated with autism. Nat Genet *34*, 27-29.

Jongeneel, C.V., Iseli, C., Stevenson, B.J., Riggins, G.J., Lal, A., Mackay, A., Harris, R.A., O'Hare, M.J., Neville, A.M., Simpson, A.J., *et al*. (2003). Comprehensive sampling of gene expression in human cell lines with massively parallel signature sequencing. Proceedings of the National Academy of Sciences of the United States of America *100*, 4702-4705.

Kandel, E., Schwartz, J., Jessell, T.M., Siegelbaum, S., and Hudspeth, A.J. (2012). Principles of Neural Science, 5th Edition edn (McGraw-Hill).

Kappler, J.A., Starr, C.J., Chan, D.K., Kollmar, R., and Hudspeth, A.J. (2004). A nonsense mutation in the gene encoding a zebrafish myosin VI isoform causes defects in hair-cell mechanotransduction. Proceedings of the National Academy of Sciences of the United States of America *101*, 13056-13061.

Katz, L.C., and Shatz, C.J. (1996). Synaptic Activity and the Construction of Cortical Circuits. Science *274*.

Kawakami, K., Abe, G., Asada, T., Asakawa, K., Fukuda, R., Ito, A., Lal, P., Mouri, N., Muto, A., Suster, M.L.*, et al*. (2010). zTrap: zebrafish gene trap and enhancer trap database. BMC Developmental Biology *10*, 105.

Kazmierczak, P., Sakaguchi, H., Tokita, J., Wilson-Kubalek, E.M., Milligan, R.A., Muller, U., and Kachar, B. (2007). Cadherin 23 and protocadherin 15 interact to form tip-link filaments in sensory hair cells. Nature *449*, 87-91.

Kennedy, T., Serafini, T., de la Torre, J., and Tessier-Lavigne, M. (1994). Netrins are diffusible chemotropic factors for commissural axons in the embryonic spinal cord. Cell *78*, 425-435.

Kidd, T., Bland, K., and Goodman, C.S. (1999). Slit Is the Midline Repellent for the Robo Receptor in Drosophila. Cell*,* 785-794.

Kindt, K.S., Finch, G., and Nicolson, T. (2012). Kinocilia mediate mechanosensitivity in developing zebrafish hair cells. Developmental Cell *23*, 329-341.

Kohsaka, H., and Nose, A. (2009). Target recognition at the tips of postsynaptic filopodia: accumulation and function of Capricious. Development *136*, 1127-1135.

Kolodkin, A.L., Matthes, D.J., and Goodman, C.S. (1993). The semaphorin Genes Encode a Family of Transmembrane and Secreted Growth Cone Guidance Molecules. Cell *75*, 1389-1399.

Komiyama, T., and Luo, L. (2006). Development of wiring specificity in the olfactory system. Current Opinion in Neurobiology *16*, 67-73.

Kornberg, T.B., and Roy, S. (2014). Cytonemes as specialized signaling filopodia. Development *141*, 729-736.

Kunes, S., and Steller, H. (1993). Topography in the Drosophila visual system. Current Opinions in Neurobiology *3*, 53-59.

Kurn, N., Chen, P., Heath, J.D., Kopf-Sill, A., Stephens, K.M., and Wang, S. (2005). Novel isothermal, linear nucleic acid amplification systems for highly multiplexed applications. Clinical Chemistry *51*, 1973-1981.

Lambert, P., Gu, R., and Corwin, J. (1997). Analysis of small hair bundles in the utricles of mature guinea pigs. American Journal of Otolaryngology *18*, 637-643.

Langmead, B., Trapnell, C., Pop, M., and Salzberg, S.L. (2009). Ultrafast and memory-efficient alignment of short DNA sequences to the human genome. Genome Biology *10*, R25.

Laumonnier, F., Bonnet-Brilhault, F., Gomot, M., Blanc, R., David, A., Moizard, M.P., Raynaud, M., Ronce, N., Lemonnier, E., Calvas, P., *et al*. (2004). X-linked mental retardation and autism are associated with a mutation in the NLGN4 gene, a member of the neuroligin family. American Journal of Human Genetics *74*, 552-557.

Lawson-Yuen, A., Saldivar, J.S., Sommer, S., and Picker, J. (2008). Familial deletion within NLGN4 associated with autism and Tourette syndrome. European Journal of Human Genetics *16*, 614-618.

Leblond, C.S., Heinrich, J., Delorme, R., Proepper, C., Betancur, C., Huguet, G., Konyukh, M., Chaste, P., Ey, E., Rastam, M., *et al*. (2012). Genetic and functional analyses of SHANK2 mutations suggest a multiple hit model of autism spectrum disorders. PLoS Genetics *8*, e1002521.

Ledent, V. (2002). Postembryonic development of the posterior lateral line in zebrafish. Development *129*, 597-604.

Lenzi, D., and Roberts, W. (1994). Calcium signalling in hair cells: multiple roles in a compact cell. Current Opinions in Neurobiology *4*, 496-502.

Lepage, S.E., and Bruce, A.E. (2008). Characterization and comparative expression of zebrafish calpain system genes during early development. Developmental Dynamics *237*, 819-829.

Liao, J.C. (2010). Organization and physiology of posterior lateral line afferent neurons in larval zebrafish. Biology Letters *6*, 402-405.

Liao, J.C., and Haehnel, M. (2012). Physiology of afferent neurons in larval zebrafish provides a functional framework for lateral line somatotopy. Journal of Neurophysiology *107*, 2615-2623.

Lopez-Schier, H., and Hudspeth, A.J. (2006). A two-step mechanism underlies the planar polarization of regenerating sensory hair cells. Proceedings of the National Academy of Sciences of the United States of America *103*, 18615-18620.

Lopez-Schier, H., Starr, C.J., Kappler, J.A., Kollmar, R., and Hudspeth, A.J. (2004). Directional cell migration establishes the axes of planar polarity in the posterior lateral-line organ of the zebrafish. Developmental Cell *7*, 401-412.

Lowery, L.A., and Van Vactor, D. (2009). The trip of the tip: understanding the growth cone machinery. Nature Reviews Molecular Cell Biology *10*, 332-343.

Luo, L., and Flanagan, J.G. (2007). Development of continuous and discrete neural maps. Neuron *56*, 284-300.

Lysakowski, A. (1999). Development of Synaptic Innervation in the Rodent Utricle. Annals of the New York Academy of Sciences *871*, 422-425.

Ma, E.Y., Rubel, E.W., and Raible, D.W. (2008). Notch signaling regulates the extent of hair cell regeneration in the zebrafish lateral line. The Journal of Neuroscience *28*, 2261-2273.

Mangos, S., Liu, Y., and Drummond, I.A. (2007). Dynamic expression of the osmosensory channel trpv4 in multiple developing organs in zebrafish. Gene Expression Patterns *7*, 480-484.

Marrs, G.S., Green, S.H., and Dailey, M.E. (2001). Rapid formation and remodeling of postsynaptic densities in developing dendrites. Nature Neuroscience *4*, 1006-1013.

Martin, P., and Parkhurst, S.M. (2004). Parallels between tissue repair and embryo morphogenesis. Development *131*, 3021-3034.

Matthews, G., and Fuchs, P. (2010). The diverse roles of ribbon synapses in sensory neurotransmission. Nature Reviews Neuroscience *11*, 812-822.

McDermott, B.M., Jr., Asai, Y., Baucom, J.M., Jani, S.D., Castellanos, Y., Gomez, G., McClintock, J.M., Starr, C.J., and Hudspeth, A.J. (2010). Transgenic labeling of hair cells in the zebrafish acousticolateralis system. Gene Expression Patterns *10*, 113-118.

McLaughlin, T., and O'Leary, D. (2005). Molecular Gradients and Development of Retinotopic Maps. Annual Reviews in Neuroscience *28*, 327-355.

Metcalfe, W., Kimmel, C., and Schabtach, E. (1985). Anatomy of the posterior lateral line system in young larvae of the zebrafish. Journal of Comparative Neurology *233*, 377-389.

Millard, T.H., and Martin, P. (2008). Dynamic analysis of filopodial interactions during the zippering phase of Drosophila dorsal closure. Development *135*, 621-626.

Mirković, I., Pylawka, S., and Hudspeth, A.J. (2012). Rearrangements between differentiating hair cells coordinate planar polarity and the establishment of mirror symmetry in lateral-line neuromasts. Biology Open *1*, 498-505.

Mizutari, K., Fujioka, M., Hosoya, M., Bramhall, N., Okano, H.J., Okano, H., and Edge, A.S. (2013). Notch inhibition induces cochlear hair cell regeneration and recovery of hearing after acoustic trauma. Neuron *77*, 58-69.

Mo, W., and Nicolson, T. (2011). Both Pre- and Postsynaptic Activity of Nsf Prevents Degeneration of Hair-Cell Synapses. PLoS One *6*, 1-13.

Montgomery, J., and Macdonald, J. (1987). Sensory tuning of lateral line receptors in antarctic fish to the movements of planktonic prey. Science *235*, 195-196.

Mosca, T., Hong, W., Dani, V., Favaloro, V., and Luo, L. (2012). Trans-synaptic Teneurin signalling in neuromuscular synapse organization and target choice. Nature *484*, 237-241.

Nagiel, A., Andor-Ardo, D., and Hudspeth, A.J. (2008). Specificity of afferent synapses onto plane-polarized hair cells in the posterior lateral line of the zebrafish. The Journal of Neuroscience *28*, 8442-8453.

Nagiel, A., Patel, S.H., Andor-Ardo, D., and Hudspeth, A.J. (2009). Activity-independent specification of synaptic targets in the posterior lateral line of the larval zebrafish. Proceedings of the National Academy of Sciences of the United States of America *106*, 21948-21953.

Nasevicius, A., and Ekker, S.C. (2000). Effective targeted gene 'knockdown' in zebrafish. Nature Genetics *26*, 216-220.

O'Donnell, M., Chance, R.K., and Bashaw, G.J. (2009). Axon growth and guidance: receptor regulation and signal transduction. Annual Review of Neuroscience *32*, 383-412.

Obholzer, N., Wolfson, S., Trapani, J.G., Mo, W., Nechiporuk, A., Busch-Nentwich, E., Seiler, C., Sidi, S., Sollner, C., Duncan, R.N., *et al*. (2008). Vesicular glutamate transporter 3 is required for synaptic transmission in zebrafish hair cells. The Journal of Neuroscience *28*, 2110-2118.

Olszewski, J., Haehnel, M., Taguchi, M., and Liao, J.C. (2012). Zebrafish larvae exhibit rheotaxis and can escape a continuous suction source using their lateral line. PLoS One *7*, e36661.

Oshima, K., Shin, K., Diensthuber, M., Peng, A.W., Ricci, A.J., and Heller, S. (2010). Mechanosensitive hair cell-like cells from embryonic and induced pluripotent stem cells. Cell *141*, 704-716.

Pak, C.W., Flynn, K.C., and Bamburg, J.R. (2008). Actin-binding proteins take the reins in growth cones. Nature Reviews Neuroscience *9*, 136-147.

Pecho-Vrieseling, E., Sigrist, M., Yoshida, Y., Jessell, T.M., and Arber, S. (2009). Specificity of sensory-motor connections encoded by Sema3e-Plxnd1 recognition. Nature *459*, 842-846.

Penzes, P., Buonanno, A., Passafaro, M., Sala, C., and Sweet, R.A. (2013). Developmental vulnerability of synapses and circuits associated with neuropsychiatric disorders. Journal of Neurochemistry *126*, 165-182.

Pujol, R., Pickett, S.B., Nguyen, T.B., and Stone, J.S. (2014). Large basolateral processes on type II hair cells are novel processing units in mammalian vestibular organs. J Comp Neurol *522*, 3141-3159.

Pujol-Marti, J., Baudoin, J.P., Faucherre, A., Kawakami, K., and Lopez-Schier, H. (2010). Progressive Neurogenesis Defines Lateralis Somatotopy. Developmental Dynamics *239*, 1919-1930.

Pujol-Marti, J., Zecca, A., Baudoin, J.P., Faucherre, A., Asakawa, K., Kawakami, K., and Lopez-Schier, H. (2012). Neuronal birth order identifies a dimorphic sensorineural map. The Journal of Neuroscience *32*, 2976-2987.

Ramirez-Weber, F.A., and Kornberg, T.B. (1999). Cytonemes: cellular processes that project to the principal signaling center in Drosophila imaginal discs. Cell *97*, 599-607.

Reichelt, A.C., Rodgers, R.J., and Clapcote, S.J. (2012). The role of neurexins in schizophrenia and autistic spectrum disorder. Neuropharmacology *62*, 1519-1526.

Rice, D.S., Northcutt, G.M., and Kurschner, C. (2001). The Lnx family proteins function as molecular scaffolds for Numb family proteins. Molecular and cellular neurosciences *18*, 525-540.

Rieger, S., and Sagasti, A. (2011). Hydrogen peroxide promotes injury-induced peripheral sensory axon regeneration in the zebrafish skin. PLoS Biol *9*, e1000621.

Roy, S., Hsiung, F., and Kornberg, T.B. (2011). Specificity of Drosophila cytonemes for distinct signaling pathways. Science *332*, 354-358.

Roy, S., Huang, H., Liu, S., and Kornberg, T.B. (2014). Cytoneme-mediated contact-dependent transport of the Drosophila decapentaplegic signaling protein. Science *343*, 1244624.

Rubel, E., Dew, L., and Roberson, D. (1995). Mammalian vestibular hair cell regeneration. Science *267*, 701-707.

Russell, I.J. (1970). The Role of the Lateral-Line Efferent System in Xenopus Laevis. Journal of Experimental Biology *54*, 621-641.

Salmons, S., and Sreter, F.A. (1976). Significance of impulse activity in the transformation of skeletal muscle type. Nature *263*, 30-34.

Sanders, T.A., Llagostera, E., and Barna, M. (2013). Specialized filopodia direct long-range transport of SHH during vertebrate tissue patterning. Nature *497*, 628-632.

Sandulescu, C.M., Teow, R.Y., Hale, M.E., and Zhang, C. (2011). Onset and dynamic expression of S100 proteins in the olfactory organ and the lateral line system in zebrafish development. Brain Res *1383*, 120-127.

Sanes, J., and Lichtman, J. (2001). Induction, assembly, maturation, and maintenance of a postynaptic apparatus. Nature Reviews Neuroscience *2*, 791-805.

Sapede, D., Gompel, N., Dambly-Chaudiere, C., and Ghysen, A. (2002). Cell migration in the postembryonic development of the fish lateral line. Development *129*, 605-614.

Sato, A., Koshida, S., and Takeda, H. (2010). Single-cell analysis of somatotopic map formation in the zebrafish lateral line system. Developmental Dynamics *239*, 2058-2065.

Sato, A., and Takeda, H. (2013). Neuronal subtypes are specified by the level of neurod expression in the zebrafish lateral line. The Journal of neuroscience *33*, 556-562.

Schmidt, J.T., and Edwards, D.L. (1983). Activity Sharpens the Map during the Regeneration of the Retinotectal Projection in Goldfish. Brain Research *269*, 29-39.

Scott, E.K., Mason, L., Arrenberg, A.B., Ziv, L., Gosse, N.J., Xiao, T., Chi, N.C., Asakawa, K., Kawakami, K., and Baier, H. (2007). Targeting neural circuitry in zebrafish using GAL4 enhancer trapping. Nature Methods *4*, 323-326.

Seiler, C., Ben-David, O., Sidi, S., Hendrich, O., Rusch, A., Burnside, B., Avraham, K.B., and Nicolson, T. (2004). Myosin VI is required for structural integrity of the apical surface of sensory hair cells in zebrafish. Developmental Biology *272*, 328-338.

Seiler, C., Finger-Baier, K.C., Rinner, O., Makhankov, Y.V., Schwarz, H., Neuhauss, S.C., and Nicolson, T. (2005). Duplicated genes with split functions: independent roles of protocadherin15 orthologues in zebrafish hearing and vision. Development *132*, 615-623.

Shargorodsky, J., Curhan, S.G., Curhan, G.C., and Eavey, R. (2010). Change in Prevalence of Hearing Loss in US Adolescents. The Journal of the American Medical Association *304*, 772-778.

Sheets, L., Kindt, K.S., and Nicolson, T. (2012). Presynaptic CaV1.3 channels regulate synaptic ribbon size and are required for synaptic maintenance in sensory hair cells. The Journal of Neuroscience *32*, 17273-17286.

Sheets, L., Trapani, J.G., Mo, W., Obholzer, N., and Nicolson, T. (2011). Ribeye is required for presynaptic Ca(V)1.3a channel localization and afferent innervation of sensory hair cells. Development *138*, 1309-1319.

Shen, K., and Bargmann, C. (2003). The immunoglobulin superfamily protein SYG-1 determines the location of specific synapses in C. elegans. Cell *112*, 619-630.

Shen, K., Fetter, R., and Bargmann, C. (2004). Synaptic specificity is generated by the synaptic guidepost protein SYG-2 and its receptor, SYG-1. Cell *116*, 869-881.

Shinza-Kameda, M., Takasu, E., Sakurai, K., Hayashi, S., and Nose, A. (2006). Regulation of Layer-Specific Targeting by Reciprocal Expression of a Cell Adhesion Molecule, Capricious. Neuron *49*, 205-213.

Sinkkonen, S.T., Chai, R., Jan, T.A., Hartman, B.H., Laske, R.D., Gahlen, F., Sinkkonen, W., Cheng, A.G., Oshima, K., and Heller, S. (2011). Intrinsic regenerative potential of murine cochlear supporting cells. Scientific Reports *1*, 26.

Sobkowicz, H.M., Slapnick, S.M., and August, B.K. (2002). Differentiation of spinous synapses in the mouse organ of corti. Synapse *45*, 10-24.

Sobkowicz, H.M., Slapnick, S.M., and August, B.K. (2003). Reciprocal synapses between inner hair cell spines and afferent dendrites in the organ of corti of the mouse. Synapse *50*, 53-66.

Sperry, R.W. (1945). Restoration of vision after crossing of optic nerves and after contralateral transplantation of eye. Journal of Neurophysiology *8*, 17-28.

Sperry, R.W. (1963). Chemoaffinity in the orderly growth of nerve fiber patterns and connections. Proceedings of the National Academy of Sciences *50*, 703-710.

Steiner, A.B., Kim, T., Cabot, V., and Hudspeth, A.J. (2014). Dynamic gene expression by putative hair-cell progenitors during regeneration in the zebrafish lateral line. Proceedings of the National Academy of Sciences of the United States of America *111*, E1393-1401.

Stone, J.S., and Rubel, E.W. (2000). Temporal, spatial, and morphologic features of hair cell regeneration in the avian basilar papilla. The Journal of Comparative Neurology *417*, 1-16.

Sudhof, T.C. (2008). Neuroligins and neurexins link synaptic function to cognitive disease. Nature *455*, 903-911.

Suli, A., Watson, G.M., Rubel, E.W., and Raible, D.W. (2012). Rheotaxis in larval zebrafish is mediated by lateral line mechanosensory hair cells. PLoS One *7*, e29727.

Tessier-Lavigne, M., and Goodman, C.S. (1996). The Molecular Biology of Axon Guidance. Science *274*, 1123-1132.

Thisse, B., Pflumio, S., Fürthauer, M., Loppin, B., Heyer, V., Degrave, A., Woehl, R., Lux, A., Steffan, T., Charbonnier, X.Q., *et al*. (2001). Expression of the zebrafish genome during embryogenesis (ZFIN Direct Data Submission: zfin.org).

Tingaud-Sequeira, A., Forgue, J., Andre, M., and Babin, P.J. (2006). Epidermal transient down-regulation of retinol-binding protein 4 and mirror expression of apolipoprotein Eb and estrogen receptor 2a during zebrafish fin and scale development. Developmental Dynamics *235*, 3071-3079.

Trachtenberg, J.T., Chen, B.E., Knott, G.W., Feng, G., Sanes, J.R., Welker, E., and Svoboda, K. (2002). Long-term in vivo imaging of experience-dependent synaptic plasticity in adult cortex. Nature *19*, 788-794.

Trapani, J.G., Obholzer, N., Mo, W., Brockerhoff, S.E., and Nicolson, T. (2009). Synaptojanin1 is required for temporal fidelity of synaptic transmission in hair cells. PLoS Genetics *5*, e1000480.

Trapnell, C., Roberts, A., Goff, L., Pertea, G., Kim, D., Kelley, D.R., Pimentel, H., Salzberg, S.L., Rinn, J.L., and Pachter, L. (2012). Differential gene and transcript expression analysis of RNA-seq experiments with TopHat and Cufflinks. Nature Protocols *7*, 562-578.

Uhm, C.S., Neuhuber, B., Lowe, B., Crocker, V., and Daniels, M. (2001). Synapse-Forming Axons and Recombinant Agrin Induce Microprocess Formation on Myotubes. Journal of Neuroscience *21*, 9678-9689.

Uthaiah, R.C., and Hudspeth, A.J. (2010). Molecular anatomy of the hair cell's ribbon synapse. The Journal of Neuroscience *30*, 12387-12399.

Varoqueaux, F., Aramuni, G., Rawson, R.L., Mohrmann, R., Missler, M., Gottmann, K., Zhang, W., Sudhof, T.C., and Brose, N. (2006). Neuroligins determine synapse maturation and function. Neuron *51*, 741-754.

Wang, X., Tsai, J.W., Imai, J.H., Lian, W.N., Vallee, R.B., and Shi, S.H. (2009). Asymmetric centrosome inheritance maintains neural progenitors in the neocortex. Nature *461*, 947-955.

Welch, J.M., Lu, J., Rodriguiz, R.M., Trotta, N.C., Peca, J., Ding, J.D., Feliciano, C., Chen, M., Adams, J.P., Luo, J., *et al*. (2007). Cortico-striatal synaptic defects and OCD-like behaviours in Sapap3-mutant mice. Nature *448*, 894-900.

West, M.C., and McDermott, B.M., Jr. (2011). Ribeye a-mCherry fusion protein: a novel tool for labeling synaptic ribbons of the hair cell. Journal of Neuroscience Methods *197*, 274-278.

Westerfield, M. (2000). The zebrafish book: A guide for the laboratory use of zebrafish (Danio rerio), 4th Edition edn (Eugene: Univ. of Oregon Press).

Whitehead, M.C., and Morest, D.K. (1985). The Development of Innervation Patterns in the Avian Cochlea. Neuroscience *14*, 255-276.

Wibowo, I., Pinto-Teixeira, F., Satou, C., Higashijima, S., and Lopez-Schier, H. (2011). Compartmentalized Notch signaling sustains epithelial mirror symmetry. Development *138*, 1143-1152.

Wilkinson, C.J., Carl, M., and Harris, W.A. (2009). Cep70 and Cep131 contribute to ciliogenesis in zebrafish embryos. BMC Cell Biology *10*, 17.

Williams, J., and Holder, N. (2000). Cell turnover in neuromasts of zebrafish larvae. Hearing Research *143*, 171-181.

Wilson, H.L., Wong, A.C.C., Shaw, S.R., Tse, W.-Y., Stapleton, G.A., Phelan, M.C., Hu, S., Marshall, J., and McDermid, H.E. (2003). Molecular characterisation of the 22q13 deletion syndrome supports the role of haploinsufficiency of SHANK3/PROSAP2 in the major neurological symptoms. Journal of Medical Genetics *40*, 575-584.

Wolpert, L. (1969). Positional information and the spatial pattern of cellular differentiation. Journal of Theoretical Biology *25*, 1-47.

Wolpert, L. (2009). Diffusible gradients are out - an interview with Lewis Wolpert. Interviewed by Richardson, Michael K. The International Journal of Developmental Biology *53*, 659-662.

Wood, W., Jacinto, A., Grose, R., Woolner, S., Gale, J., Wilson, C., and Martin, P. (2002). Wound healing recapitulates morphogenesis in Drosophila embryos. Nature Cell Biology *4*, 907-912.

Yamagata, M., and Sanes, J. (1995). Lamina–specific cues guide outgrowth and arborization of retinal axons in the optic tectum. Development *121*, 189-200.

Yamagata, M., and Sanes, J. (2008). Dscam and Sidekick proteins direct lamina-specific synaptic connections in vertebrate retina. Nature *451*, 465-469.

Yamagata, M., Weiner, J., and Sanes, J. (2002). Sidekicks: Synaptic Adhesion Molecules that Promote Lamina-Specific Connectivity in the Retina. Cell *110*, 649-660.

Yan, J., Oliveira, G., Coutinho, A., Yang, C., Feng, J., Katz, C., Sram, J., Bockholt, A., Jones, I.R., Craddock, N., *et al*. (2005). Analysis of the neuroligin 3 and 4 genes in autism and other neuropsychiatric patients. Molecular Psychiatry *10*, 329-332.

Yoshida, Y. (2012). Semaphorin signaling in vertebrate neural circuit assembly. Frontiers in Molecular Neuroscience *5*, 71.